Electronic Supplementary Material (ESI) for ChemComm.
This journal is © The Royal Society of Chemistry 2022

Supporting Information

Probing flux of mitochondrial potassium using an azacrown-diketopyrrolopyrrole based highly sensitive probe

G. Dinesh Kumar,[a] Marzena Banasiewicz,[b] Antoni Wrzosek,[c] Rafal P. Kampa,[c] Manon H. E. Bousquet,[d] Damian Kusy,[a] Denis Jacquemin,*[d] Adam Szewczyk,*[c] and Daniel T. Gryko*[a]

[a] Institute of Organic Chemistry, Polish Academy of Sciences, Kasprzaka 44/52, 01-224 Warsaw, Poland. E-mail: dtgryko@icho.edu.pl

[b] Institute of Physics, Polish Academy of Sciences, Al. Lotników 32/46, 02-668 Warsaw, Poland.

[c] Nencki Institute of Experimental Biology of Polish Academy of Sciences, Pasteur 3, 02-093 Warsaw, Poland. E-mail: a.szewczyk@nencki.gov.pl.

[d] CEISAM UMR 6230, CNRS, Université de Nantes, 44000 Nantes, France. E-mail :Denis.Jacquemin@univ-nantes.fr

Table of contents

Section S1: General Information

All reagents and solvents were purchased from commercial sources and were used as received unless otherwise noted. Reagent grade solvents (CH_2Cl_2, hexanes) were distilled prior to use. Transformations with moisture- and oxygen-sensitive compounds were performed under a stream of argon. The reaction progress was monitored by means of thin-layer chromatography (TLC), which was performed on Kieselgel 60. The identity and purity of prepared compounds were proved by ^{1}H NMR and ^{13}C NMR as well as by mass spectrometry (via EI-MS or ESI-MS). HRMS (ESI-TOF) and HRMS (EI): double-focusing magnetic sector instruments with EBE geometry were utilized. NMR spectra were measured on 400 or 500 or 600 MHz instruments. Chemical shifts (δ, ppm) were determined with tetramethylsilane (TMS) as the internal reference; J values are given in Hz. All melting points for crystalline products were measured with an automated melting point apparatus and are given without correction.

UV/Vis absorption spectra were recorded on a PerkinElmer Lambda 35 Spectrometer. Fluorescence spectra were recorded on a FLS1000 of Edinburgh Instruments. All linear optical studies were performed with freshly prepared air-equilibrated solutions at room temperature (298 K). Acetonitrile was spectrophotometric grade and was used without further purification. Quartz cells (10 mm) were used for the measurements of absorption and emission spectra. As a standard, Rh6G (Φ_{fl} = 0.94 in EtOH) was used to determine fluorescence quantum yields.

Section S2: Synthesis

The synthetic strategy used to prepare DPP-based probes is based on the synthesis of asymmetrical DPPs incorporating a single bromoaryl substituent followed by Buchwald-Hartwig amination with a corresponding azacrown ether. Hence, DPP **S5** was prepared from 4-bromobenzonitrile (**S2**) and pyrrolidin-2-one **S1** following our previously developed strategy in 48% yield (Scheme S1). Subsequently the desired crown-DPP **S9** was obtained by Buchwald-Hartwig amination with 1-aza-18-crown-6 (**S8**) in 23 % yield (Scheme S2).

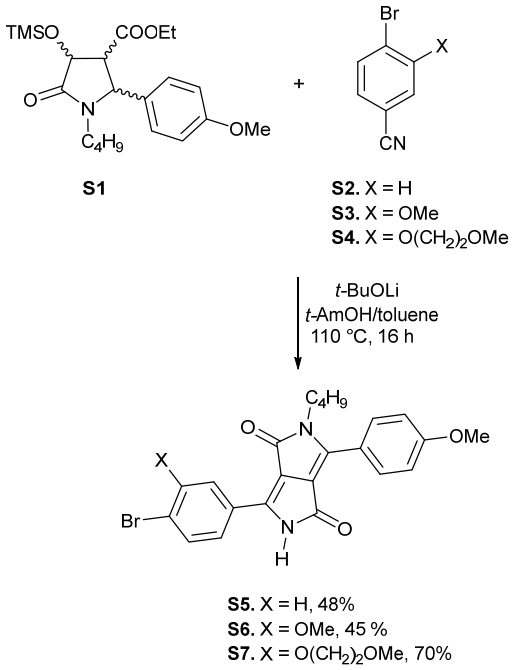

S1

S2. X = H
S3. X = OMe
S4. X = $O(CH_2)_2OMe$

S5. X = H, 48%
S6. X = OMe, 45 %
S7. X = $O(CH_2)_2OMe$, 70%

Scheme S1. The synthesis of diketopyrrolopyrroles **S5**-S**7**.

It is well known that the presence of an additional alkoxy group at an ortho position relative to an 18-azacrown-6 moiety increases the binding constant with K^+ as well as its selectivity versus this cation. In order to exploit this beneficial property, following similar synthetic procedures we designed DPPs **S10** and **S12** possessing MeO and $MeOCH_2CH_2O$ groups, respectively. We also designed DPP **S11** possessing a 15-azacrown-5 macrocycle as a model. The synthesis of these three DPPs was achieved following the aforementioned pathway, i.e., synthesis of unsymmetrical bromophenyl-DPPs **S6** and **S7** followed by optimized Buchwald-Hartwig amination with 1-aza-18-crown-6 or 1-aza-15-crown-5 to provide crown DPPs **S10** and **S11** in 15% and 50% yield respectively (Scheme S1, Fig. S1). Nitrile **S4**, obtained in two steps from 4-bromo-3-methoxy benzonitrile, was reacted with pyrrolidin-2-one **S1** forming DPP **S7** in high yield (70%). The latter dye was used for amination with 1-aza-18-crown-6 (**S8**) to afford DPP **1** in 18% yield (Scheme S1, Fig. S1).

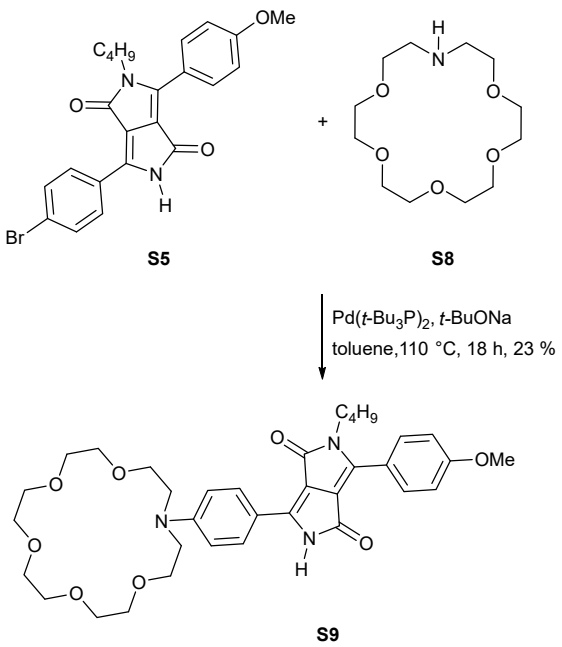

Scheme S2. The synthesis of DPP **S9** via Buchwald-Hartwig amination.

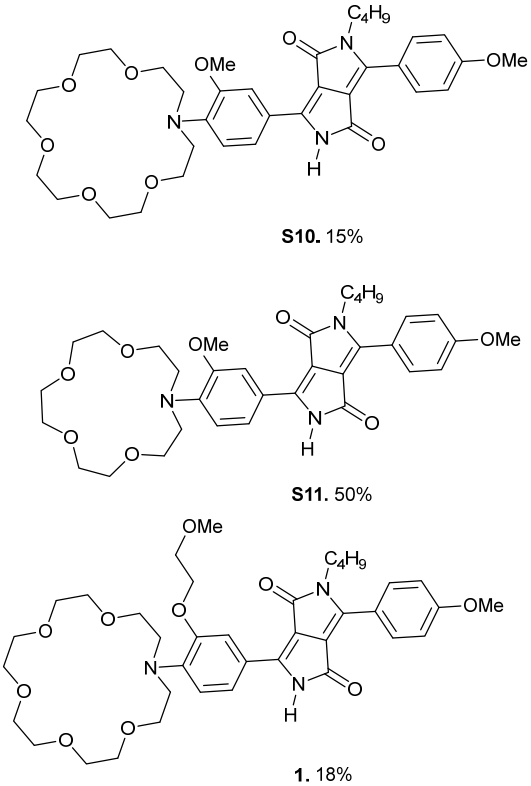

Fig. S1. The structures of crown-DPPs **S10**-**S11** and **1**.

The photophysical properties of unsymmetrically substituted DPPs strongly depend on the nature of both aryl substituents. Previously, it was found that the replacement of 4-$MeOC_6H_4$ with 4-$CF_3C_6H_4$ can render DPPs' fluorescence inert to changes in solvent polarity. This provided us with motivation to prepare analogues of DPPs **S9**-**S11** and **1** possessing 4-trifluoromethylphenyl substituents at position 2. The 4-trifluoromethylphenyl pyrrolidin-2-one **S15** was synthesized following the general procedure developed by us. The multicomponent reaction of 4-trifluoromethylbenzaldehyde with butylamine and diethyl oxalacetate afforded pyrrolidone **S13** (Scheme S3). Subsequent reduction gave lactam **S14** which was finally protected with TMS to give **S15** in 62% overall yield. The condensation of pyrrolidone **S15** with 4-bromobenzonitrile followed by Buchwald-Hartwig amination with 1-aza-18-crown-6 (**S8**) led to the formation of DPP **S17** in 29% yield.

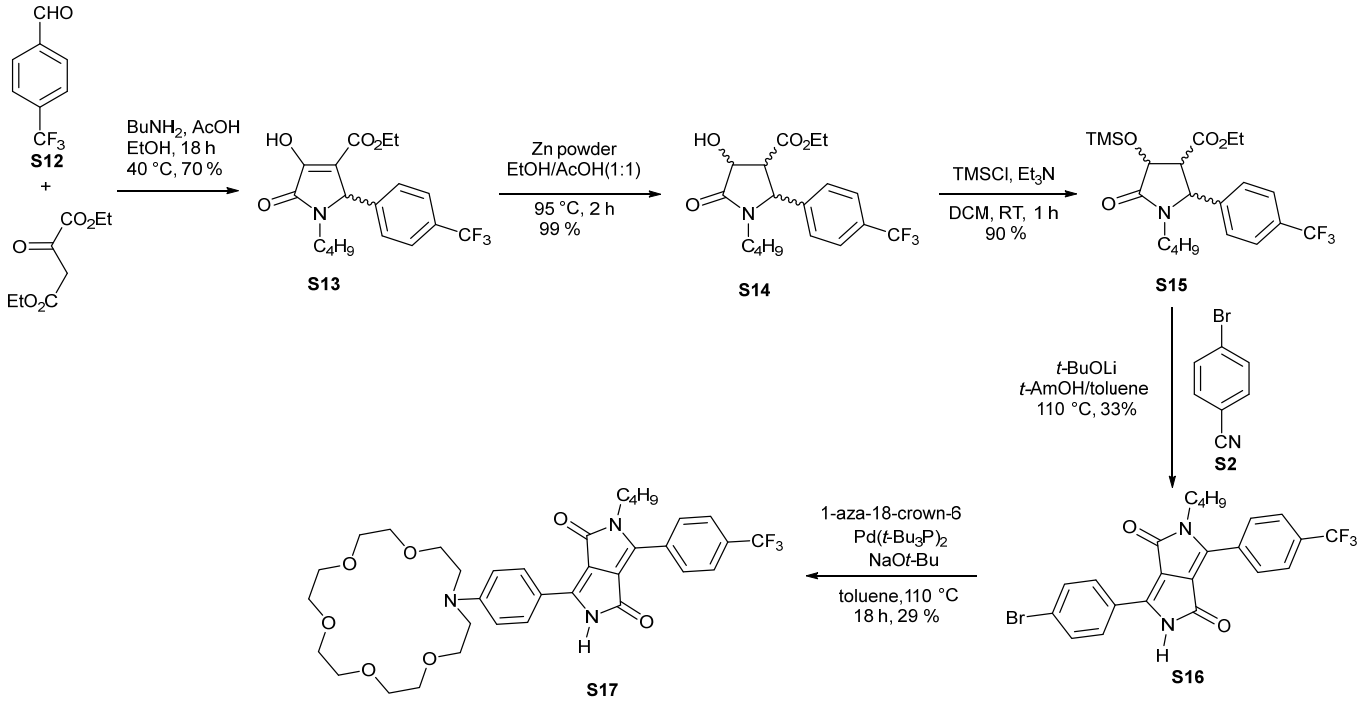

Scheme S3. Synthesis of diketopyrrolopyrrole **17**.

Finally DPP **1** was transformed into DPP **2** possessing a triphenylphosphonium salt using standard procedures (Scheme S4).

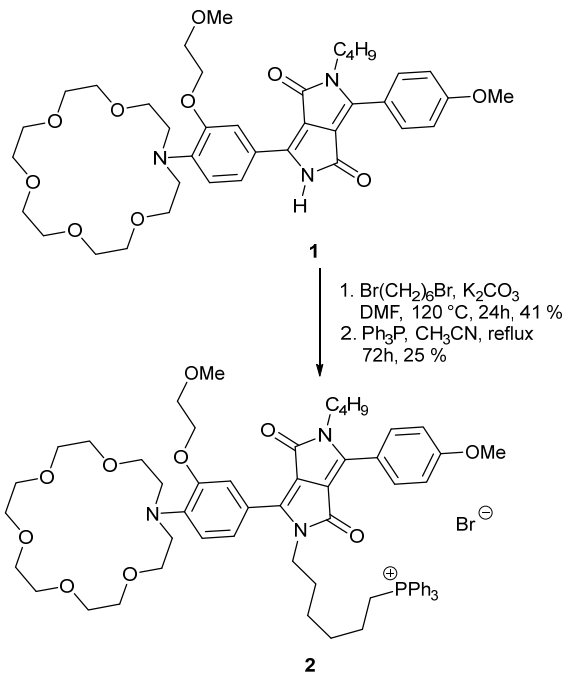

Scheme S4. The transformation of DPP **1** into mitochondrion probe **2**.

Section S3: Experimental Procedure

All reagents and solvents were purchased from commercial sources and were used as received unless otherwise noted. Reagent grade solvents (DCM, hexanes) were distilled prior to use. Transformations with moisture- and oxygen-sensitive compounds were performed under a stream of argon. The reaction progress was monitored by means of thin-layer chromatography (TLC), which was performed on Kieselgel 60. The identity and purity of prepared compounds were proved by 1H NMR and 13C NMR, 19F NMR as well as by mass spectrometry (via EI-MS or ESI-MS). HRMS (ESI-TOF) and HRMS (EI): double-focusing magnetic sector instruments with EBE geometry were utilized. NMR spectra were measured on 400 or 500 or 600 MHz instruments. Chemical shifts (δ, ppm) were determined with tetramethylsilane (TMS) as the internal reference; J values are given in Hz. All melting points for crystalline products were measured with an automated melting point apparatus and are given without correction. Pyrrolidone **S1** was obtained following the literature procedure.[1]

Synthesis of 4-bromo-3-(2-methoxyethoxy)benzonitrile (S4)

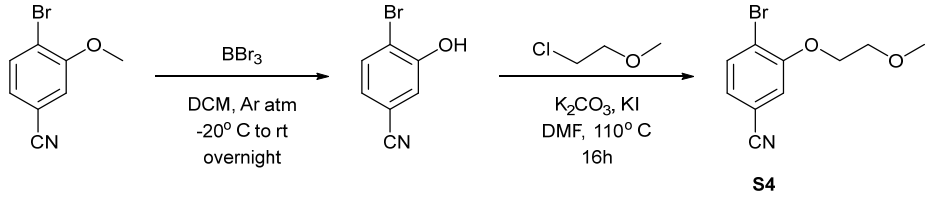

S4

4-bromo-3-hydroxybenzonitrile was synthesized according to following known literature procedure.[2]

A suspension of 4-bromo-3-hydroxybenzonitrile (0.8 g, 4 mmol), chloroethyl methyl ether(0.37mL, 4 mmol), KI (0.33g, 2 mmol) and K_2CO_3 (0.84g, 6 mmol) in 20 mL DMF was heated at 110 °C for 16 h. Then reaction mixture was cooled to room temperature and dissolved in 100 mL ethyl acetate and 50 mL water. Organic phase was separated and washed with 50 mL sat. NaCl, dried over Na_2SO_4. The solvent was evaporated to afford as brown solid in 97 % yield, 1.0 g. m.p. = 184 °C. ^{1}H NMR (500 MHz, $CDCl_3$) δ 7.65 (d, *J* = 8.1 Hz, 1H), 7.14 (m, 2H), 4.21 (t, *J* = 4.9 Hz, 2H), 3.82 (t, *J* = 4.6 Hz, 2H), 3.48(s, 3H). ^{13}C NMR (126 MHz, $CDCl_3$) δ 155.8, 134.3, 125.5, 118.5, 118.1, 116.0, 112.1, 70.6, 69.4, 59.5. HRMS (EI, m/z): [$M^{+\bullet}$] Calcd. for $C_{10}H_{10}BrNO_2$: 254.9895; found, 254.9904.

General procedure for the synthesis of DPP derivatives S5-S7:

In flame dried Schlenk flask, a mixture of appropriate nitrile (1 eq.) and lithium *tert*-butoxide (4 eq.) was heated to 110 °C under argon. To this solid mixture, *tert*-amyl alcohol (5 mL) was added in one portion followed by dropwise addition of pyrrolidone **S1** (1 eq.) dissolved in dry toluene (3 mL). The resulting dark solution was left to stir at this temperature for overnight. After cooling to room temperature reaction mixture was diluted with water (100 mL) and extracted with DCM

(100 mL), water phase was one more time washed with DCM (50 mL). The combined organic phases were dried over Na2SO4, filtered and concentrated in vacuum. The resulting crude compound was chromatographed on silica gel (DCM/MeOH = 9: 1) and crystallization from DCM/n-hexanes allowed to obtain the desired DPP product.

2-Butyl-3-(4-methoxyphenyl)-6-(4-bromophenyl)-2,5-dihydropyrrolo[3,4-*c*]pyrrole-1,4-dione (S5).

4-Bromobenzonitrile (**S2**, 1.0 g, 5.5 mmol), lithium *tert*-butoxide (1.8 g, 22 mmol) and pyrrolidone **S1** (2.2 g, 5.5 mmol) in combined solvent were used to obtain **S5** as red crystals in 48 % yield, 1.2 g. m.p. = 290 °C. ^{1}H NMR (500 MHz, $CDCl_3$) δ 10.68 (s, 1H), 8.15 (d, *J* = 8.0 Hz, 2H), 7.82 (d, *J* = 8.5 Hz, 2H), 7.47 (d, *J* = 8.1 Hz, 2H), 6.95 (d, *J* = 8.5 Hz, 2H), 3.92 (s, 3H), 3.78 (t, *J* = 7.6 Hz, 2H), 1.65 (quint, *J* = 7.1 Hz, 2H), 1.32 (m, 2H), 0.90 (t, *J* = 7.3 Hz, 3H). ^{13}C NMR (126 MHz, $CDCl_3$) δ 163.5, 162.7, 162.1, 148.9, 142.6, 132.1, 131.0, 129.4, 126.8, 125.8, 120.2, 114.1, 55.5, 42.2, 31.5, 20.05, 13.6. HRMS (ESI, m/z): $[M+Na]^+$ Calcd. for $C_{23}H_{21}BrN_2O_3Na$: 475.3360; found, 475.3380.

2-Butyl-3-(4-methoxyphenyl)-6-(4-bromo-3-methoxyphenyl)-2,5-dihydropyrrolo[3,4-*c*]pyrrole-1,4-dione (S6).

4-Bromo-3-methoxybenzonitrile (**S3**, 1.0 g, 4.7 mmol), lithium *tert*-butoxide (1.5 g, 18.8 mmol) and pyrrolidone **S1** (1.92 g, 4.7 mmol) in combined solvent were used to obtain **S6** as orange-red crystals in 45 % yield, 1.0 g. m.p. = 292 °C. ^{1}H NMR (600 MHz, $CDCl_3$) δ 10.87 (s, 1H), 8.07 (s, 1H), 7.80 (d, *J* = 8.8 Hz, 2H), 7.69 (d, *J* = 8.2 Hz, 1H), 7.18 (d, *J* = 7.3 Hz, 1H), 7.08 (d, *J* = 8.8 Hz, 2H), 4.04 (s, 3H), 3.94 (s, 3H), 3.85 (t, *J* = 7.9 Hz, 2H), 1.65 (quint, *J* = 7.5 Hz, 2H), 1.32 (m, 2H), 0.90 (t, *J* = 7.3 Hz, 3H). ^{13}C NMR (150 MHz, $CDCl_3$) δ 163.3, 163.2, 159.9, 159.6, 156.7, 154.0, 134.2, 131.3, 127.3, 119.9, 119.1, 116.9, 115.5, 114.9, 113.6, 111.1, 56.5, 55.6, 42.6, 31.3, 19.8, 13.4. HRMS (ESI, m/z): $[M+Na]^+$ Calcd. For $C_{24}H_{23}BrN_2O_4Na$: 505.0739; found, 505.0726.

2-Butyl-3-(4-methoxyphenyl)-6-(4-bromo-3-methoxyethoxyphenyl)-2,5-dihydropyrrolo[3,4-*c*]pyrrole-1,4-dione (S7).

4-Bromo-3-methoxyethoxybenzonitrile (**S4**, 1.0 g, 3.9 mmol), lithium *tert*-butoxide (1.25 g, 15.6 mmol) and pyrrolidone **S1** (1.6 g, 3.9 mmol) in combined solvent were used to obtain **S7** as orange-red crystals in 70 % yield, 1.4 g. m.p. = 284 °C. ^{1}H NMR (600 MHz, $CDCl_3$) δ 8.12 (s, 1H), 7.80 (d, *J* = 9.0 Hz, 2H), 7.69 (d, *J* = 8.2 Hz, 1H), 7.38 (d, *J* = 9.9 Hz, 1H), 7.08 (d, *J* = 8.8 Hz, 2H), 4.40 (t, *J* = 4.5 Hz, 2H), 4.02 (t, *J* = 4.4 Hz, 2H), 3.92(s, 3H), 3.86 (t, *J* = 7.8 Hz, 2H), 3.62 (s, 3H), 3.57 (s, 1H), 1.65 (quint, *J* = 7.5 Hz, 2H), 1.32 (m, 2H), 0.90 (t, *J* = 7.4 Hz, 3H). ^{13}C NMR (150 MHz, $CDCl_3$) δ 163.3, 159.9, 159.7, 155.7, 153.7, 134.3, 131.3, 127.3, 119.9, 119.2, 117.0, 115.5, 114.8, 113.6, 112.1, 108.8, 70.7, 68.4, 59.3, 55.6, 42.5, 31.3, 19.8, 13.4. HRMS (ESI, m/z): $[M+H]^+$ Calcd. for $C_{26}H_{26}BrN_2O_5$: 525.1025; found, 525.1008.

2-Butyl-3-(4-trifluoromethylphenyl)-6-(4-bromophenyl)-2,5-dihydropyrrolo[3,4-*c*]pyrrole-1, 4-dione (S16).

4-Bromobenzonitrile (**S2**, 1.0 g, 5.5 mmol), lithium *tert*-butoxide (1.75 g, 22 mmol) and pyrrolidone **S15** (2.5 g, 5.5 mmol) in combined solvent were used to obtain **S16** as red crystals in 33 % yield, 900 mg. m.p. = 283 ˚C. ^{1}H NMR (500 MHz, $CDCl_3$) δ 9.27 (s, 1H), 8.16 (d, *J* = 8.7 Hz, 2H), 7.92 (d, *J* = 8.1 Hz, 2H), 7.82 (d, *J* = 8.4 Hz, 2H), 7.64 (d, *J* = 8.7 Hz, 2H), 3.82 (t, *J* = 7.7 Hz, 2H), 1.60 (quint, *J* = 7.6 Hz, 2H), 1.28 (m, 2H), 0.88 (t, *J* = 7.4 Hz, 3H). ^{13}C NMR (126 MHz, CDCl3) δ 162.7, 162.2, 146.2, 144.5, 132.6, 131.3, 129.2, 129.1, 129.0, 127.2, 126.1, 125.9, 125.9, 111.7, 110.0, 42.0, 31.6, 20.0, 13.6. HRMS (ESI, m/z): $[M+H]^+$ Calcd. for $C_{23}H_{17}BrF_3N_2O_2$: 489.0426; found, 489.0413.

General procedure for Buchwald-Hartwig amination of DPP derivatives S9-S11 and 1:

A mixture of appropriate DPP (1 eq.), 1-aza-18-crown-6 (2 eq.), sodium *tert*-butoxide (4 eq.) and bis(tri-*tert*-butylphosphine)palladium(0) (0.05 eq.) were placed in a dried Schenk flask under argon atmosphere followed by 10 mL dry toluene were added. The reaction mixture was stirred at 110 ˚C for 18 h. After cooling to room temperature, reaction mixture was diluted with water (100 mL) and extracted with DCM (100 mL), aqueous phase was one more time washed with DCM (50 mL). The combined organic phases were dried over Na_2SO_4, filtered and concentrated in vacuum. The crude product was purified by column chromatography over silica gel using a step gradient of MeOH in DCM as eluent (from 0% to 10%). Crystallization from DCM/hexanes allowed to obtain desired product.

2-Butyl-3-(4-methoxyphenyl)-6-(1,4,7,10,13-pentaoxa-16-azacyclooctadecane,16-(4-phenyl)-2,5-dihydropyrrolo[3,4-*c*]pyrrole-1, 4-dione (S9).

DPP (**S5**, 0.25 g, 0.55 mmol), 1-aza-18-crown-6 (**S8**, 0.29 g, 1.1 mmol), sodium *tert*-butoxide (0.21 g, 2.2 mmol), and bis(tri-*tert*-butylphosphine)palladium(0) (15 mg, 0.05 mmol) in 10 mL of dry toluene were used to obtain product **S9** as a red crystals in 23 % yield, 80 mg. m.p. = 208 ˚C. ^{1}H NMR (500 MHz, $CDCl_3$) δ 9.35 (s, 1H), 8.27 (d, *J* =7.8 Hz, 2H), 7.8 (s, 2H), 7.03 (d, *J* = 8.6 Hz, 2H), 6.80 (s, 2H), 3.87 (s, 3H), 3.73-3.65 (m, 26H), 1.63 (quint, *J* =7.3 Hz, 2H), 1.3 (m, 2H), 0.88 (t, *J* = 7.3 Hz, 3H). ^{13}C NMR (126 MHz, $CDCl_3$) δ 163.7, 162.4, 161.3, 161.2, 150.8, 145.2, 144.4, 144.3, 130.5, 130.2, 121.2, 115.3, 114.2, 111.6, 110.0, 106.5, 70.9, 70.8, 70.7, 68.5, 55.4, 51.5, 41.9, 31.7, 20.0, 13.7. HRMS (ESI, m/z): $[M+Na]^+$ Calcd. for $C_{35}H_{45}N_3O_8Na$: 658.3104; found, 658.3085.

2-Butyl-3-(4-methoxyphenyl)-6-(1,4,7,10,13-pentaoxa-16-azacyclooctadecane,16-(2-methoxyphenyl-4-yl)-2,5-dihydropyrrolo[3,4-*c*]pyrrole-1, 4-dione (S10).

DPP (**S6**, 0.25 g, 0.51 mmol), 1-aza-18-crown-6 (**S8**, 0.22 g, 1.03 mmol), sodium *tert*-butoxide (0.16 g, 2.06 mmol), and bis(tri-*tert*-butylphosphine)palladium(0) (20 mg, 0.05 mmol) in 10 mL of dry toluene were used to obtain **S10** as red crystals in 15 % yield, 50 mg. m.p. = 188 ˚C. ^{1}H NMR (500 MHz, $CDCl_3$) δ 9.46 (s, 1H), 8.17 (s, 1H), 7.79 (d, *J* =8.2 Hz, 2H), 7.7 (s, 1H), 7.05 (d, *J* = 8.6 Hz, 2H), 6.99 (s, 1H), 3.89 (s, 6H), 3.7-3.61 (m, 26H), 1.63 (quint, *J* =7.0 Hz, 2H), 1.3 (m, 2H), 0.88 (t, *J* = 7.4 Hz, 3H). ^{13}C NMR (126 MHz, $CDCl_3$) δ 163.7, 162.6, 161.5, 151.0, 145.6, 144.8, 143.7, 130.5,

121.0, 117.7, 114.3, 112.0, 110.1, 70.7, 70.2, 69.9, 69.2, 55.9, 52.6, 41.8, 31.6, 20.0, 13.7. HRMS (EI, m/z): [$M^{+\bullet}$] Calcd. for $C_{36}H_{47}N_3O_9$: 665.3312; found, 665.3304.

2-Butyl-3-(4-methoxyphenyl)-6-(1,4,7,10-tetraoxa-13-azacyclopentadecane,16-(2-methoxyphenyl-4-yl)-2,5-dihydropyrrolo[3,4-*c*]pyrrole-1, 4-dione (S11).

DPP (**S6**, 0.25 g, 5.1 mmol), 1-aza-15-crown-5 (0.23 g, 10.3 mmol), sodium *tert*-butoxide (0.2 g, 20.4 mmol), and bis(tri-*tert*-butylphosphine)palladium(0) (15 mg, 0.05 mmol) in 10 mL of dry toluene were used to obtain **S11** as red crystals in 50 % yield, 160 mg. m.p. = 210 ˚C. ^{1}H NMR (600 MHz, $CDCl_3$) δ 9.82 (s, 1H), 8.17 (s, 1H), 7.79 (s, 1H), 7.77 (d, *J* = 8.3 Hz, 2H), 7.03 (d, *J* = 8.6 Hz, 2H), 6.99 (d, *J* = 8.2 Hz, 1H), 3.92 (m, 6H), 3.89-3.80 (s, 6H), 3.73-3.64 (m, 13H), 3.2 (t, *J* = 8.9 Hz, 2H), 1.61 (quint, *J* = 7.0 Hz, 2H), 1.3 (m, 2H), 0.86 (t, *J* = 7.2 Hz, 3H). ^{13}C NMR (150 MHz, $CDCl_3$) δ 163.9, 162.5, 161.4, 150.7, 145.2, 143.6, 130.5, 130.4, 121.7, 121.1, 119.1, 117.1, 114.2, 112.0, 110.2, 107.4, 71.0, 70.4, 70.0, 69.7, 69.6, 69.1, 65.2, 55.9, 55.4, 53.5, 47.7, 41.7, 31.6, 20.0, 13.6. HRMS (ESI, m/z): $[M+Na]^+$ Calcd. for $C_{34}H_{43}N_3O_8Na$: 644.2948; found, 644.2941.

2-Butyl-3-(4-methoxyphenyl)-6-(1,4,7,10,13-Pentaoxa-16-azacyclooctadecane,16-(2-methoxyethoxyphenyl-4-yl)-2,5-dihydropyrrolo[3,4-*c*]pyrrole-1, 4-dione (1).

DPP (**S7**, 0.5 g, 0.94 mmol), 1-aza-18-crown-6 (**S8**, 0.5 g, 1.9 mmol), sodium *tert*-butoxide (0.37 g, 3.8 mmol), and bis(tri-*tert*-butylphosphine)palladium(0) (25 mg, 0.05 mmol) in 10 mL of dry toluene were used to obtain **1** as red crystals in 18 % yield, 120 mg. m.p. = 182 ˚C. ^{1}H NMR (500 MHz, $CDCl_3$) δ 8.19 (s, 1H), 7.79 (d, *J* = 8.6 Hz, 2H), 7.03 (d, *J* = 8.8 Hz, 4H), 3.82 (t, *J* =7.8 Hz, 2H), 3.68-3.59 (m, 29H), 3.38(s, 6H), 1.63 (quint, *J* =7.2 Hz, 2H), 1.3 (m, 2H), 0.88 (t, *J* = 7.2 Hz, 3H). ^{13}C NMR (126 MHz, $CDCl_3$) δ 163.7, 162.7, 161.6, 149.6, 145.3, 144.8, 130.6, 129.4, 121.7, 121.6, 120.9, 115.6, 114.5, 114.3, 114.1, 113.0, 110.2, 71.1, 70.8, 70.2, 69.6, 69.4, 69.3, 69.2, 69.1, 69.0, 68.9, 67.5, 58.9, 55.5, 52.8, 41.8, 31.6, 20.0, 13.7. HRMS (ESI, m/z): $[M+H]^+$ Calcd. for $C_{38}H_{52}N_3O_{10}$: 710.3653; found, 710.3666.

2-Butyl-3-(4-trifluoromethylphenyl)-6-(1,4,7,10,13-pentaoxa-16-azacyclooctadecane,16-(4-phenyl)-2,5-dihydropyrrolo[3,4-*c*]pyrrole-1,4-dione (S17).

DPP (**S16**, 0.1 g, 0.2 mmol), 1-aza-18-crown-6 (**S8**, 0.11 g, 0.4 mmol), sodium *tert*-butoxide (0.08 g, 0.8 mmol), and bis(tri-*tert*-butylphosphine)palladium(0) (5 mg, 0.05 mmol) in 10 mL of dry toluene were used to obtain **S17** as red crystals in 29 % yield, 50 mg. m.p. = 205 ˚C. ^{1}H NMR (500 MHz, $CDCl_3$) δ 10.05 (s, 1H), 8.32 (s, 2H), 7.92 (d, *J* =8.0 Hz, 2H), 7.75 (d, *J* = 8.5 Hz, 2H), 6.76 (d, *J* = 9.0 Hz, 2H), 3.83 (t, *J* =7.0 Hz, 2H), 3.73-3.65 (m, 24H), 1.63 (quint, *J* = 7.5 Hz, 2H), 1.3 (m, 2H), 0.88 (t, *J* = 7.5 Hz, 3H). ^{13}C NMR (126 MHz, $CDCl_3$) δ 164.3, 161.9, 151.5, 147.6, 141.0, 132.3, 131.5, 131.2, 131.1, 130.9, 130.8, 129.0, 128.9, 128.8, 125.6, 125.5, 125.0, 124.8, 122.8, 114.9, 112.4, 111.8, 111.7, 106.2, 70.8, 70.7, 68.5, 51.5, 41.9, 31.7, 20.0, 13.7. HRMS (ESI, m/z): $[M+Na]^+$ Calcd. for $C_{35}H_{42}F_3N_3O_7Na$: 696.2873; found, 696.2889.

Preparation of mitochondrial probe (2):

A suspension of unsymmetrical DPP **1** (100 mg, 0.14 mmol) and K_2CO_3 (40 mg, 0.28 mmol) in dry DMF (5 mL) was stirred at 120°C under argon atmosphere for 5 min. Then 1, 6-dibromohexane (0.22 mL, 1.4 mmol) was added and the mixture was stirred at 120 °C under argon for 24 h. Thereafter, the mixture was cooled down to room temperature and water (50 mL) was added. The product was extracted with DCM three times. The combined organic layers were dried over anhydrous Na_2SO_4, filtered and the solvent was evaporated under reduced pressure. The product was purified by column chromatography over silica gel using a step gradient of MeOH in DCM as eluent (from 0% to 10%). Compound was obtained as an orange red semi solid in 41% yield, 50 mg. HRMS (ESI, m/z): $[M+Na]^+$ Calcd.for $C_{44}H_{62}BrN_3O_{10}Na$: 894.3516; found, 894.3496.

Alkylated crude compound of **1** (50 mg, 0.06 mmol) and triphenylphosphine (0.15 g, 0.57 mmol) were added into a flask containing 5 mL of acetonitrile. The mixture was refluxed for 72 h. After removal of solvent in vacuo, the remaining solid was purified by column chromatography with gradient solvent from CH_2Cl_2 to CH_2Cl_2/MeOH (v/v = 9/1). Compound **2** was obtained as orange-red crystals by recrystallization from diethyl ether in 25% yield, 15 mg. m.p. = 94 °C. ^{1}H NMR (600 MHz, CD_3CN): δ 7.86-7.62 (m, 15H), 7.46 (dd, *J* = 6.6 Hz, 2H), 7.24 (dd, *J* = 8.4 Hz, 2H), 7.09 (d, *J* = 9.0 Hz, 1H), 6.99 (d, *J* = 8.4 Hz, 2H), 4.01 (t, *J* = 6.6 Hz, 2H), 3.85-3.40 (m, 28H), 2.81 (t, *J* = 7.8 Hz, 2H), 2.54 (t, *J* = 7.2 Hz, 2H), 1.39-1.27 (m, 19H), 0.88 (t, *J* = 6.6 Hz, 3H). ^{13}C NMR (126 MHz, $CDCl_3$) δ 173.8, 163.4, 162.9, 153.0, 148.7, 139.6, 138.2, 136.1, 135.8, 134.7, 134.6, 133.2, 132.9, 131.7, 131.2, 130.6, 125.8, 125.1, 119.8, 116.2, 115.2, 114.8, 70.5, 70.1, 65.1, 59.3, 56.3, 42.1, 36.9, 35.6, 35.2, 35.1, 34.4, 32.6, 32.1, 31.8, 31.6, 30.6, 30.5, 30.3, 30.2, 30.1, 29.9, 29.6, 29.4, 26.6, 26.3, 23.4, 22.7, 22.3, 20.5, 14.4, 13.9.; HRMS (ESI, m/z): $[M+H]^+$ Calcd. for $C_{62}H_{78}N_3O_{10}P^+$: 1055.5425; found, 1055.5405.

Ethyl-1-butyl-4-hydroxy-5-oxo-2-(4-Trifluoromethylphenyl)-2,5-dihydro-1H-pyrrole-3-carboxylate (S13).

A 250 mL round-bottom flask equipped with a magnetic stirring bar, was charged with ethanol (100 mL), 4-trifluoromethyl benzaldehyde **S12** (7.3 mL, 53 mmol) and *n*-butylamine (5.25 mL, 53 mmol), reaction mixture was kept at room temperature, with constant stirring for 15 minutes. Next diethyl oxalacetate (10.0 g, 53 mmol) was added in one portion, followed by dropwise addition of acetic acid (6.1 mL, 106 mmol). Reaction mixture was heat up to 40 °C, and vigorously stirred overnight. Then reaction mixture was cooled to room temperature and diluted with water (200 mL), and extracted with DCM (200mL×2). Organic phase was dried over anhydrous Na_2SO_4, filtered and concentrated in vacuo. Yellowish solid was recrystallized from EtOAc to obtain product **S13** as white crystals 70 %, 14.0 g. m.p. = 198-199 °C. ^{1}H NMR (600 MHz, $CDCl_3$) δ 9.02 (s, 1H), 7.61 (d, *J* = 8.2 Hz, 2H), 7.30 (d, *J* = 8.0 Hz, 2H), 5.14 (s, 1H), 4.13 (q, *J* = 7.1 Hz, 2H), 3.78 (m, 1H), 2.63 (m, 1H), 1.48 – 1.41 (m, 2H), 1.28 – 1.22 (m, 2H), 1.12 (t, *J* = 7.1 Hz, 3H), 0.86 (t, *J* = 7.4 Hz, 3H); ^{13}C NMR (151 MHz, $CDCl_3$) δ 164.8, 163.6, 157.7, 139.3, 131.2, 128.1, 125.8, 122.9, 112.4, 61.2, 60.0, 40.3, 30.3, 19.9, 13.9, 13.6. ^{19}F NMR (470 MHz, $CDCl_3$) δ -62.71. HRMS (ESI, m/z): $[M+Na]^+$ Calcd. for $C_{18}H_{20}F_3NO_4Na$: 394.3562; found, 394.3520.

Ethyl-1-butyl-4-hydroxy-2-(4-Trifluoromethylphenyl)-5-oxopyrrolidine-3-carboxylate (S14).

Compound **S13** (14.0 g, 37.7 mmol) was dissolved in 150 mL mixture of EtOH/AcOH (1:1) and zinc powder (15.0 g, 226.2 mmol) was added and reaction mixture vigorously stirred at 95 °C for 1h. A second portion of zinc powder (15.0 g, 226.2 mmol) was added and stirring was continued at 95 °C until completion of the reaction. After cooling to room temperature reaction mixture was diluted with EtOAc (100 mL) the excess of zinc and the inorganic salts were filtered off. The filtrate was then diluted with water (150 mL). The aqueous layer was extracted with EtOAc (100 mL), and the combined organic phases were washed with saturated $NaHCO_3$ solution until neutral and finally dried over Na_2SO_4, filtered and concentrated in vacuo to obtain liquid product **S14** as mixture of diastereoisomers in 85% yield, 11.9 g. Careful analysis of ^{1}H NMR spectra of crude **S14** showed the ratio 2:1 of major isomer **S14** with the all-trans configuration in relation to the rest three minor compounds.

Crude compound (11.9 g, 31.9 mmol) was dissolved in dry EtOH (75 mL), freshly powdered K_2CO_3 (11.2 g, 68.5 mmol) was added in one portion. Reaction mixture was stirred at room temperature for 30 minutes. Next reaction mixture was diluted with EtOAc (100 mL) the excess of inorganic salts were filtered off. The filtrate was then washed with water (100 mL x 2), organic phase was dried over Na_2SO_4, filtered and concentrated in vacuum to obtain yellowish liquid product in 99.5 %, 11.8 g. ^{1}H NMR spectra showed 10:1 ratio of major isomer **S14a** with the all-trans configuration in relation to the rest two minor compounds. ^{1}H NMR (500 MHz, $CDCl_3$) δ 7.63 (d, *J* = 8.0 Hz, 2H), 7.44 (d, *J* = 8.0 Hz, 2H), 4.75 (d, *J* = 7.5 Hz, 1H), 4.65 (d, *J* = 8.0 Hz, 1H), 4.15 (m, 2H), 3.7-3.65 (m, 1H), 3.03 (t, *J* = 8.5 Hz, 1H), 2.45 (quint, *J* = 7.5 Hz, 1H), 1.32-1.11 (m, 8H), 0.79 (t, *J* = 7.5 Hz, 3H); ^{13}C NMR (126 MHz, $CDCl_3$) δ 173.6, 171.1, 142.3, 131.1, 129.4, 129.0, 126.1, 125.3, 72.1, 61.6, 55.9, 40.6, 28.5, 19.9, 13.9, 13.6. HRMS (EI, m/z): [$M^{+\bullet}$] Calcd. for $C_{18}H_{22}F_3NO_4$: 373.3722; found, 373.1507.

Ethyl-1-butyl-2-(4-trifluoromethylphenyl)-5-oxo-4-((trimethylsilyl)oxy)pyrrolidine-3-carboxylate (S15).

To cooled to ~0 °C solution of **S14a** (11.8 g, 31.6 mmol) in dry DCM (100 mL), dry Et_3N (8.0 mL, 56.8 mmol) was added, next TMSCl (6.0 mL, 47.4 mmol) was added drop wise. After addition cooling bath was removed, and reaction mixture was allowed to reach room temperature and stirring was continued at room temperature for 1.5 h. Next reaction mixture was diluted with water (100 mL), phases were separated and organic phase was dried over anhydrous Na_2SO_4, filtered and concentrated in vacuo gives 90% yield, 12.8 g of product **S15** without chromatographic purification. ^{1}H NMR spectra showed 10:1 ratio of major isomer **S15** with the all-trans configuration in relation to the rest two minor compounds, used for next reaction without further purification. ^{1}H NMR (500 MHz, $CDCl_3$) δ 7.63 (d, *J* = 8.0 Hz, 2H), 7.40 (d, *J* = 8.0 Hz, 2H), 4.70 (d, *J* = 7.5 Hz, 1H), 4.56 (d, *J* = 8.0 Hz, 1H), 4.16 (m, 2H), 3.69-3.63 (m, 1H), 2.91 (t, *J*

= 7.5 Hz, 1H), 2.52 (m, 1H), 1.39 – 1.31 (m, 4H), 1.24-1.17 (m, 3H), 0.81 (t, *J* = 11.5 Hz, 3H), 0.21 (s, 9H). ^{13}C NMR (101 MHz, $CDCl_3$) δ 171.6, 171.1, 142.5, 131.0, 130.7, 129.3, 127.7, 125.9, 73.1, 61.5, 60.5, 56.6, 45.7, 40.6, 28.6, 19.8, 14.0, 13.6, 0.1. HRMS (EI m/z): [$M^{+\bullet}$] Calcd. for $C_{21}H_{30}F_3NO_4Si$: 445.5542; found, 445.5510.

Section S4: Photophysical studies

The photophysical properties of DPPs **S7**, **S9-S11** and **S17** were studied in toluene and MeCN as prototypical non-polar and polar solvents (Table S1, Figures in ESI). From a structural point of view these DPPs represent D-A-D' systems where the azacrownphenyl is a strongly electron-donating group, the 4-$MeOC_6H_4$ is a weakly electron-donating substituent, and the DPP core is electron-deficient. DPPs **S7**, **S9-S11** and **S17** absorb at approx. 530 nm and emit at 540-580 nm in toluene. There is a small but noticeable hypsochromic shift of absorption in CH_3CN as compared to toluene (506-525 nm). Simultaneously emission shifts bathochromically to ~580 nm. Replacing $MeOC_6H_4$ with 4-$CF_3C_6H_4$ effectively increases the strength of the acceptor in the donor-acceptor system, by going from a quadrupolar-like D-A-D' structure to a dipolar like D-A-A' architecture. This should lead to a bathochromic shift of absorption and emission which is indeed observed experimentally (**S17** vs. **S9**: abs. 540 nm vs. 530 nm, em. 578 nm vs. 555 nm in toluene, Table S1). Solvatochromic trends are the same as for DPPs **S9**-**S11**. Interestingly, adding a triphenylphosphonium moiety strongly affects the photophysical properties shifting absorption hypsochromically and emission bathochromically to 590 nm. At the same time, the emission maxima does not show any solvent polarity effects (Table S1).

In all cases the fluorescence quantum yields are very high (80-90%) and the difference between toluene and CH_3CN is trifling in spite of the nature of the considered transitions. This observation is in strong contrast to solvatochromic behavior of 6-(3,5-bis(trifluoromethyl)phenyl)-2-butyl-3-(4-(dimethylamino)phenyl)-2,5-dihydropyrrolo[3,4-*c*]pyrrole-1,4-dione which showed very bright emission in toluene that almost totally quenched in CH_3CN.

Table 1. Photophysical properties of DPPs in toluene and CH_3CN.

Compound	solvent	$^{max}\lambda_{abs}$ [nm]	$^{max}\lambda_{ems}$ [nm]	Stokes shift [cm^{-1}]	Φ_{fl}[a]
S7	toluene	508	540	1200	0.77
	CH_3CN	498	538	1400	0.66
S9	toluene	529	555	900	0.78
	CH_3CN	525	563	1300	0.87
S10	toluene	528	566	1300	0.88
	CH_3CN	506	581	2500	0.84
S11	toluene	531	564	1100	0.85
	CH_3CN	519	582	2100	0.86
1	toluene	530	569	1300	0.77
	CH_3CN	514	583	2300	0.81
S17	toluene	540	578	1200	0.88
	CH_3CN	530	599	2200	0.87
2	toluene	519	592	2400	0.80
	CH_3CN	499	591	3100	0.48

[a]Determined using Rhodamine 6G in EtOH.

Table S2. Changes of fluorescence of DPPs **S7**, **S9-S11** and **S17** in the presence of 5 eq. KPF_6 and $PhSO_3H$ in CH_3CN.

DPP	KPF_6 (5 eq.)		$PhSO_3H$ (5 eq.)	
	Enhancement of fluorescence	λ_{em} (nm)	Enhancement of fluorescence	λ_{em} (nm)
S7	1.02	536	1.01	537
S9	0.99	564	0.55	550
S10	0.80	536	0.83	550
S11	0.96	582/536	0.65	551
S17	1.02	596	0.49	536

Having the fundamental photophysical properties measured, we moved on to investigation of the influence of both K^+ cations and protonation on the absorption and emission of DPPs **S7**, **S9-S11** and **S17** (Table S2). The influence of KPF_6 addition on the fluorescence of these DPPs strongly depends on the presence of the additional alkoxy substituents. In their absence (DPPs **S9** and **S17**) there is essentially no effect even in the presence of a huge excess of KPF_6 (Fig. S9 & S34). In contrast, for DPP **S10** which bears MeO substituent that assist coordination, the effect is spectacular and the addition of just one equivalent of K^+ shifts emission hypsochromically from 580 to 525 nm (Fig. 3). Decreasing the size of macrocycle to 15-crown-5 (DPP **S11**, too small to accommodate K^+) makes the response a very weak one, and hundreds of equivalents of KPF_6 are necessary to induce comparable changes (Fig. 4). The addition of benzenesulfonic acid yields the same trend, however, there is no difference in strength of the bathochromic shift between

DPPs bearing differently sized crowns (Figs. S3, S5, S10, S13, S16, S19, S21, S26, S30, S33, S35, S38, S40). The presence of auxiliary alkoxy groups does not help in obtaining a more marked response to benzenesulfonic acid either.

Section S5: Absorption and emission spectra

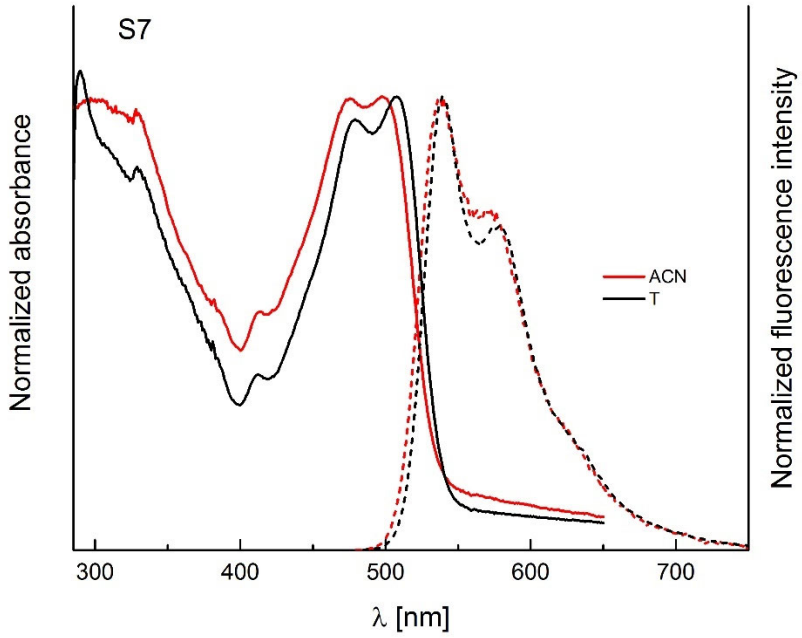

Fig. S1. The absorption and emission spectra of DPP **S7** in acetonitrile and in toluene.

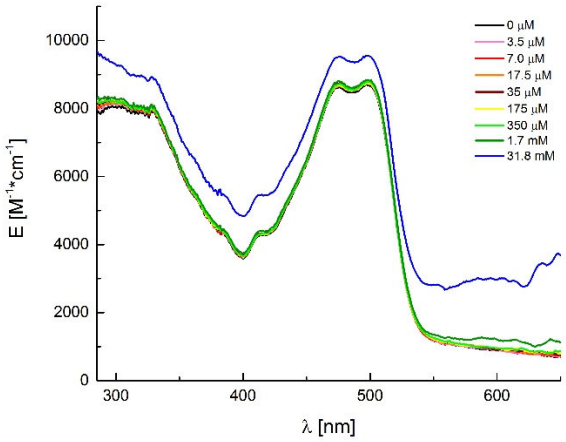

Fig. S2. The effect of KPF_6 addition on the absorption spectra of DPP **S7** measured in CH_3CN.

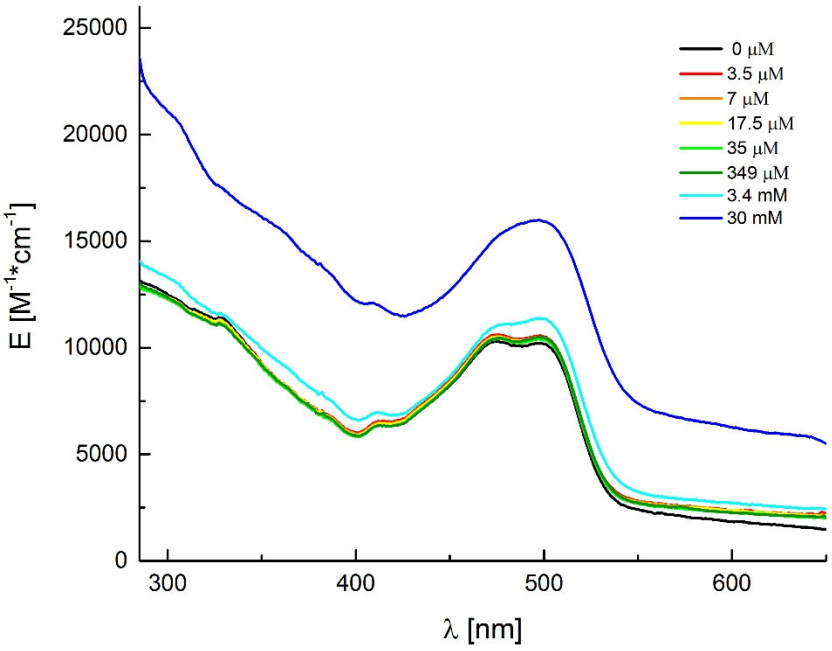

Fig. S3. The effect of BENZENESULFONIC ACID addition on the absorption spectra of DPP **S7** measured in CH_3CN.

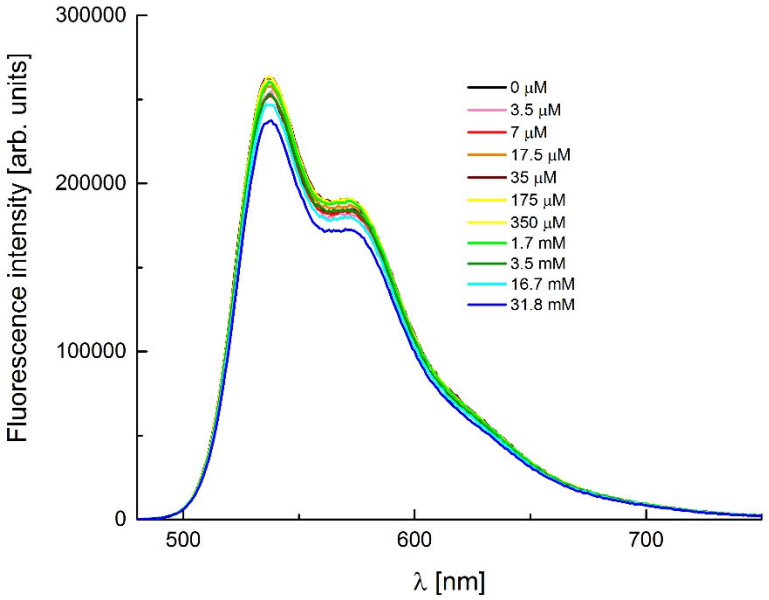

Fig. S4. The effect of KPF_6 addition on the emission spectra of DPP **S7** measured in CH_3CN.

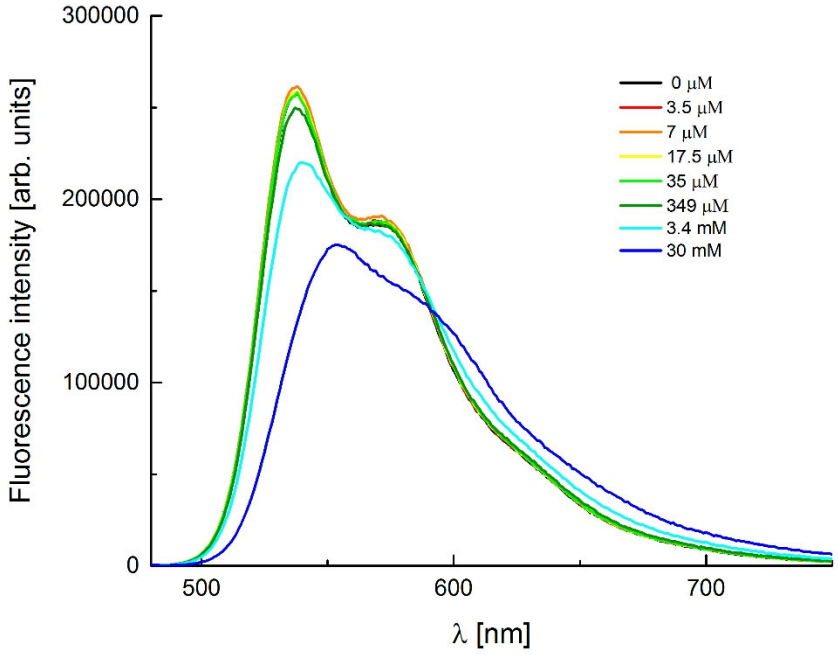

Fig. S5. The effect of BENZENESULFONIC ACID addition on the emission spectra of DPP **S7** measured in CH_3CN.

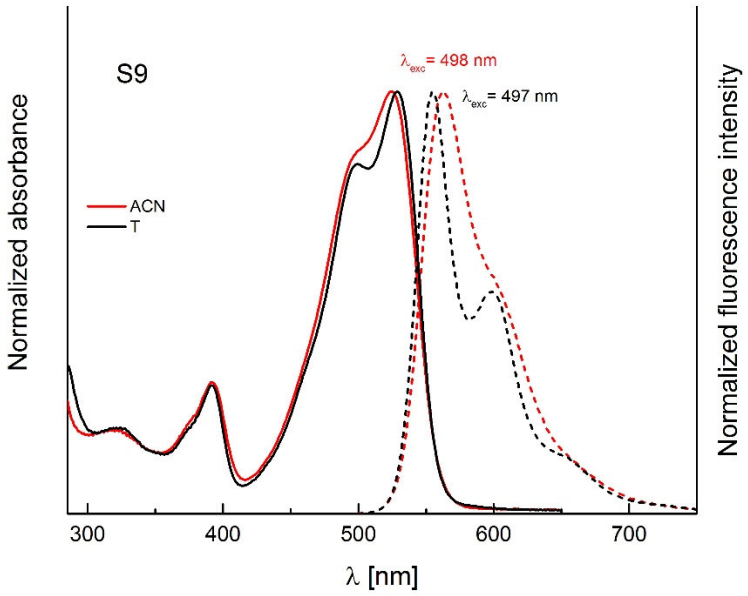

Fig. S6. The absorption and emission spectra of DPP **S9** in acetonitrile and in toluene.

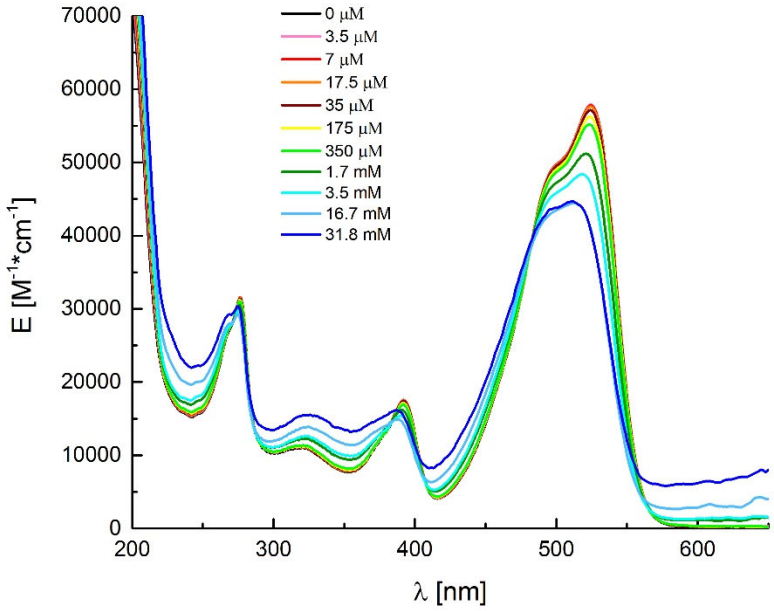

Fig. S7. The effect of KPF_6 addition on the absorption spectra of DPP **S9** measured in CH_3CN.

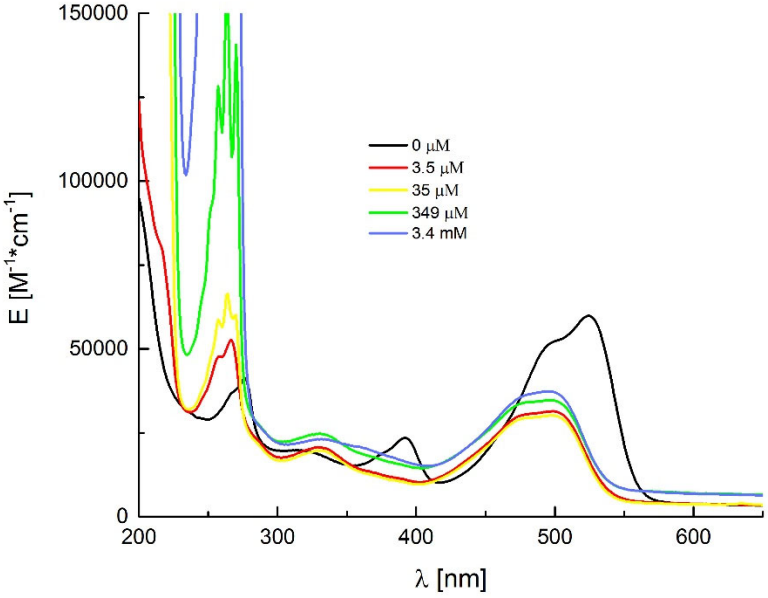

Fig. S8. The effect of BENZENESULFONIC ACID addition on the absorption spectra of DPP **S9** measured in CH_3CN.

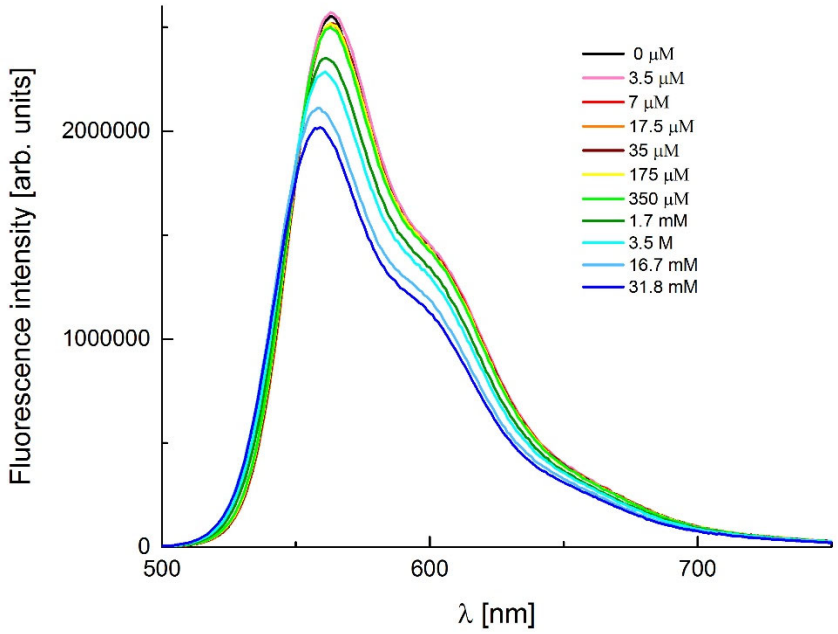

Fig. S9. The effect of KPF_6 addition on the emission spectra of DPP **S9** measured in CH_3CN.

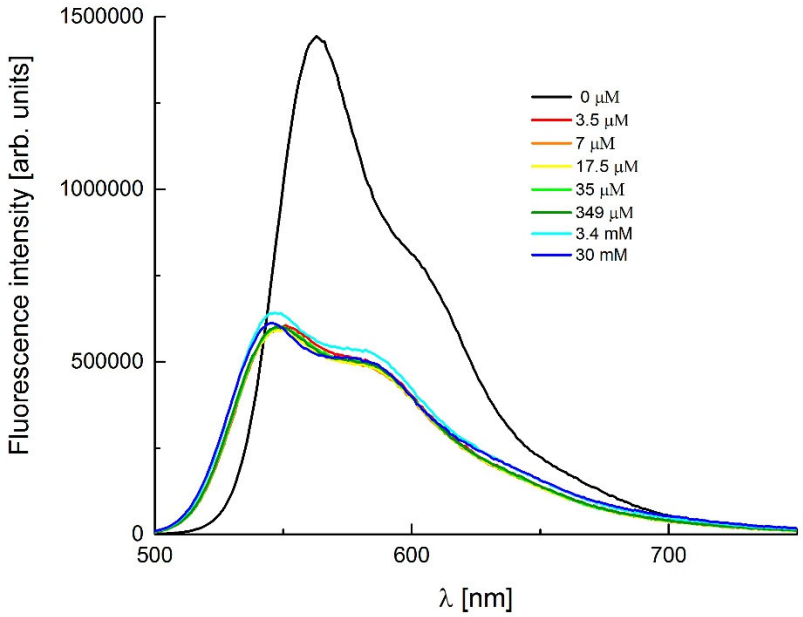

Fig. S10. The effect of BENZENESULFONIC ACID addition on the emission spectra of DPP **S9** measured in CH_3CN.

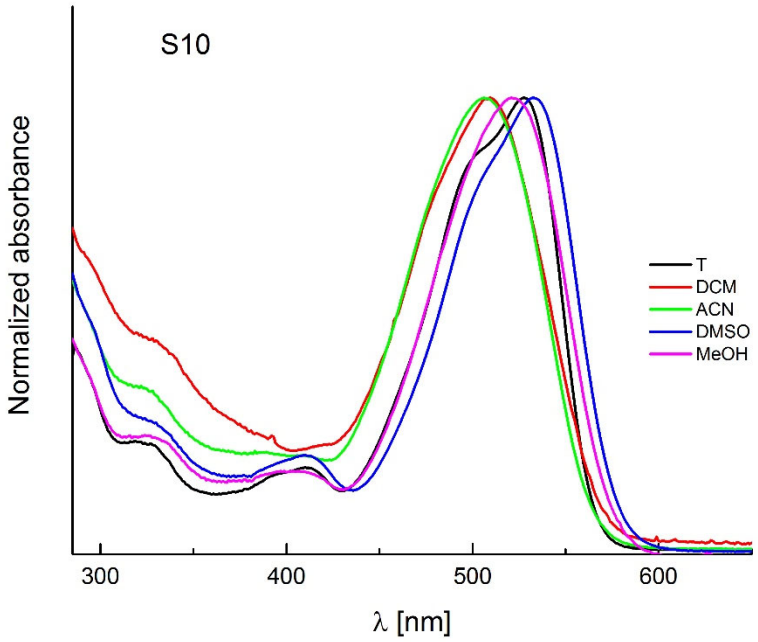

Fig. S11. The absorption and emission spectra of DPP **S10** in various solvents.

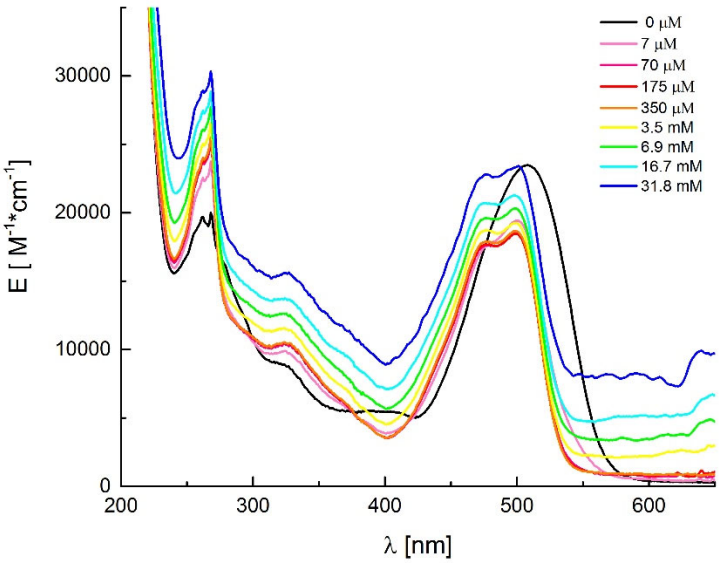

Fig. S12. The effect of KPF_6 addition on the absorption spectra of DPP **S10** measured in CH_3CN.

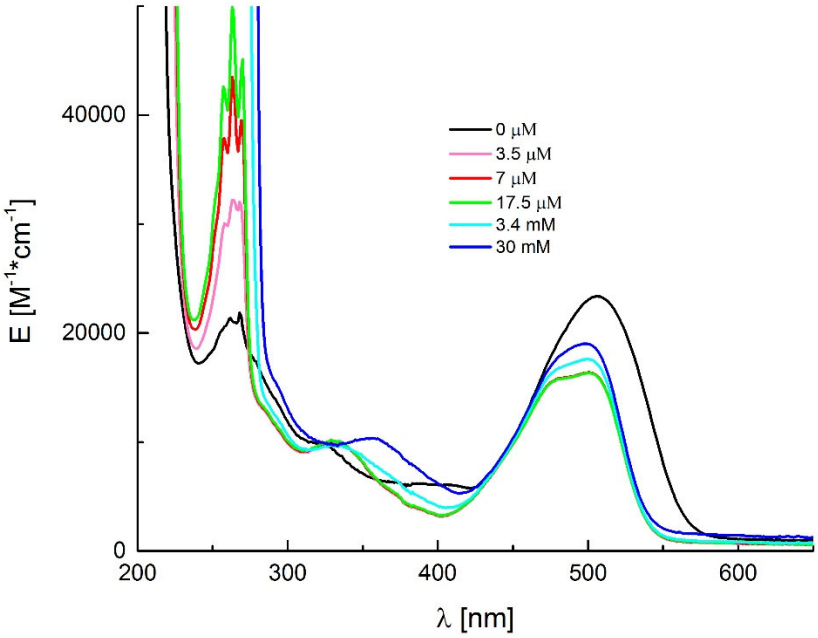

Fig. S13. The effect of BENZENESULFONIC ACID addition on the absorption spectra of DPP **S10** measured in CH_3CN.

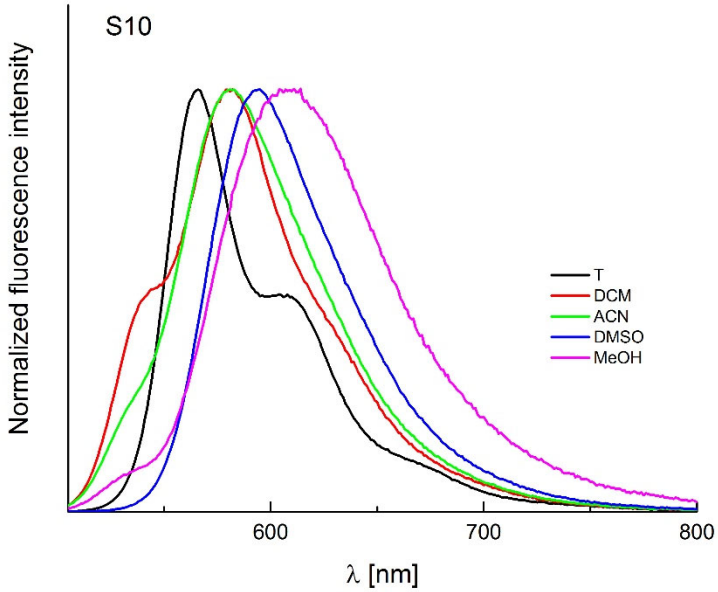

Fig. S14. The emission spectra of DPP **S10** in various solvents.

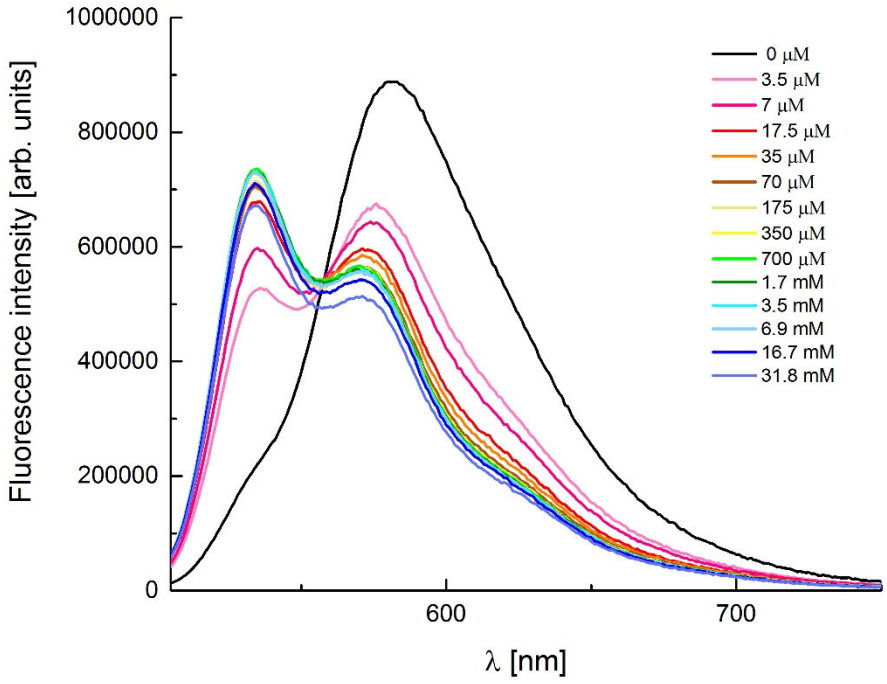

Fig. S15. The effect of KPF_6 addition on the emission spectra of DPP **S10** measured in CH_3CN.

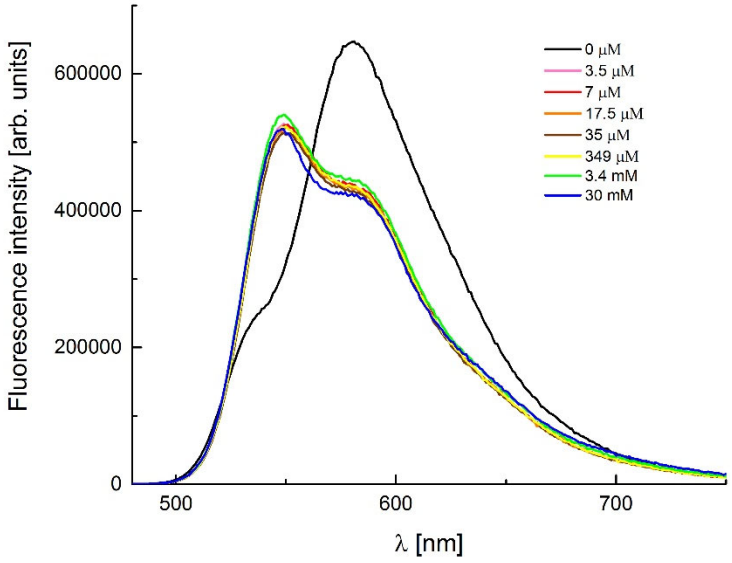

Fig. S16. The effect of BENZENESULFONIC ACID addition on the emission spectra of DPP **S10** measured in CH_3CN.

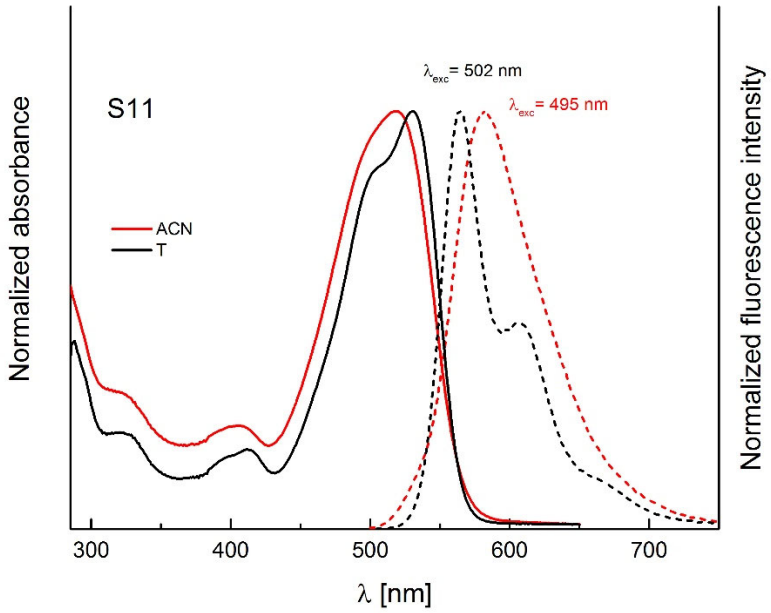

Fig. S17. The absorption and emission spectra of DPP **S11** in acetonitrile and in toluene.

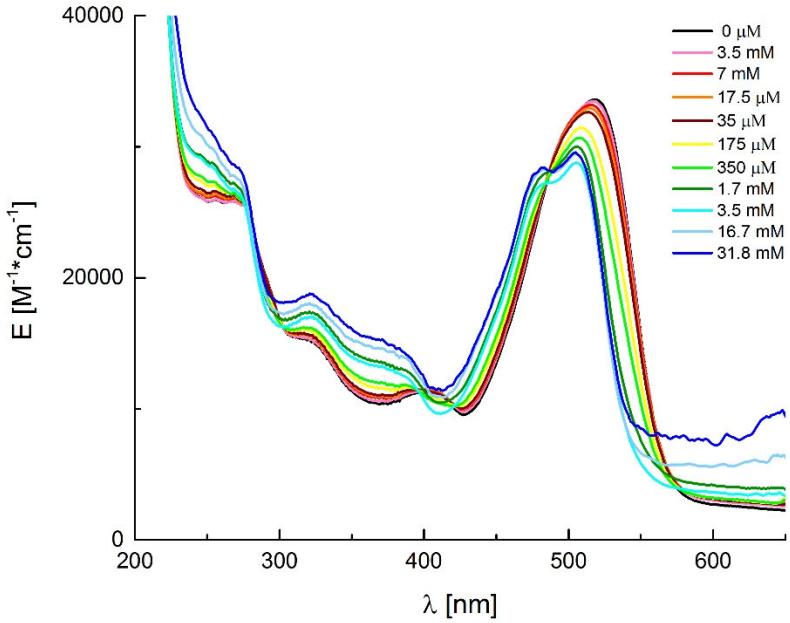

Fig. S18. The effect of KPF_6 addition on the absorption spectra of DPP **S11** measured in CH_3CN.

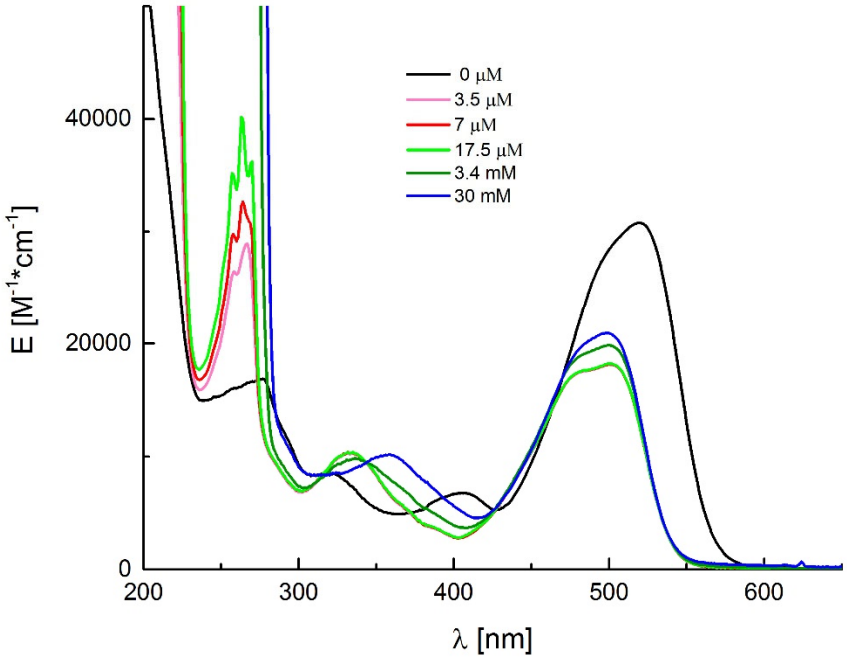

Fig. S19. The effect of BENZENESULFONIC ACID addition on the absorption spectra of DPP **S11** measured in CH_3CN.

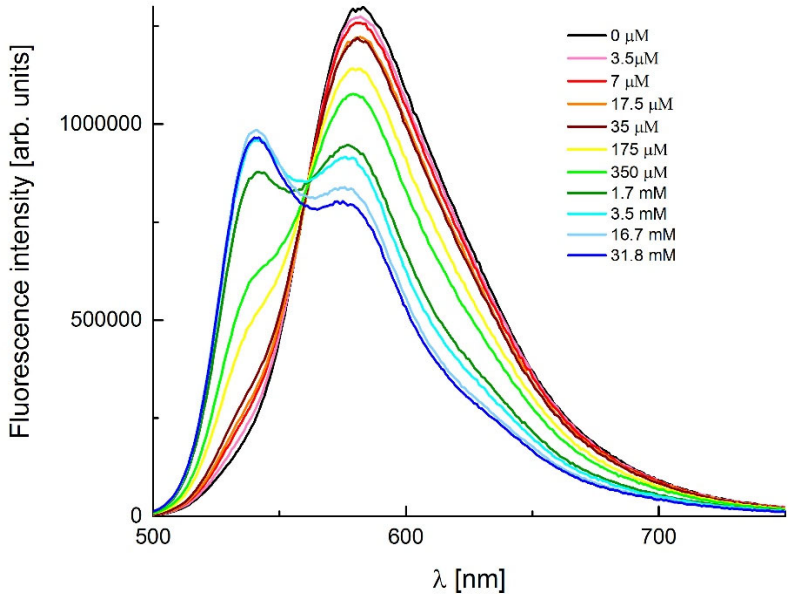

Fig. S20. The effect of KPF_6 addition on the emission spectra of DPP **S11** measured in CH_3CN.

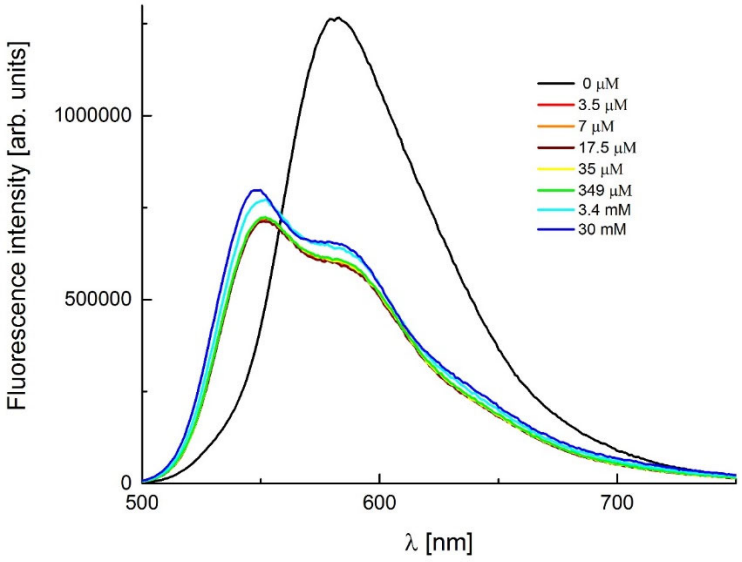

Fig. S21. The effect of BENZENESULFONIC ACID addition on the emission spectra of DPP **S11** measured in CH_3CN.

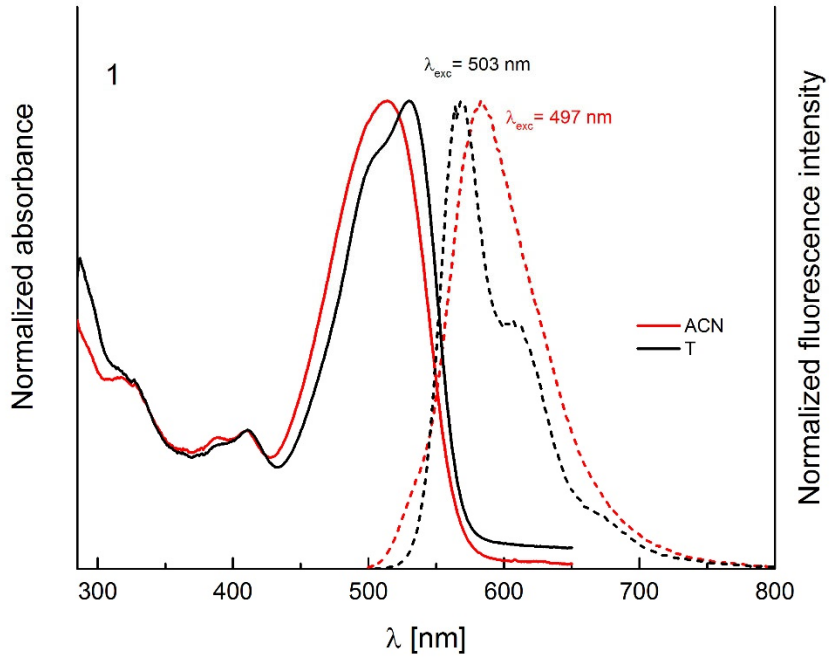

Fig. S22. The absorption and emission spectra of DPP **1** in acetonitrile and in toluene.

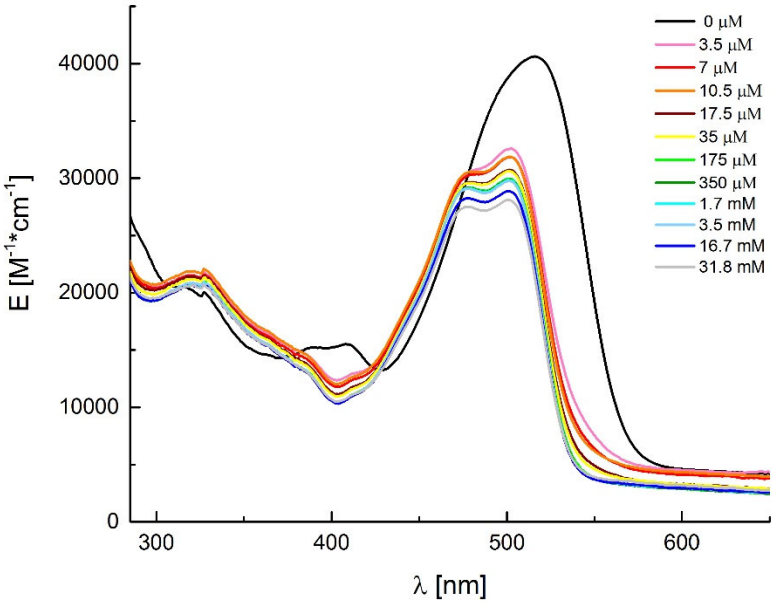

Fig. S23. The effect of KPF_6 addition on the absorption spectra of DPP **1** measured in CH_3CN.

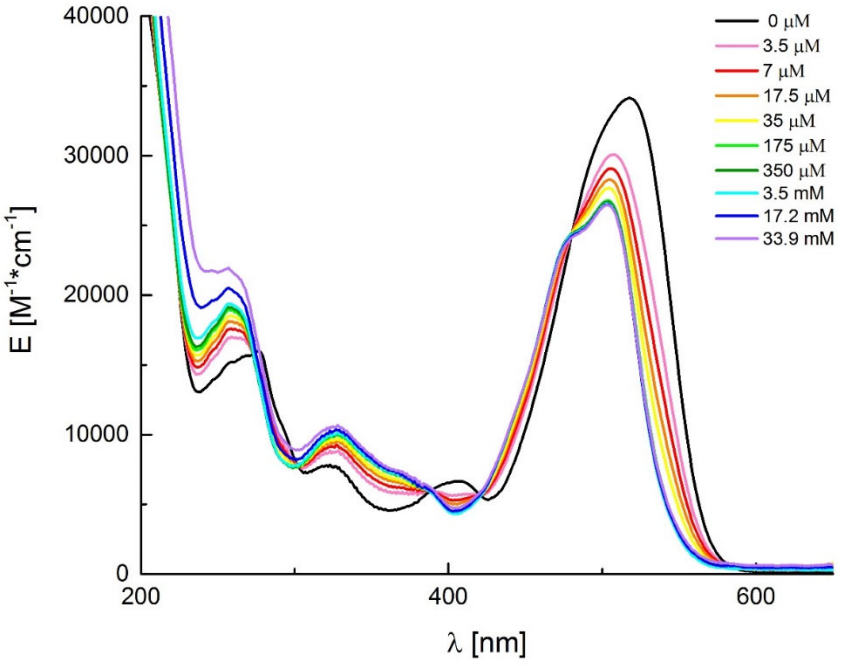

Fig. S24. The effect of sodium perchlorate addition on the absorption spectra of DPP **1** measured in CH_3CN.

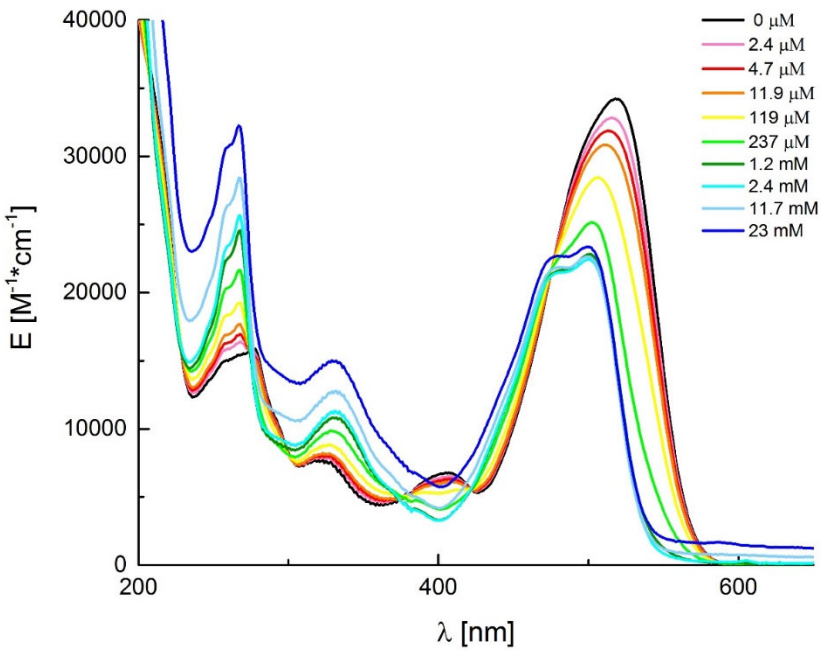

Fig. S25. The effect of magnesium perchlorate addition on the absorption spectra of DPP **1** measured in CH_3CN.

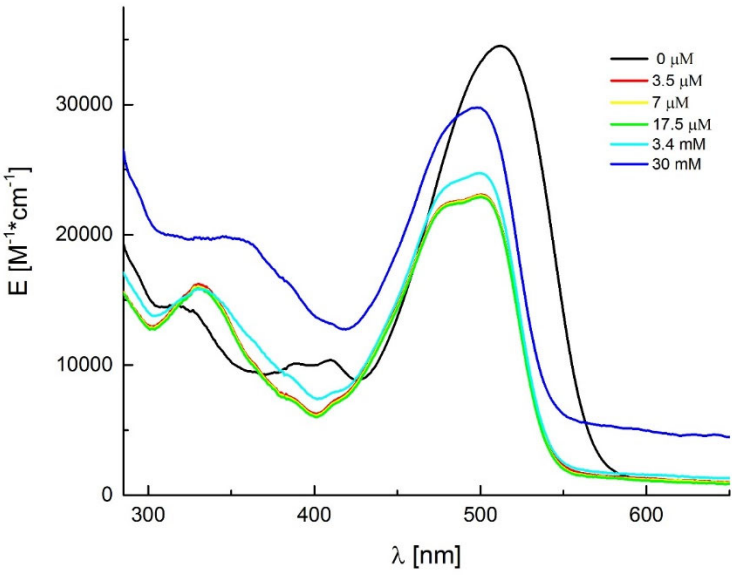

Fig. S26. The effect of benzenesulfonic acid addition on the absorption spectra of DPP **1** measured in CH_3CN.

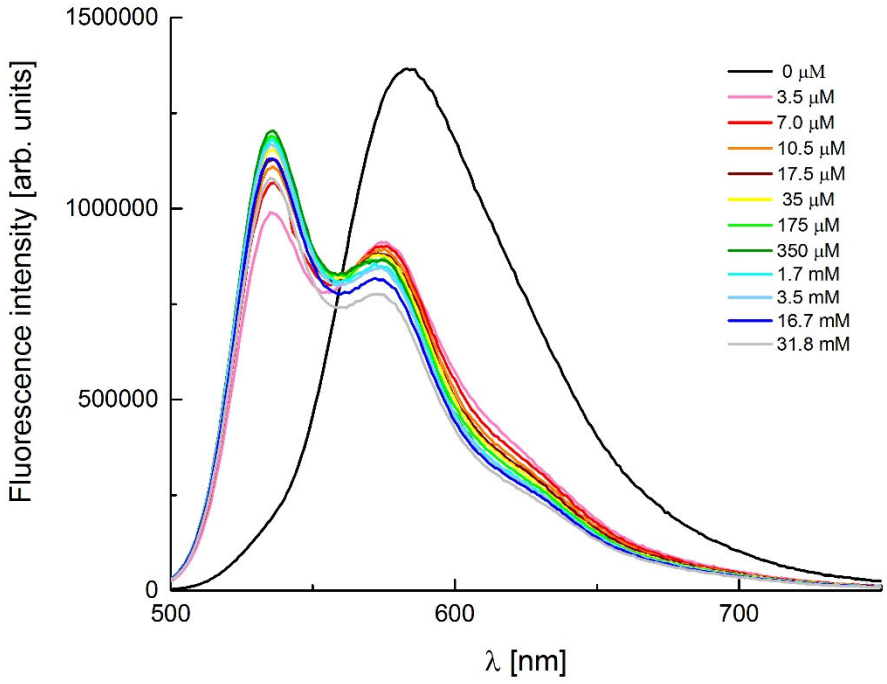

Fig. S27. The effect of KPF_6 addition on the emission spectra of DPP **1** measured in CH_3CN.

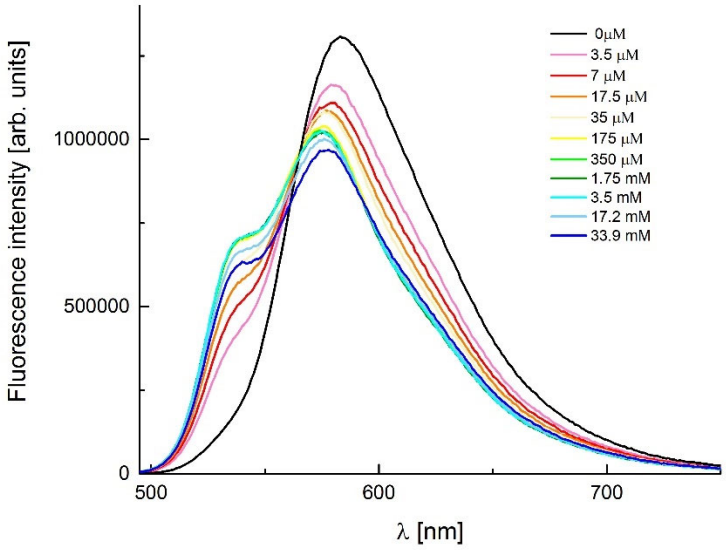

Fig. S28. The effect of sodium perchlorate addition on the emission spectra of DPP **1** measured in CH_3CN.

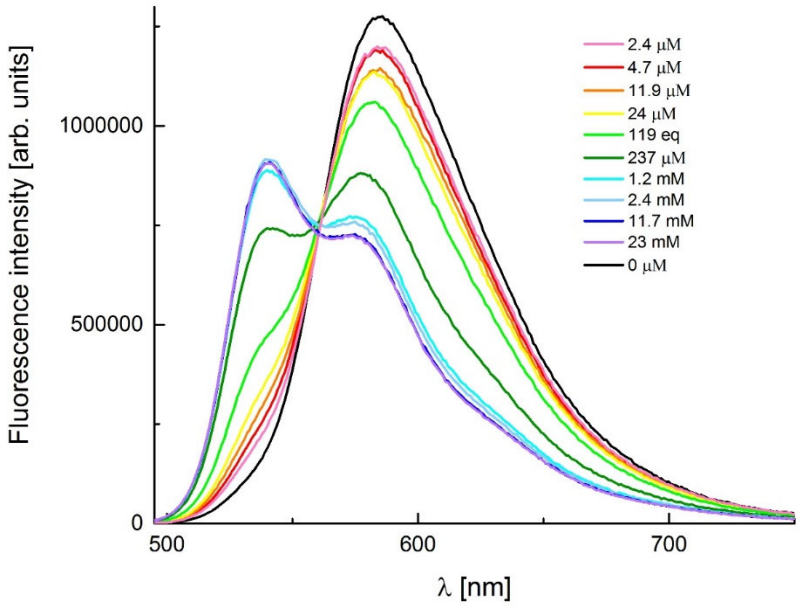

Fig. S29. The effect of magnesium perchlorate addition on the emission spectra of DPP **1** measured in CH_3CN.

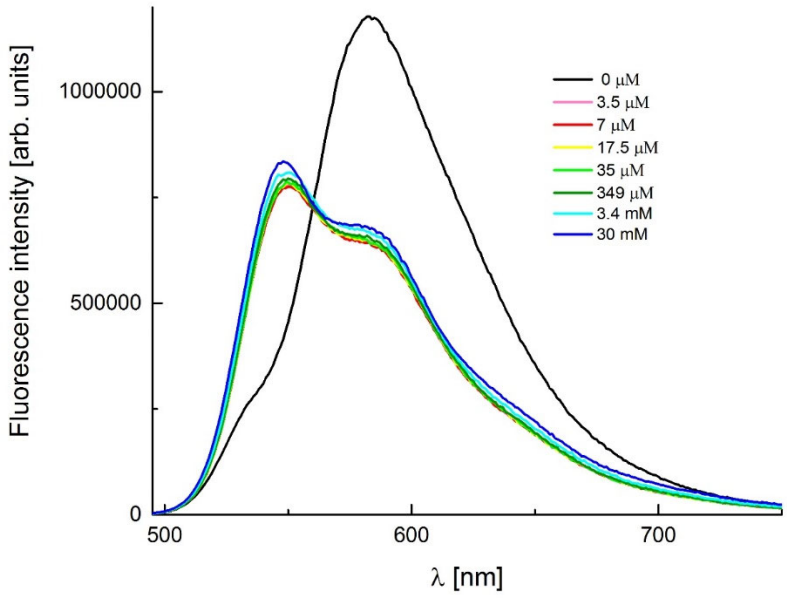

Fig. S30. The effect of BENZENESULFONIC ACID addition on the emission spectra of DPP **1** measured in CH_3CN.

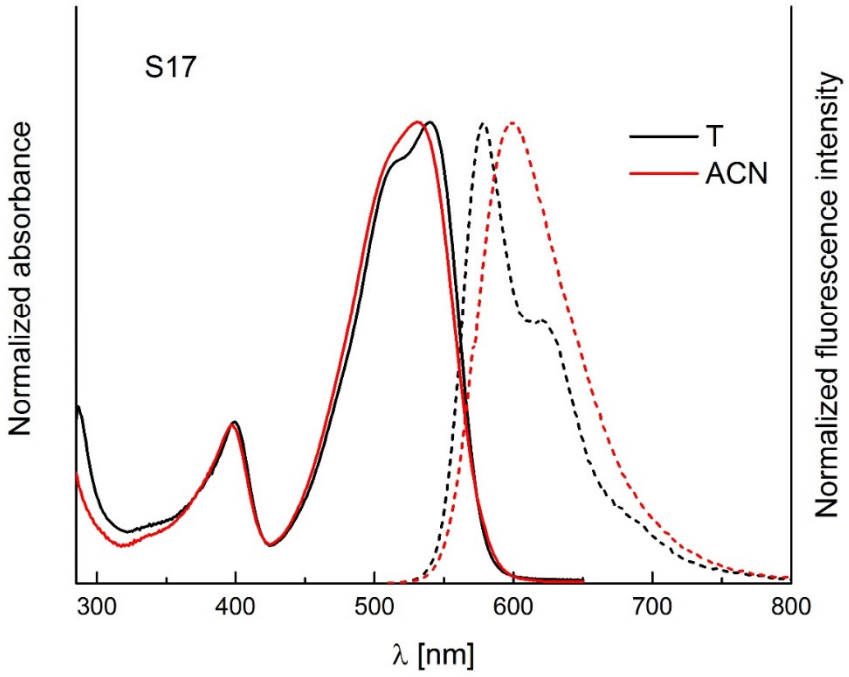

Fig. S31. The absorption and emission spectra of DPP **S17** in acetonitrile and in toluene.

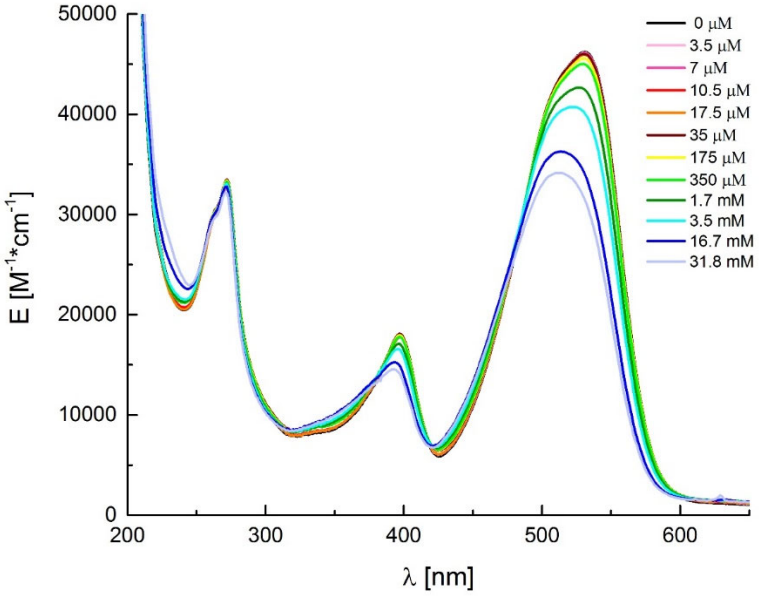

Fig. S32. The effect of KPF_6 addition on the absorption spectra of DPP **S17** measured in CH_3CN.

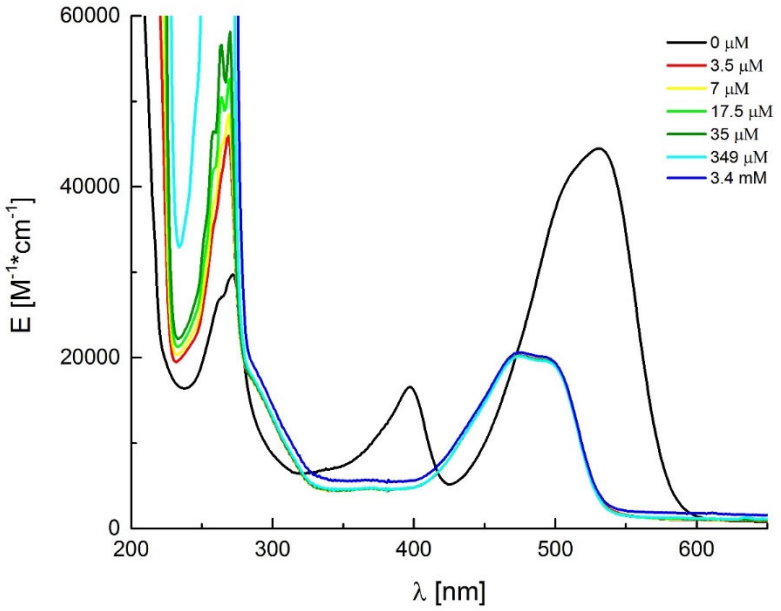

Fig. S33. The effect of BENZENESULFONIC ACID addition on the absorption spectra of DPP **S17** measured in CH_3CN.

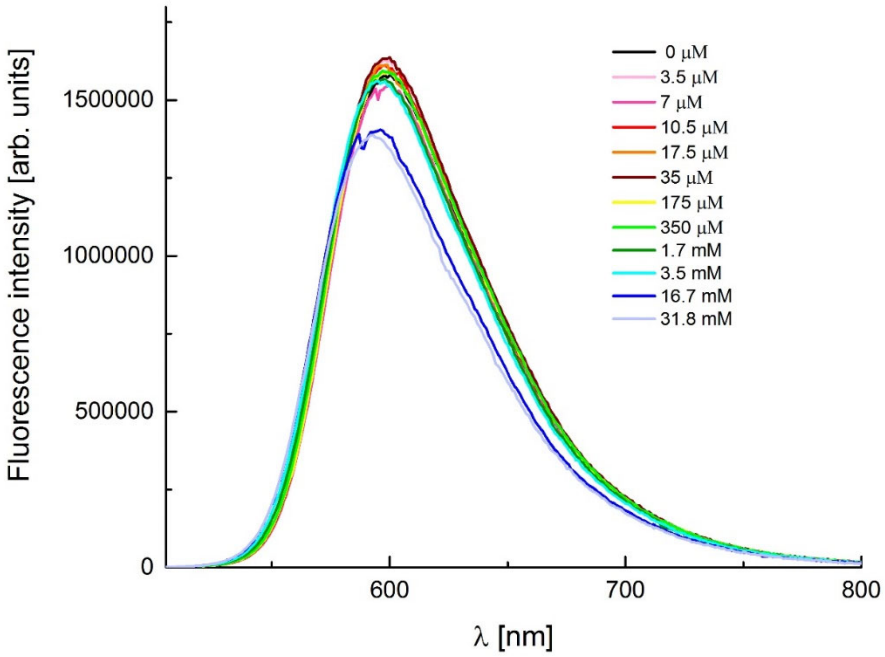

Fig. S34. The effect of KPF_6 addition on the emission spectra of DPP **S17** measured in CH_3CN.

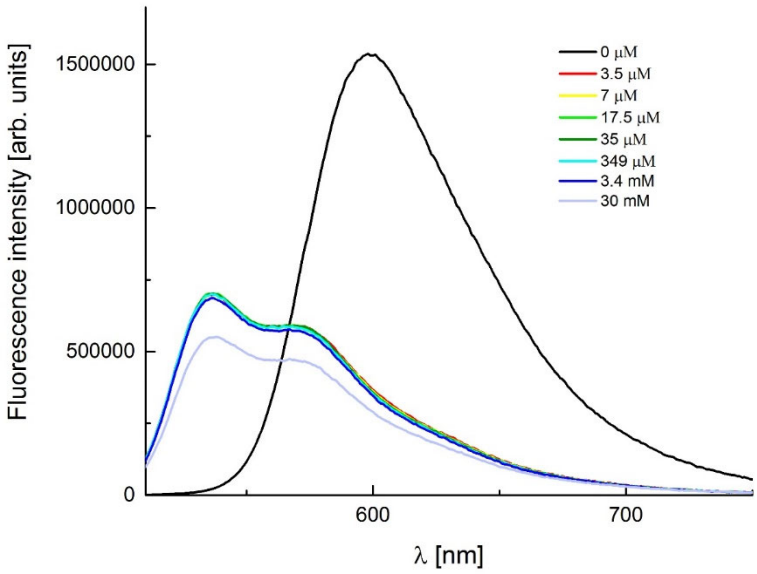

Fig. S35. The effect of BENZENESULFONIC ACID addition on the emission spectra of DPP **S17** measured in CH_3CN.

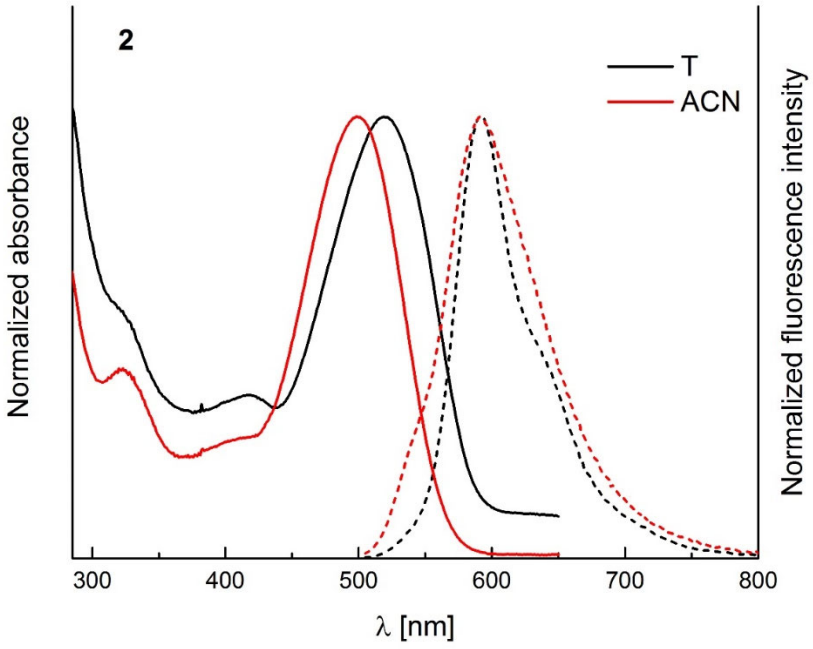

Fig. S36. The absorption and emission spectra of DPP **2** in acetonitrile and in toluene.

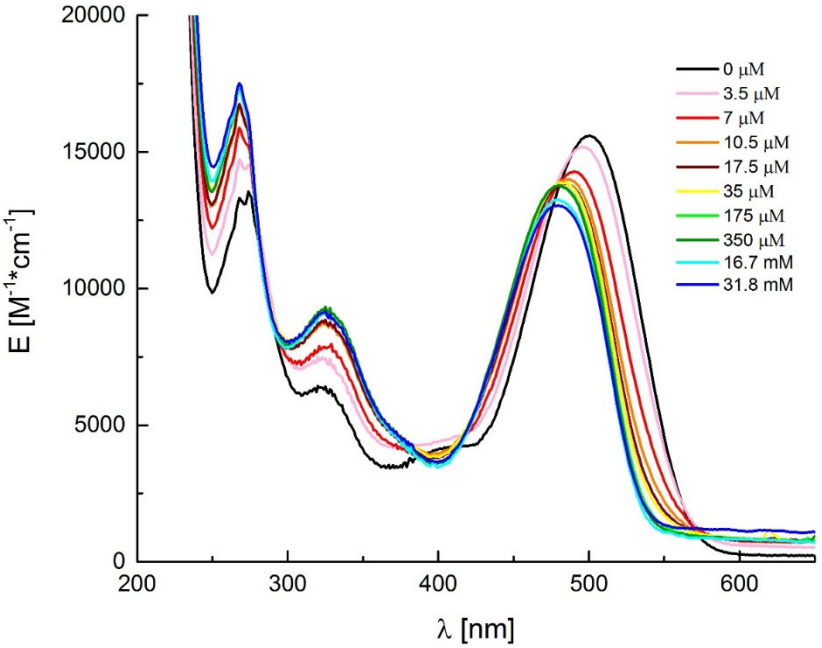

Fig. S37. The effect of KPF_6 addition on the absorption spectra of DPP **2** measured in CH_3CN.

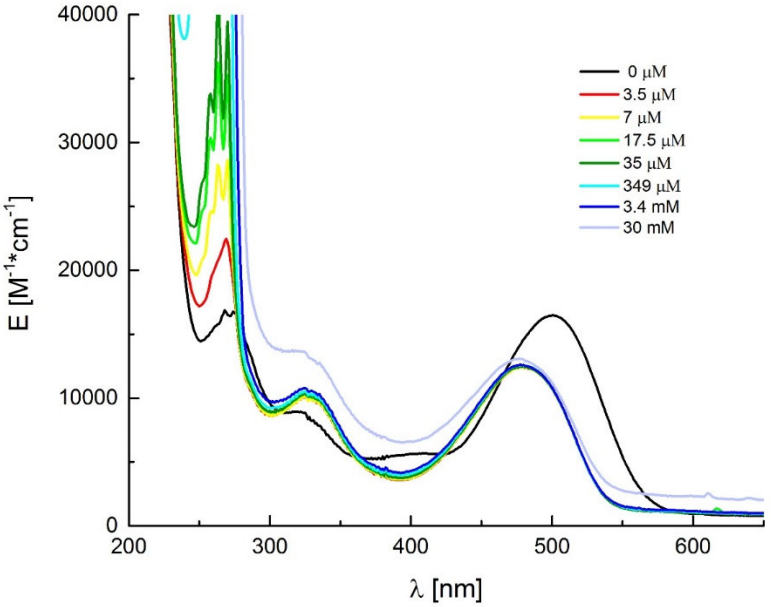

Fig. S38. The effect of BENZENESULFONIC ACID addition on the absorption spectra of DPP **2** measured in CH_3CN.

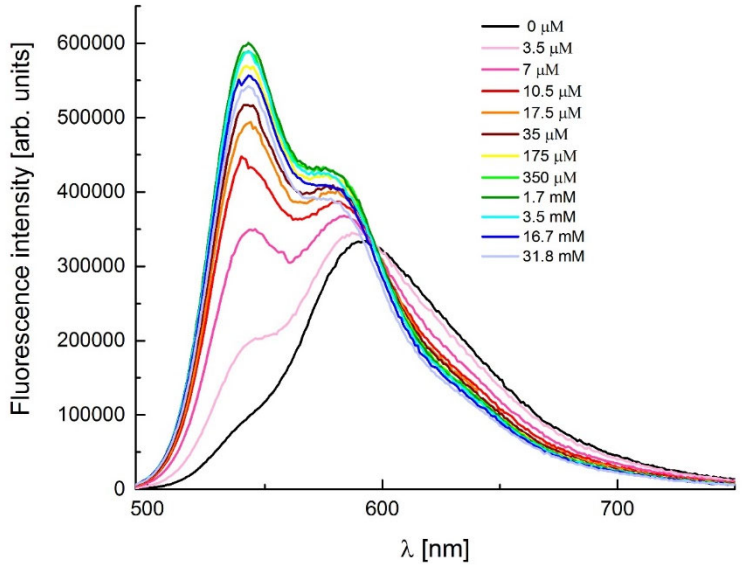

Fig. S39. The effect of KPF_6 addition on the emission spectra of DPP **2** measured in CH_3CN.

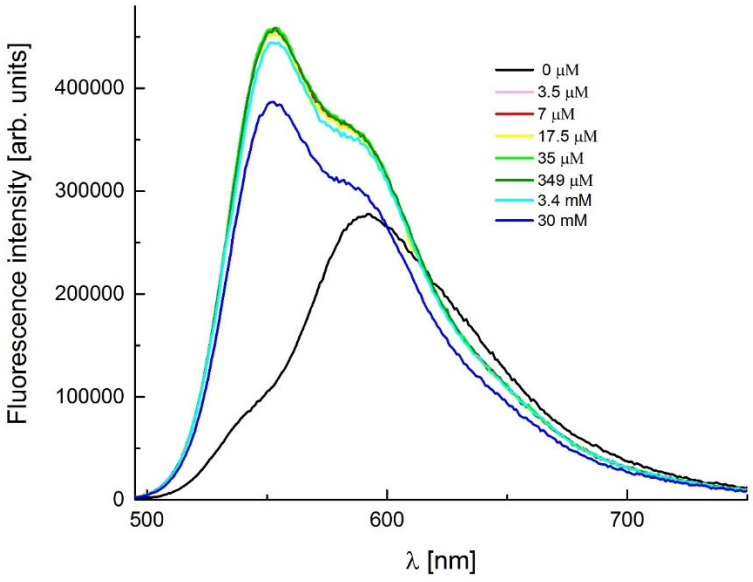

Fig. S40. The effect of BENZENESULFONIC ACID addition on the emission spectra of DPP **2** measured in CH_3CN.

Photostability measurements

Photostability of DPP **2** was determined through the variation in absorption of each sample at the appropriate absorption maximum wavelength (λ_{abs}) with respect to irradiation time. Toluene was selected as the solvent. Concentrations giving similar optical densities (A ≈ 1) were used. Quartz cells of samples were irradiated with a 300 W Xe lamp (Asahi spectra MAX-350, light power: 0.115 W/cm^2) for 180 min at 25 °C equipped with a UV/vis mirror module through a glass fiber. The absorption spectra were measured at appropriate times during the irradiation. BODIPY (difluoro{2-[1-(3,5-dimethyl-2*H*-pyrrol-2-ylidene-*N*)ethyl]-3,5-dimethyl-1*H*-pyrrolato-*N*}boron), DPP (2,5-dimethyl-3,6-bis(3,4-dimethoxyphenyl)pyrrolo[3,4-*c*]pyrrole-1,4(2*H*,5*H*)-dione) and Alexa Fluor 555 were used as references.

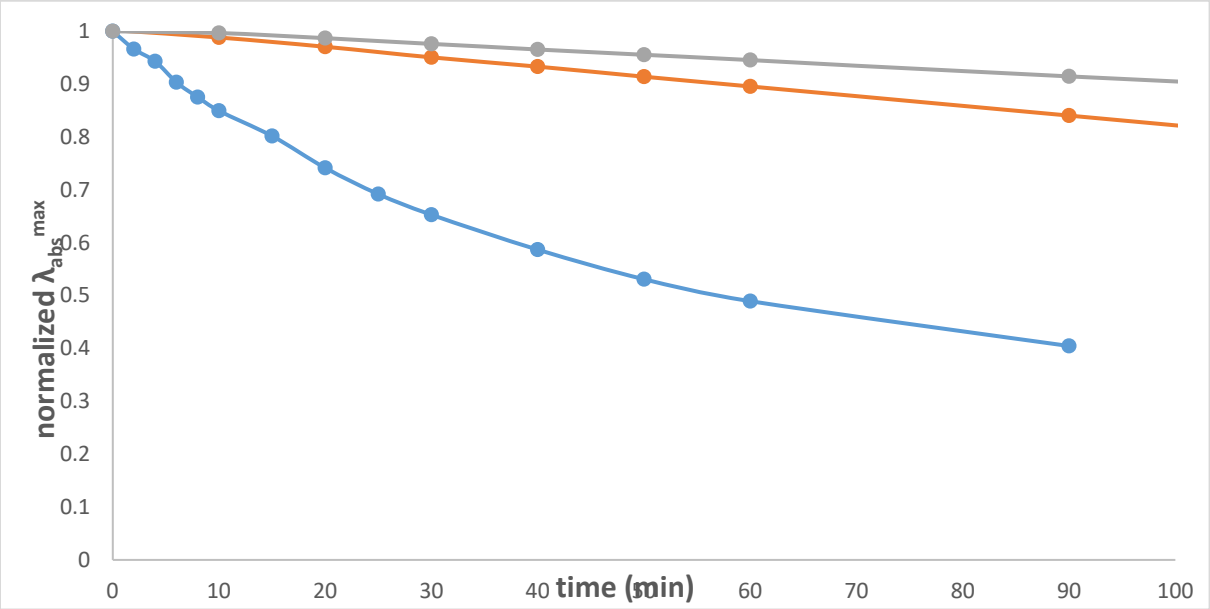

Fig. S41. Photostability of DPP **2** measured in CH_3CN (DPP **2** – blue line, BODIPY 493/503 – gray line, DPP (2,5-dioctyl-3,6-bis(3,4,5-trimethoxyphenyl)pyrrolo[3,4-c]pyrrole-1,4(2H,5H)-dione – orange line).

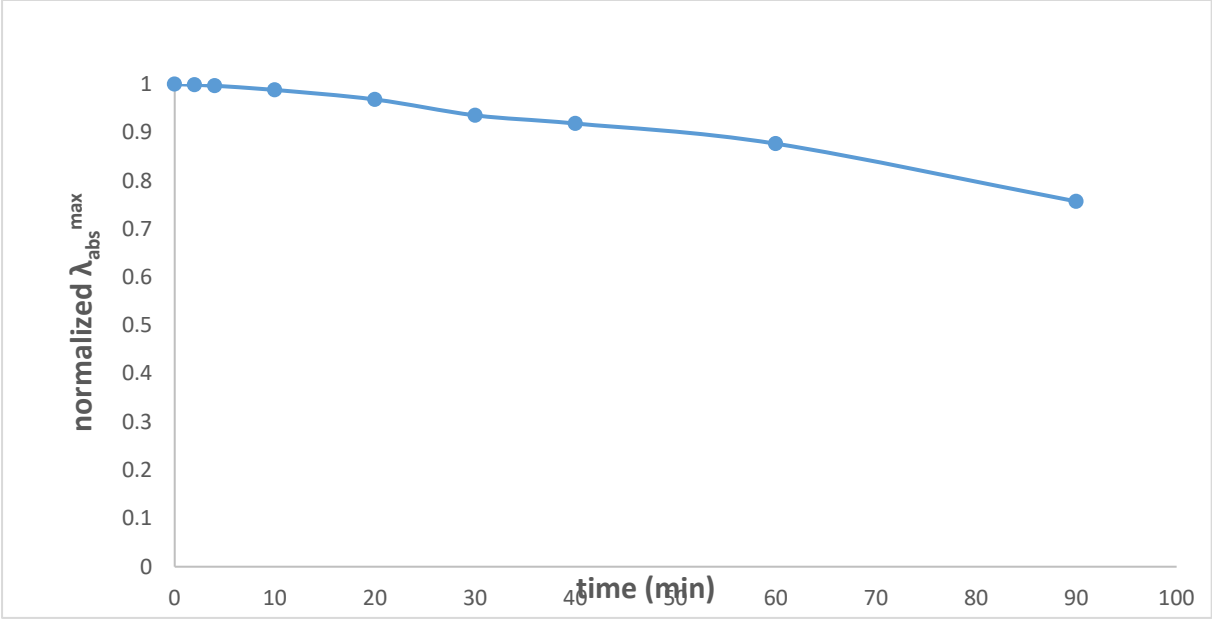

Fig. S42. Photostability of DPP **2** measured in water (containing 10% of DMSO).

Section S6: IMAGING

Cell culture conditions. The rat embryonic cardiomyoblast-derived H9C2 and endothelial EA.hy 926 cell lines were cultured at 37 ˚C in a humidified atmosphere containing 5% CO_2 in DMEM supplemented with 10% foetal bovine serum, 2 mM glutamine, 100 U/ml penicillin, and 100 µg/ml streptomycin.

Fluorescence localization of crown-diketopyrrolopyrroles within the cells. The cardiac H9C2 cells were loaded with fluorophores in DMEM medium supplemented with 10% foetal bovine serum, 2 mM glutamine, 100 U/ml penicillin, and 100 µg/ml streptomycin at 37 ˚C in a humidified atmosphere containing 5% CO_2 for 15 to 30 minutes with the crown-diketopyrrolopyrroles compounds at the final concentration ranging from 200 to 500 nM. The final concentration of the MitoTracker™ Green FM was 150 nM. Both fluorophores were dissolved in DMSO. Before measurements, the incubation medium was replaced with FluoroBrite™ DMEM. The measurements were performed with use of Olympus IX83 confocal microscope with the water objective 60x UPLSAPO 60XW. Registered data were transferred to the ImageJ and analyzed for presentation.

The research was carried out on "live" unfixed cells. The given run of the experiment, the control, the administration of valinomycin and naringenin, and the change of the incubation medium to 200 mM KCl were performed on the same cells. The research was carried out on "live" unfixed cells. The given run of the experiment, the control, the administration of valinomycin and

naringenin, and the change of the incubation medium to 200 mM KCl were performed on the same Petri dish.

H9C2 cells, which had been incubated for 30 minutes with DPP **2** at 37°C at 5% CO_2, were washed with incubation medium (FloroBrite) and measurements were made under control conditions Fig A. Then valinomycin and nigericin were added to the control medium to a final concentration of 30 µM and 10 uM respectively and after 5 min of incubation the measurements were performed for 5 mM KCl conditions. After that, the incubation medium was changed to a medium containing 200 mM KCl with appropriate concentrations of valinomycin and nigericin. And the fluorescence intensity was measured for 200 mM KCl conditions. Measurements performed only in the presence of valinomycin transport only potassium ions, which in the case of the cell membrane would do the job. However, in the case of mitochondria, the process is more complicated. Administration of valinomycin alone would change only the electrical potential ΔΨ of the inner mitochondrial membrane which would lead to activation of the respiratory chain and an increase in pH. The addition of nigericin reduces the transmembrane ΔpH (Kang, Chen et al. 2017).

Kang, P. T., C. L. Chen, P. Lin, W. M. Chilian and Y. R. Chen (2017). "Impairment of pH gradient and membrane potential mediates redox dysfunction in the mitochondria of the post-ischemic heart." Basic Res Cardiol 112(4): 36.

The number of cells used for the measurement is usually 100,000 if we take into account their volume (assuming that they are a sphere) $4/3\pi r^3$ (radius of the cell 50 µm) then compared to the volume of 2 ml of incubation medium, if the concentration on both sides of the biological membrane is equalized, the concentration will be close to the value of 5 mM as it is in incubation medium.

mean from both samples	B3-A	YG2-A	B3-A/YG2-A
Probe	5,77E+05	1,57E+05	3,81E+00
Probe_valinomycin_nigeri	4,44E+05	1,72E+05	2,56E+00
Probe_valinomycin_nigeri	6,14E+05	1,09E+05	5,65E+00
Control	18052	4170	4,32901679
Pearson r (B3 vs YG2):	-0,82		

In response to this comment the measurements were performed using a flow cytometer and the results confirmed those obtained for the confocal microscopy measurements. Only the extreme values of potassium ions were used to define the limit of changes in the value of the fluorescence intensity ratio for green and red colors. Further studies with potassium titration are planned, but require a separate approach to demonstrate the biological usefulness of a given fluorescent probe.

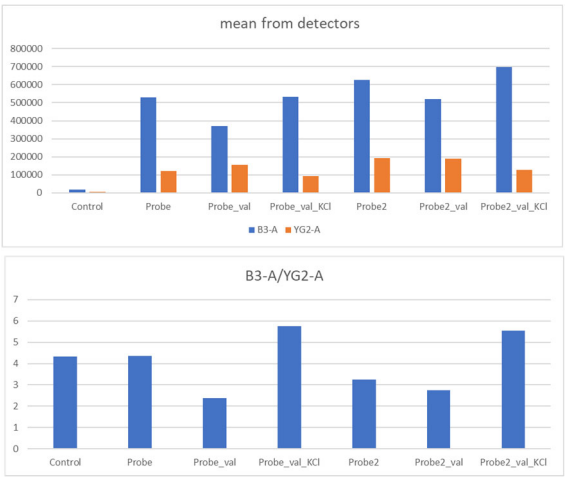

Figure 43. Measurements made using flow cytometry for different KCl concentrations. Probe_val is for valinomycin and nigericin. Data from two experiments.

In order to determine the viability of cells under the influence of the tested crown-diketopyrrolopyrroles, an annexin V-based apoptosis and necrosis test (RealTime-Glo ™ Annexin V Apoptosis and Necrosis Assay, Promega) was performed, allowing the simultaneous examination of the effect of the substances on the induction of apoptotic and necrotic cell death.

Section S7: Confocal fluorescence microscopy images

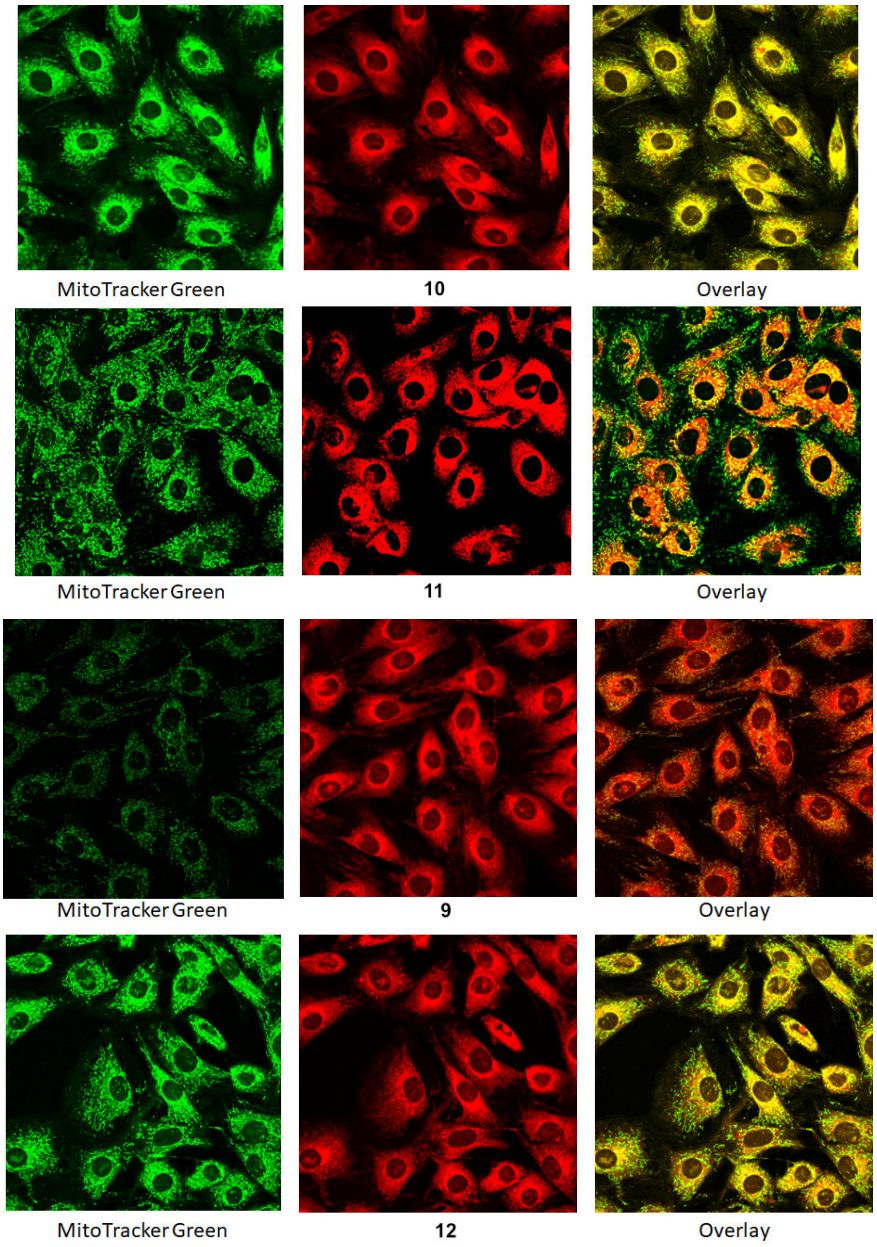

Fig. S44. Intracellular localization of **S10, S11, S9** and **1** compounds as detected using confocal fluorescence microscopy.

The fluorescence of MitoTracker™ Green (green) as a well-established marker for mitochondria, and the fluorescence of the **S10**, **S11**, **S9** and **S12** (red) compounds were recorded with 559 nm excitation wavelength and emission range 610–750 nm. Overlay picture recorded simultaneously for two fluorophore in living H9C2 cells line.

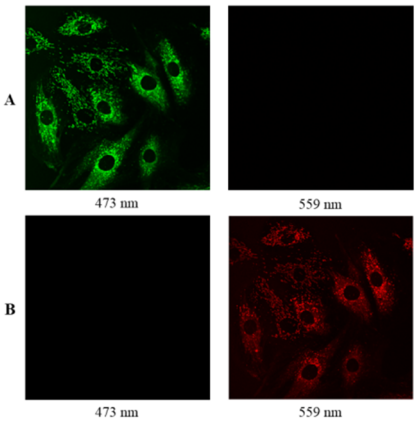

Fig. S45. Separation of the fluorescence emission wavelength with excitation with laser line 473 nm (A) and 559 nm (B). Detection channels were set for fluorescence green and red light respectively.

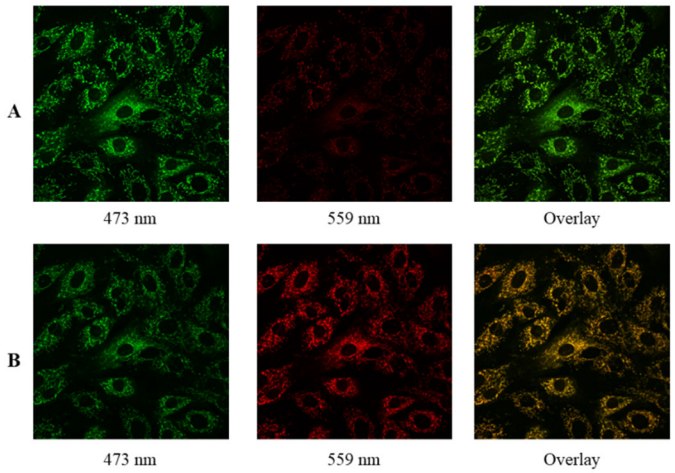

Fig. S46. Changes in the fluorescence of the **2** compound in the different intracellular K^+ concentration caused by nigericin. A control condition. B in the presence of nigericin (10 µM).

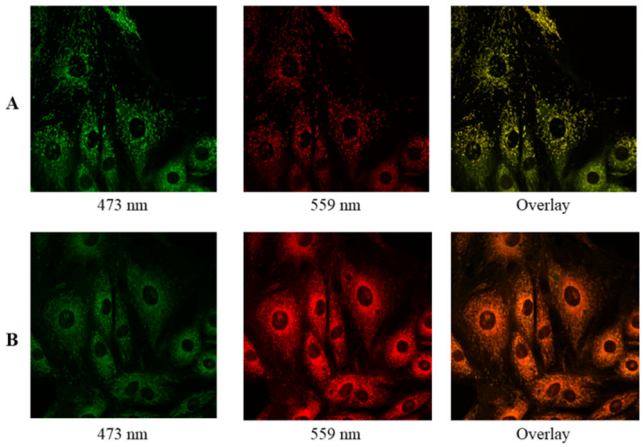

Fig. S47. Changes in the fluorescence of the **2** compound in the different intracellular K^+ concentration caused by valinomycin. A control condition. B in the presence of valinomycin (30 μM).

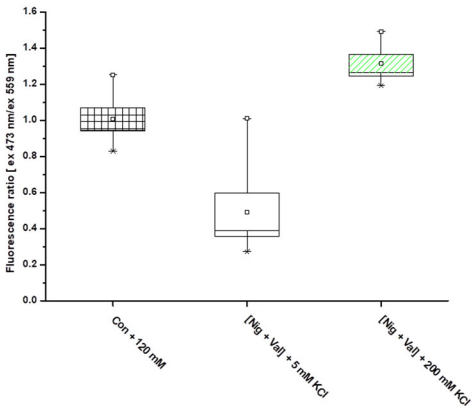

Fig. S48. Changes in the ratio (473 nm/559 nm) of the fluorescence intensity at the different excitation wavelength as measured with use of ImageJ. The ratio is statistically different for each conditions as measured in paired sample t Test at the level 0.05.

Penetration into the cell depends on a number of factors and under our conditions, after many trials, we decided to load the cells with the dye in the presence of Pluronic 127 detergent and FBS in the incubation medium. This is due to the fact that research on living cells is taken into account and the dye entering the cell accumulates in the inner mitochondrial membrane and

mitochondria. Too rapid accumulation could damage the performance of the mitochondrial activity system and produce undesirable results. It turned out that the penetration of the dye into the cell without FBS in the environment is extremely fast, but it is easier to control the charge level of the cell in the presence of FBS by changing the time of loading. In our opinion, it is more important to obtain a stable dye balance. In the ratiometric measurements of fluorescence the level of dyes loading is less important.

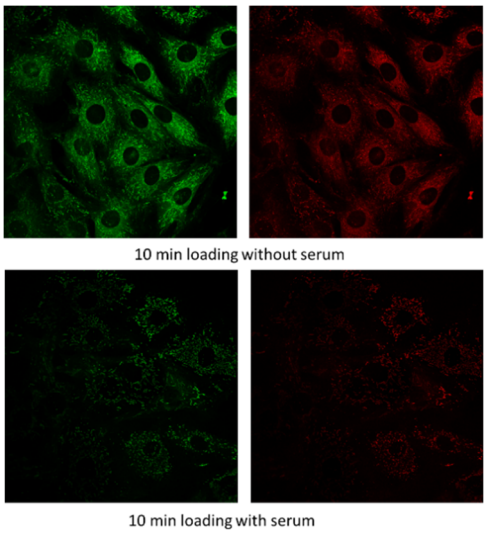

Figure 49. Different level loading of dye **6** in the presence and absence of serum.

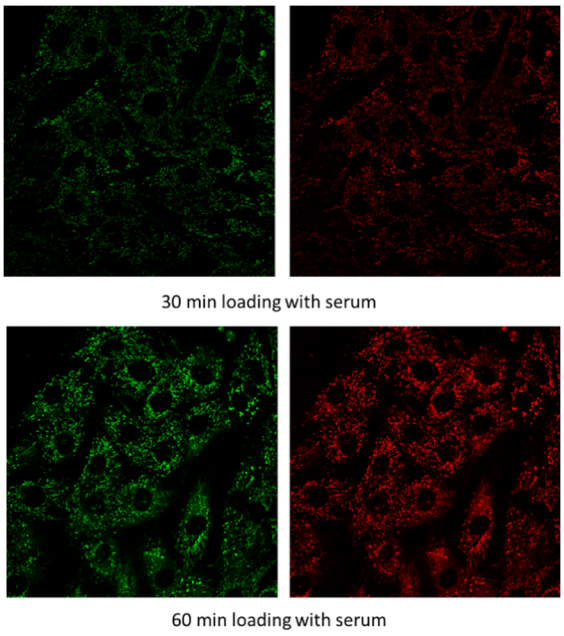

Figure 50. Different time loading of dye **6** in the presence of serum in incubation medium.

Pearson's correlation coefficient and Mander's overlap coefficient (MOC).

For pair of two signal channels Mitotracker Green and DPP **1** Pearson's Coefficient: r=0.597, Manders' Coefficients (original): M1=0.997 (fraction of Mitotracker Green overlapping DPP **1**), M2=0.763 (fraction of DPP **1** overlapping Mitotracker Green).

For pair of two signal channels Mitotracker Green and DPP **2** Pearson's Coefficient: r=0.793, Manders' Coefficients (original): M1=0.888 (fraction of Mitotracker Green overlapping DPP **2**) M2=0.993 (fraction of DPP **2** overlapping Mitotracker Green).

For pair of two signal channels: Mitotracker Green and DPP **2** (B) Pearson's Coefficient: r=0.788, Manders' Coefficients (original): M1=0.944 (fraction of Mitotracker Green overlapping DPP **2**), M2=0.968 (fraction of DPP **2** overlapping Mitotracker Green).

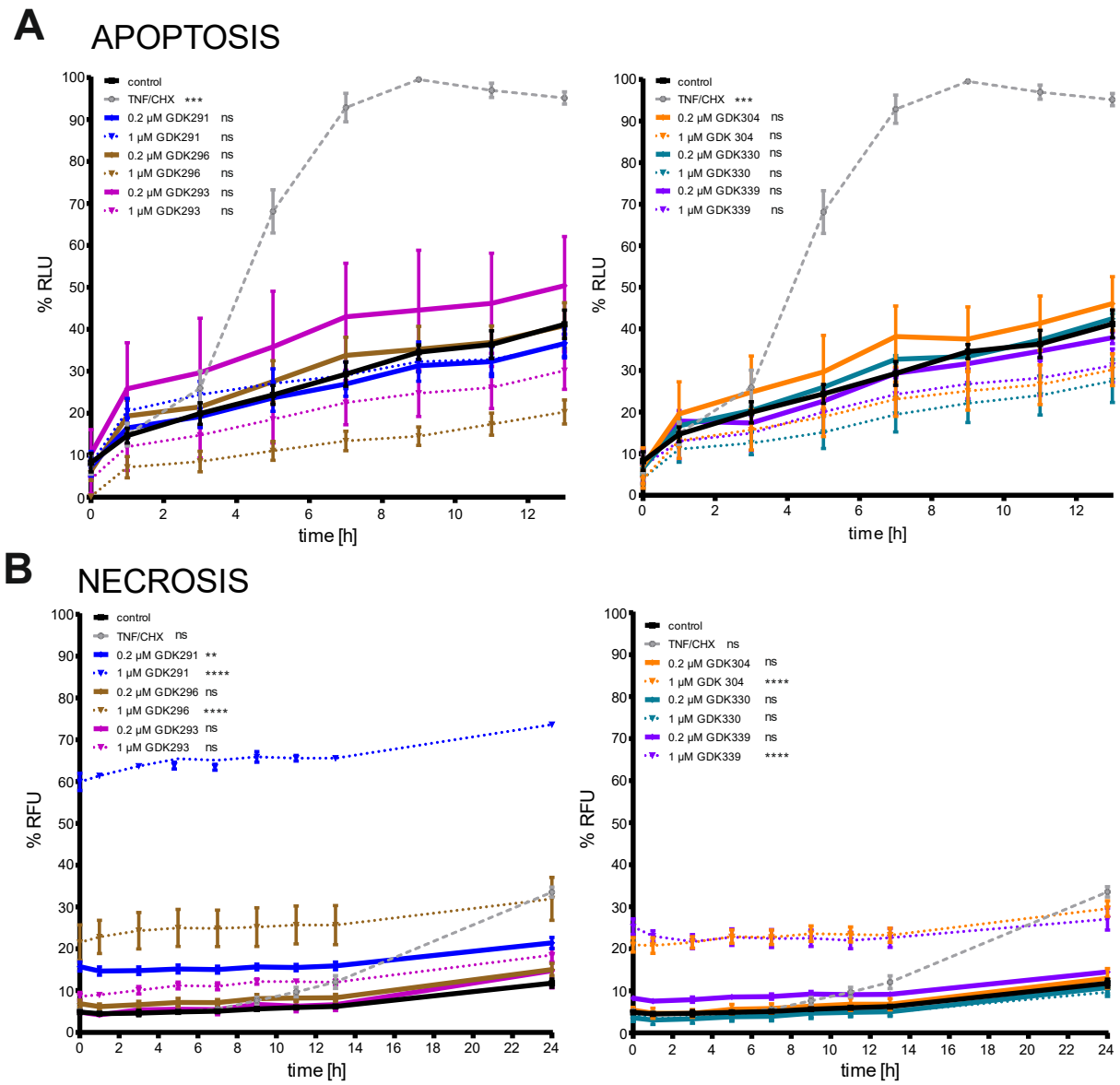

Fig. S51. Effect of crown-diketopyrrolopyrroles on apoptosis and necrosis of the EA.hy 926 cells.

Change in luminescence as a measure of apoptosis (A) and fluorescence (B) over the time. Statistical significance relative to the control was determined by two-way ANOVA with Tukey's test for n = 3 ($p < 0.0001$ (****); $p > 0.05$ (ns).

Section S8: Theoretical calculations

Methods

For the calculations, the selected protocol follows one that has been extensively described and tested before,[3] and is only briefly outlined below. In this approach, the ground and excited state geometries are optimized at the PCM[4]-(TD-)M06-2X[5] 6-31+G(d) level, the vibrational frequencies are obtained at the exact sale level of theory, the total and transition energies are determined at CC2/*aug*-cc-pVTZ level, and the solvent corrections (here acetonitrile) on these CC2 energies are included at the PCM(LR+cLR[6])-TD-M06-2X/6-311+G(2d,p) level. All (TD-)DFT calculations have been performed with the Gaussian16.A03 program,[7] whereas the CC2 calculations have been achieved with Turbomole 7.3,[8] applying the RI density fitting approach. This approach allows to obtain 0-0 energies that correspond to the crossing point between the measured absorption and emission curves. Finally, the vibronic calculations shown in the ESI was performed with the FCClasses code within the TD approach and the vertical-gradient vibronic model. Temperature effects were considered (298 K) and a broadening function was used (Gaussian, HWMH: 200 cm^{-1}).[9]

Studies

To gain further insights into the photophysics of these DPPs, we conducted a computational study. In the performed computations, we used model compounds (denoted with an added **M**, Fig. S20) in which the crown ether groups were replaced by NMe_2 moieties. This decision was justified by computational savings as well as the non-conjugated nature of the crown ether. We computed the 0-0 energies to be 2.24, 2.24, and 2.17 eV for **9M**, **10M**, and **17M** respectively. These values can be rightfully compared to the experimental absorption-fluorescence crossing point, which has the values 2.28, 2.28, and 2.20 eV. Naturally, the selected level of theory can restore the experimental values with high accuracy. In addition, as can be seen in Fig. 48 for **9M**, the shape of the absorption spectrum with the presence of two maxima is globally reproduced when vibronic calculations are made.

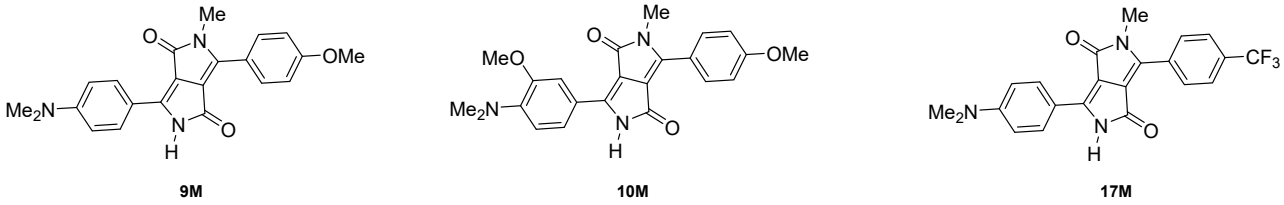

Fig. S52. Structures used in computational studies

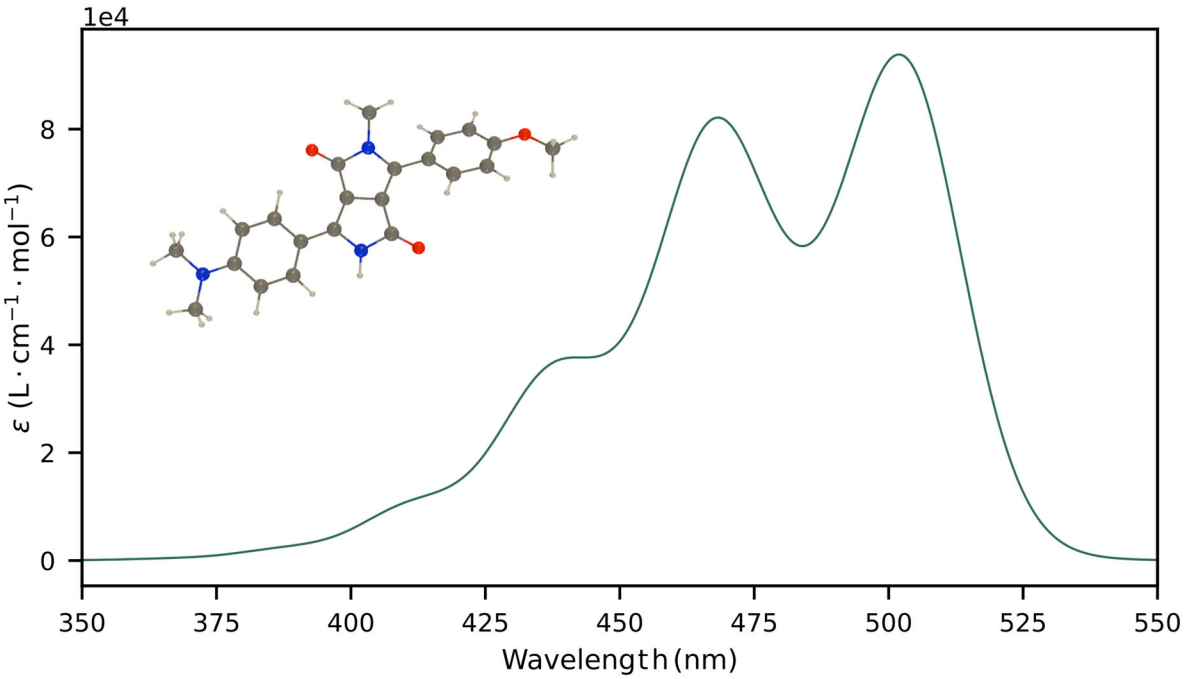

Fig. S53. Vibrationally-resolved absorption spectrum of **9M** calculated with PCM-TD-M06-2X/6-31+G(d), using the TD-VG vibronic model.

Plots displaying density differences for the three dyes are presented in Figure S22. In **9M**, the 4-$Me_2NC_6H_4$ is nearly coplanar with the DPP with a twist of only 6° as compared to a value of 33° for the 4-$MeOC_6H_4$. As can be further seen in Figure 5, the amino group, which is perfectly coplanar in both ground and excited states with the benzene ring, acts as the main donor. The DPP unit acts as the acceptor, while the methoxy group has a weak impact. When adding the secondary OMe (in **10M**), the steric clash between the two donating groups induces a twist of the NMe_2 as compared to the phenyl (40° in the ground, and 35° in the excited state). The latter however remains coplanar with the DPP as in **9M**. Nevertheless, the twist of the NMe_2 in **10M** makes it slightly less donating than in **9M**, though the topologies remain vastly similar, as consistent with the D-A-D' architecture. We note that the non-planarity of NMe_2 in **10M** hints at a more flexible structure, thus likely able to accommodate complexation. When one turns to **17M**, the pattern significantly changes with a clearer charge-transfer character, as well as the CF_3-bearing ring acting as the acceptor in a D-A-A' structure. The above noted differences are reflected in the excited-state dipole moments that attain 7.8, 6.4, and 16.5 D in **9M**, **10M**, and **17M**, respectively. It is noted experimentally that these series of dyes are especially emissive. To explain this, let us first note that TD-DFT yields very large oscillator strengths for the $S_1 \rightarrow S_0$ transition (ca. 1.0 for all three compounds), which is indicative of a very large radiative constant. At the same time TD-DFT reveals that, at the optimal S_1 geometry, there is only a triplet available

below the S_1, but the gap is hugged between the singlet and triplet (> 1.2 eV), which is clearly detrimental for ISC to occur. These two facts are consistent with a bright emission.

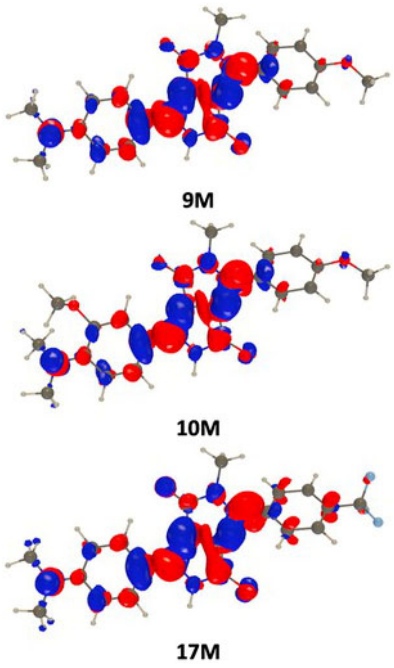

Fig. S54. Density difference plot for the model dyes of **9M**, **10M**, and **17M**. The blueberry and crimson lobed indicate regions of decreased and increase of density upon absorption. Contour threshold $1x10^{-3}$.

As a simple way to model complexation, we have used a structure in which **10M** has been protonated. In this case, the CT character is lost (see Figure S23), consistent with the blueshift and the stronger vibrationally resolved character of the experimental band after complexation (Figure 4).

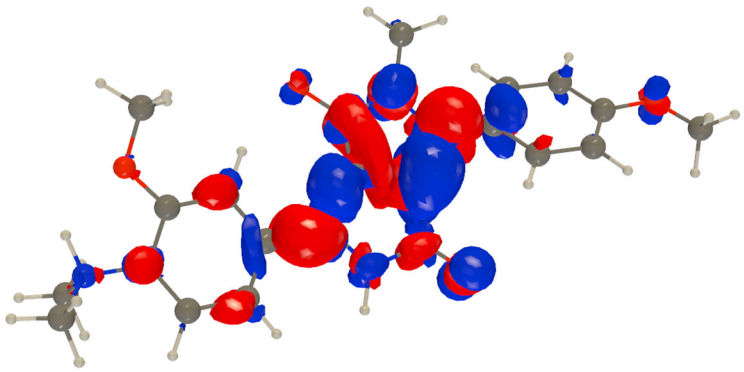

Fig. S55. Density difference plot for the model dyes of **10M+H$^+$** Contour threshold $1x10^{-3}$.

Section S9: ^{1}H NMR and ^{13}C NMR Spectra

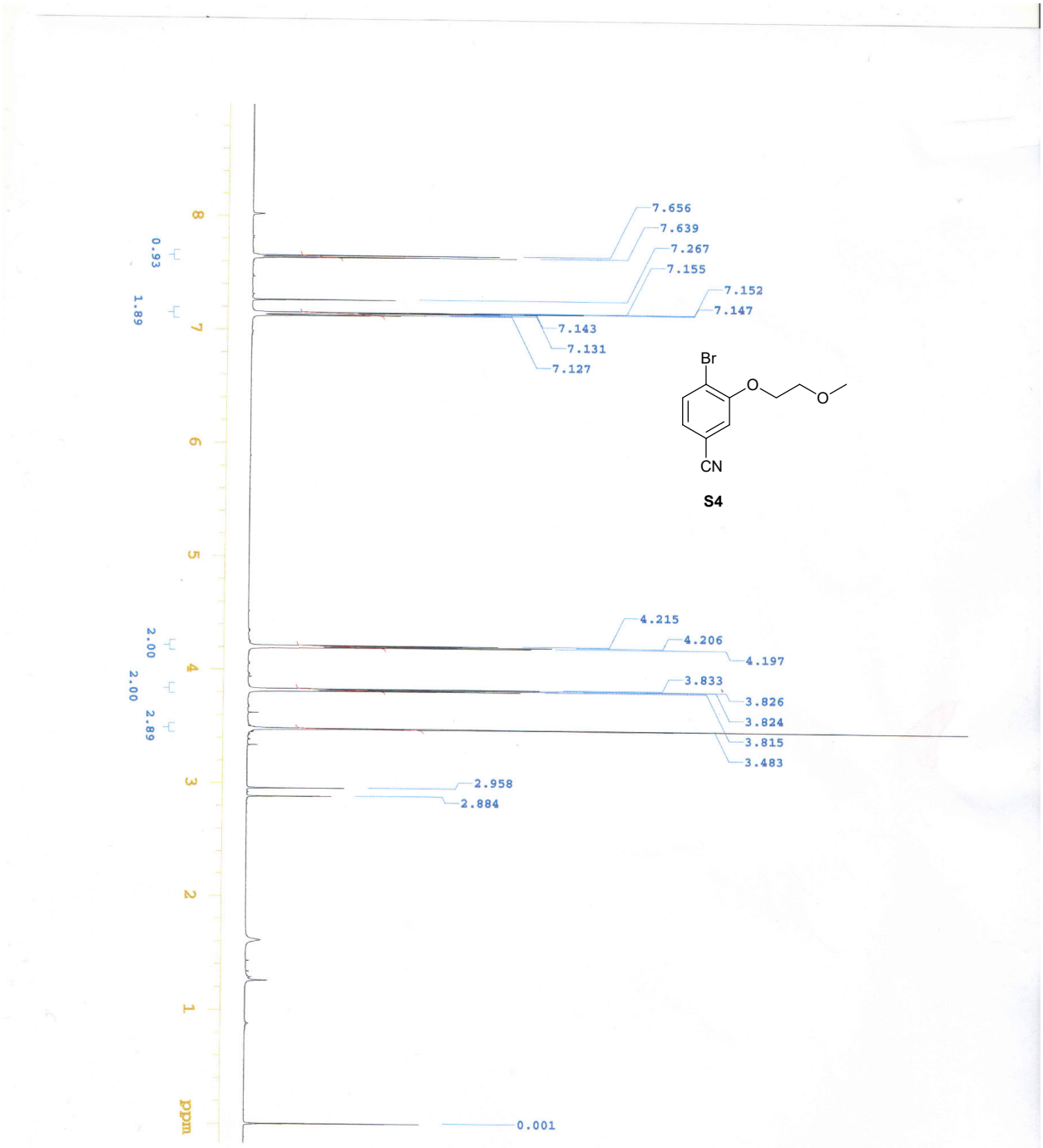

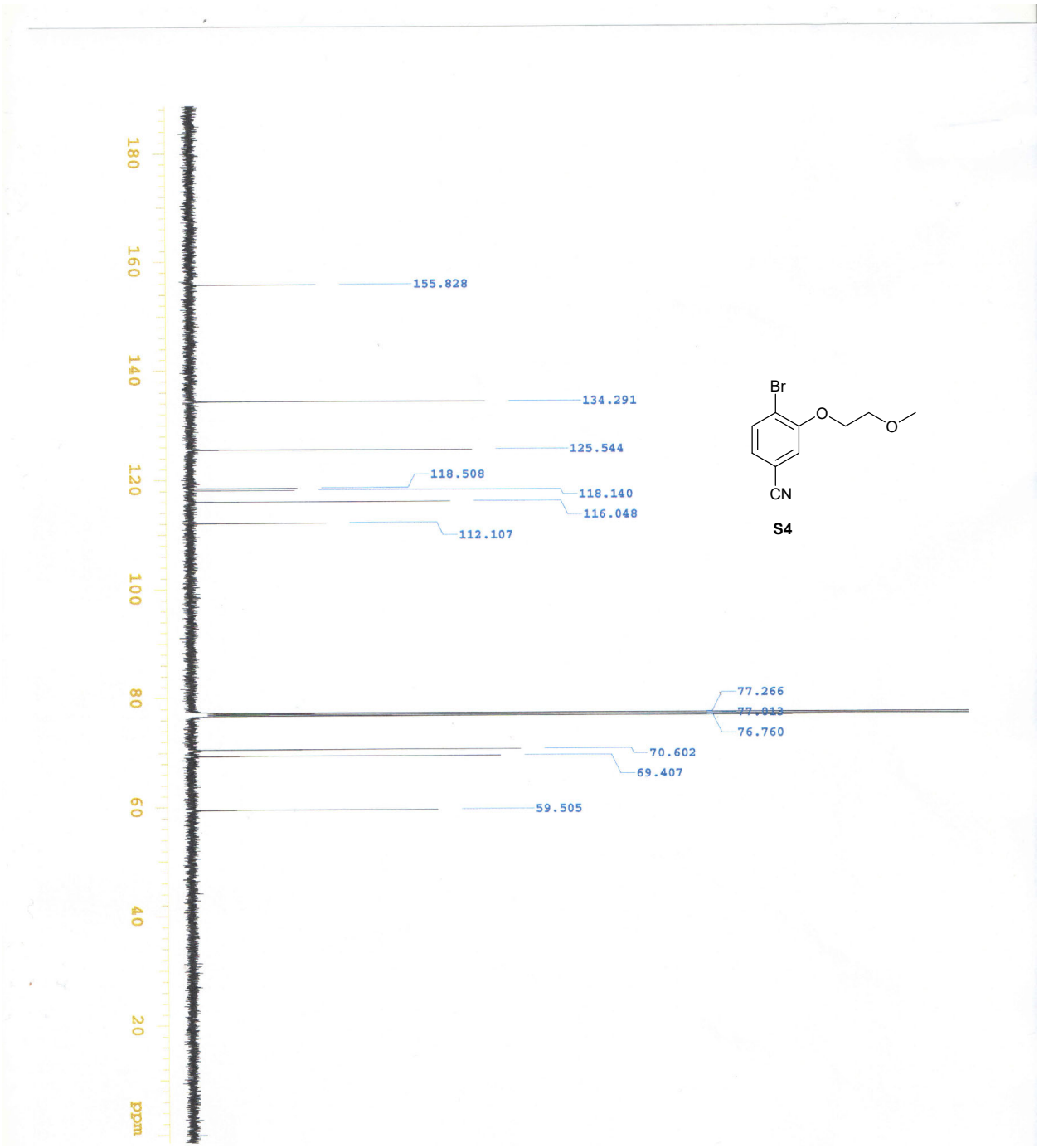
155.828
134.291
125.544
118.508
118.140
116.048
112.107
77.266
77.013
76.760
70.602
69.407
59.505
180
160
140
120
100
80
60
40
20
ppm
Br
O
O
CN
S4

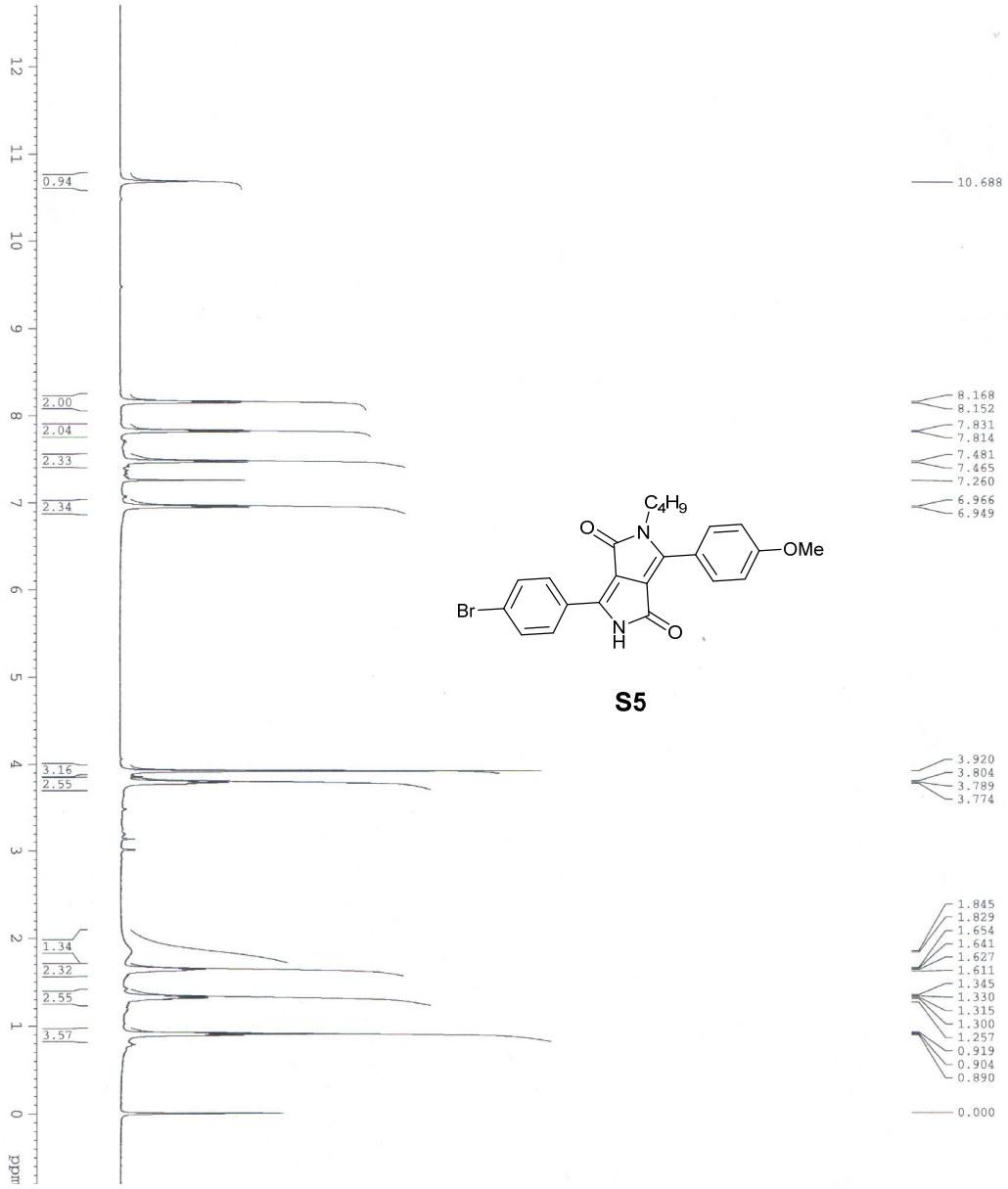
12
11
10
9
8
7
6
5
4
3
2
1
0
ppm
0.94
2.00
2.04
2.33
2.34
3.16
2.55
1.34
2.32
2.55
3.57
10.688
8.168
8.152
7.831
7.814
7.481
7.465
7.260
6.966
6.949
3.920
3.804
3.789
3.774
1.845
1.829
1.654
1.641
1.627
1.611
1.345
1.330
1.315
1.300
1.257
0.919
0.904
0.890
0.000
C4H9
O
N
OMe
Br
N
H
O

S5

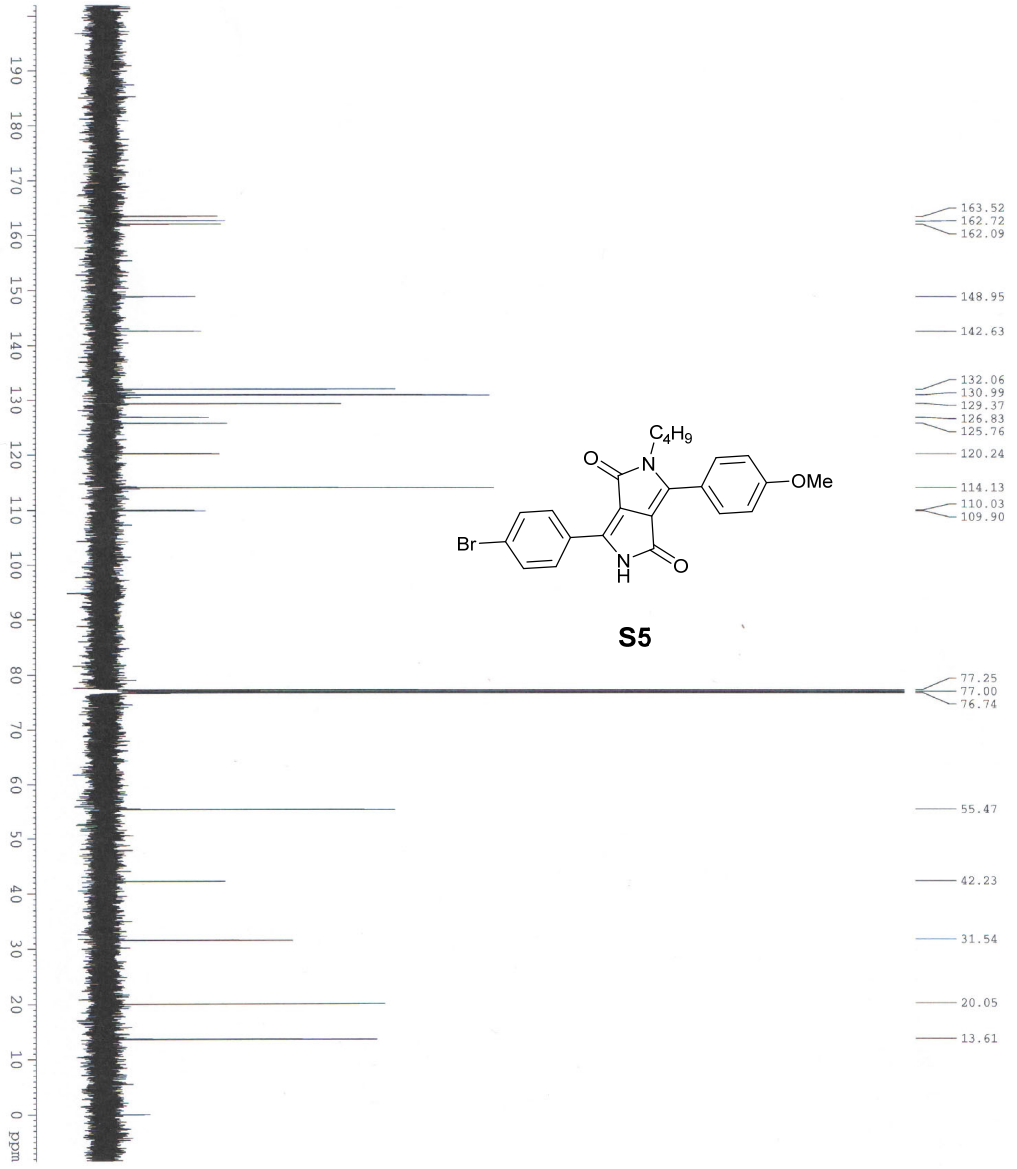
190 180 170 160 150 140 130 120 110 100 90 80 70 60 50 40 30 20 10 0 ppm
163.52
162.72
162.09
148.95
142.63
132.06
130.99
129.37
126.83
125.76
120.24
114.13
110.03
109.90
77.25
77.00
76.74
55.47
42.23
31.54
20.05
13.61
C4H9
O
N
OMe
Br
N
H
O

S5

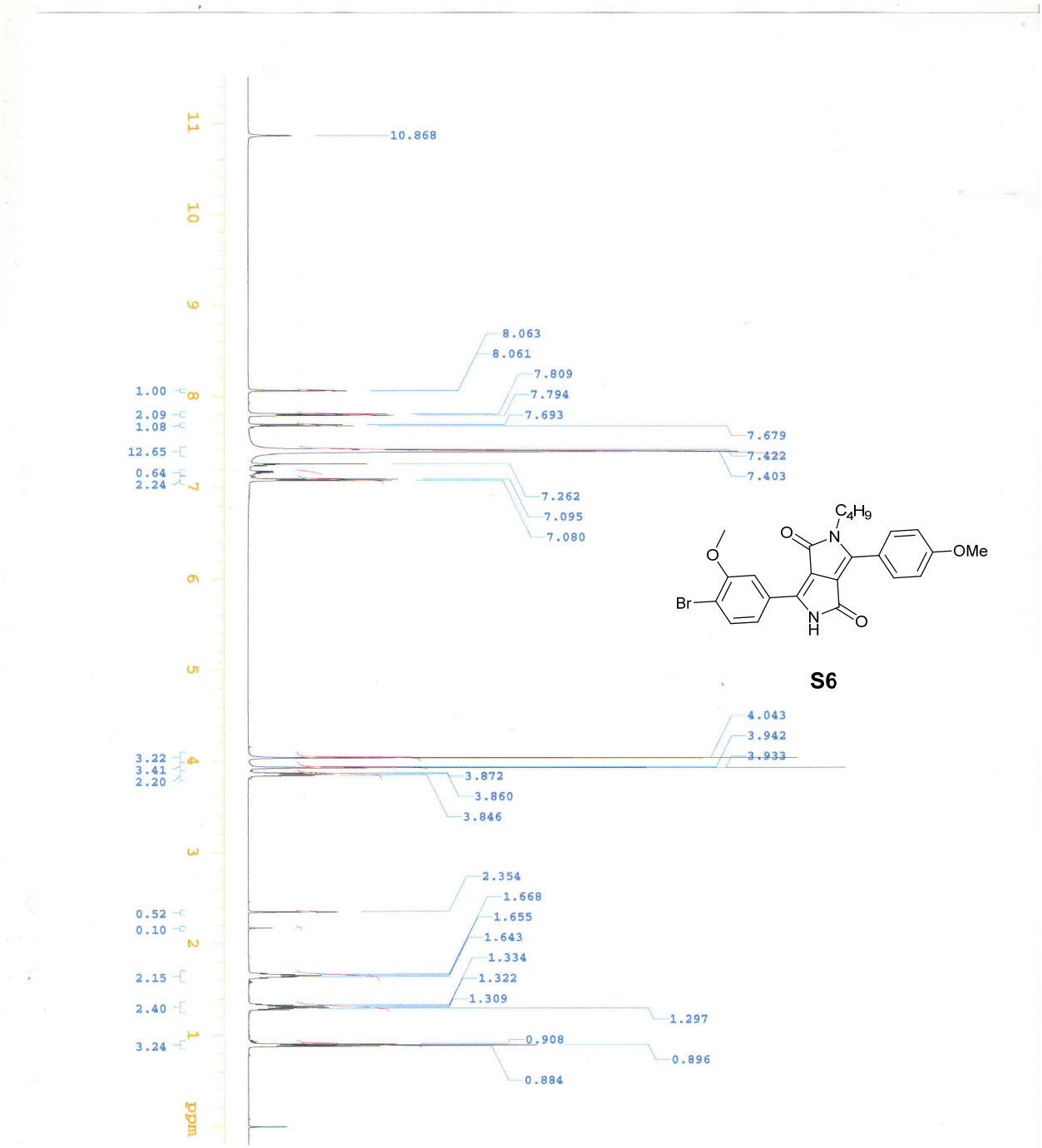
10.868
8.063
8.061
7.809
7.794
7.693
7.679
7.422
7.403
7.262
7.095
7.080
4.043
3.942
3.933
3.872
3.860
3.846
2.354
1.668
1.655
1.643
1.334
1.322
1.309
1.297
0.908
0.896
0.884
1.00
2.09
1.08
12.65
0.64
2.24
3.22
3.41
2.20
0.52
0.10
2.15
2.40
3.24
ppm
C4H9
N
O
O
OMe
Br
O
N
H
O

S6

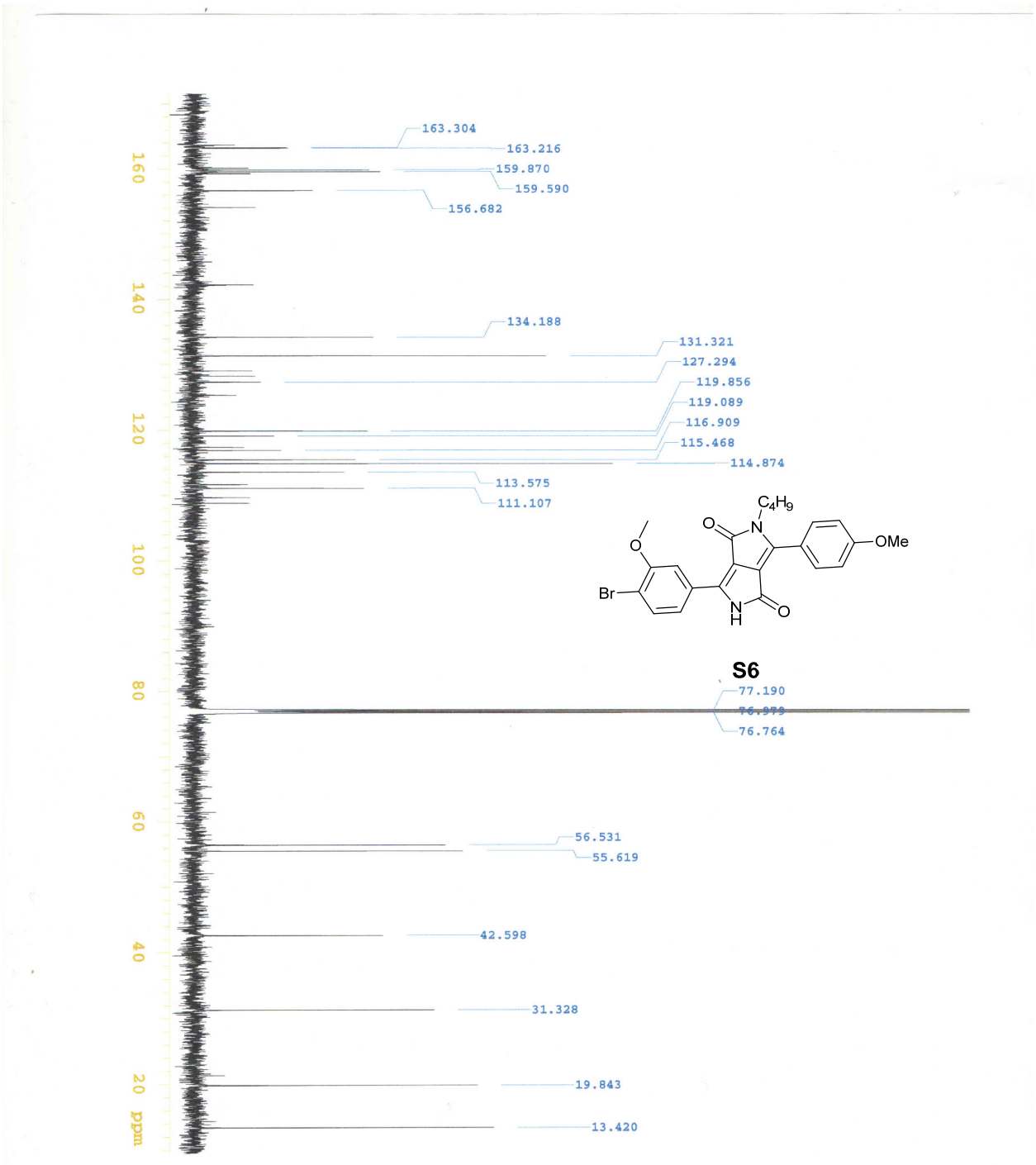
163.304
163.216
159.870
159.590
156.682
134.188
131.321
127.294
119.856
119.089
116.909
115.468
114.874
113.575
111.107
77.190
76.979
76.764
56.531
55.619
42.598
31.328
19.843
13.420
160
140
120
100
80
60
40
20
ppm
C4H9
O
N
O
OMe
O
Br
N
H
O

S6

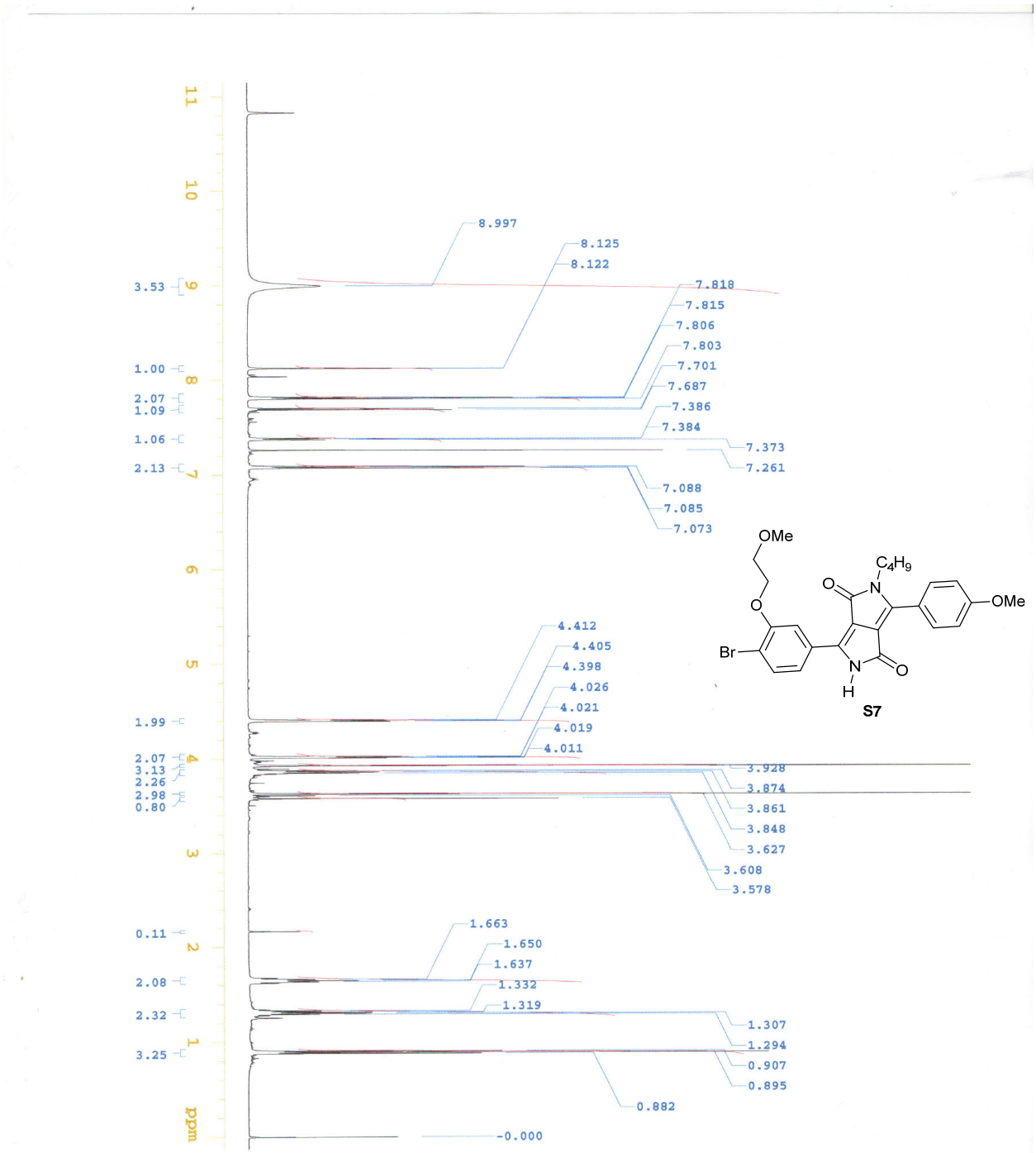
8.997
8.125
8.122
7.818
7.815
7.806
7.803
7.701
7.687
7.386
7.384
7.373
7.261
7.088
7.085
7.073
4.412
4.405
4.398
4.026
4.021
4.019
4.011
3.928
3.874
3.861
3.848
3.627
3.608
3.578
1.663
1.650
1.637
1.332
1.319
1.307
1.294
0.907
0.895
0.882
-0.000
3.53
1.00
2.07
1.09
1.06
2.13
1.99
2.07
3.13
2.26
2.98
0.80
0.11
2.08
2.32
3.25
ppm
OMe
C4H9
O
N
O
OMe
O
Br
N
O
H
S7

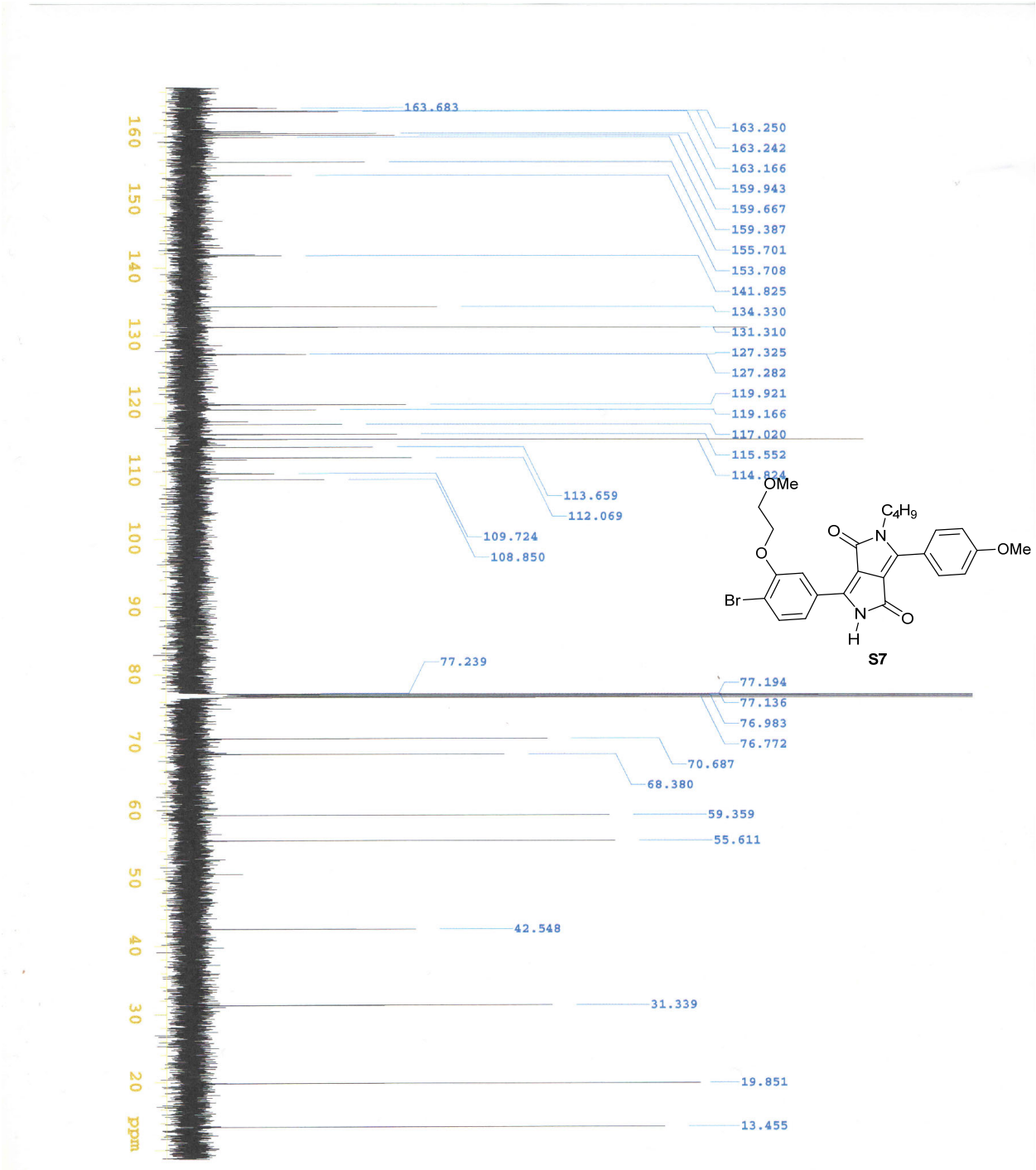
163.683
163.250
163.242
163.166
159.943
159.667
159.387
155.701
153.708
141.825
134.330
131.310
127.325
127.282
119.921
119.166
117.020
115.552
114.824
113.659
112.069
109.724
108.850
77.239
77.194
77.136
76.983
76.772
70.687
68.380
59.359
55.611
42.548
31.339
19.851
13.455
ppm
OMe
C_4H_9
O
N
OMe
O
Br
N
O
H
S7

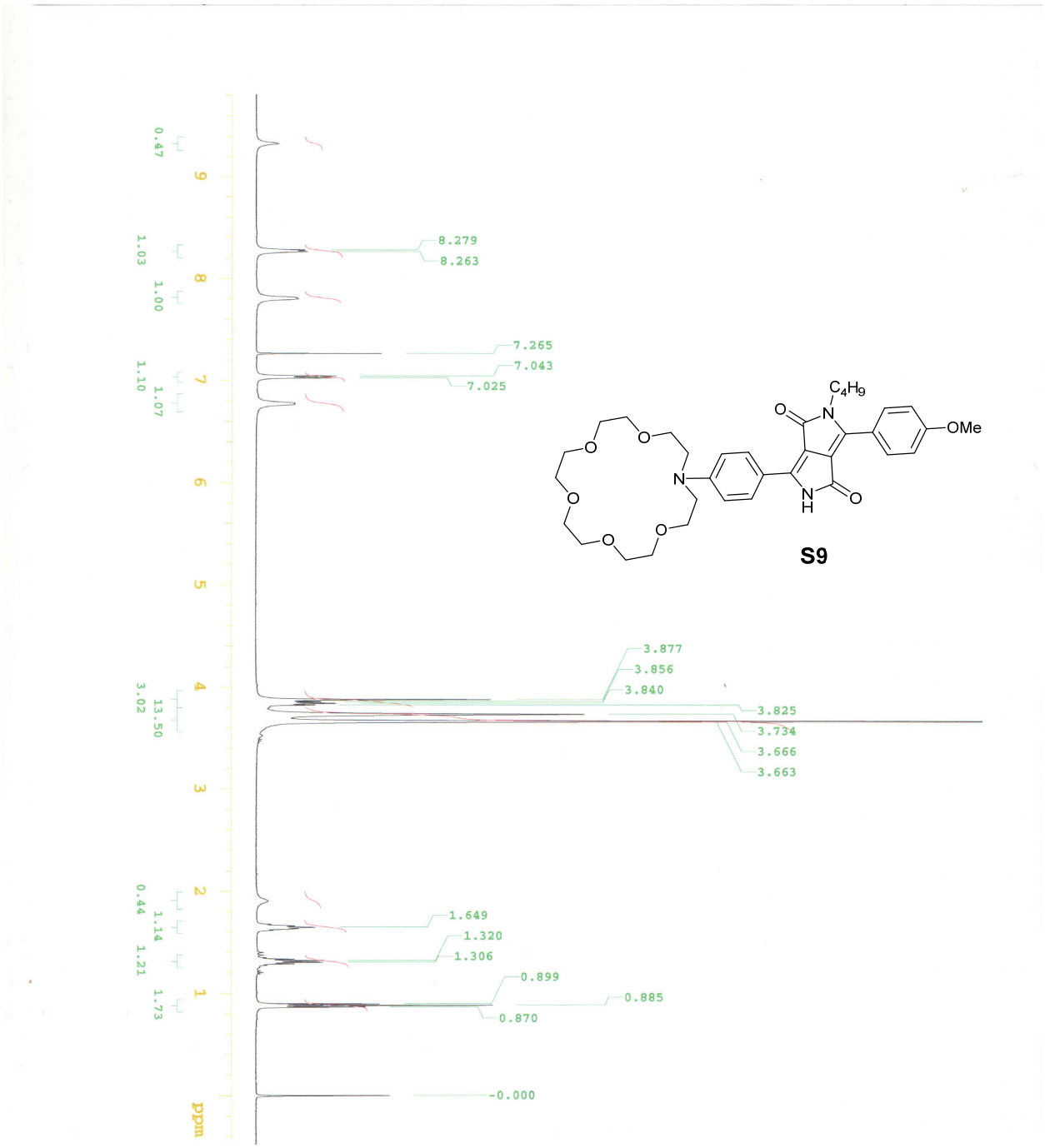
8.279
8.263
7.265
7.043
7.025
3.877
3.856
3.840
3.825
3.734
3.666
3.663
1.649
1.320
1.306
0.899
0.885
0.870
-0.000
ppm
0.47
1.03
1.00
1.10
1.07
3.02
13.50
0.44
1.14
1.21
1.73
C4H9
OMe
S9

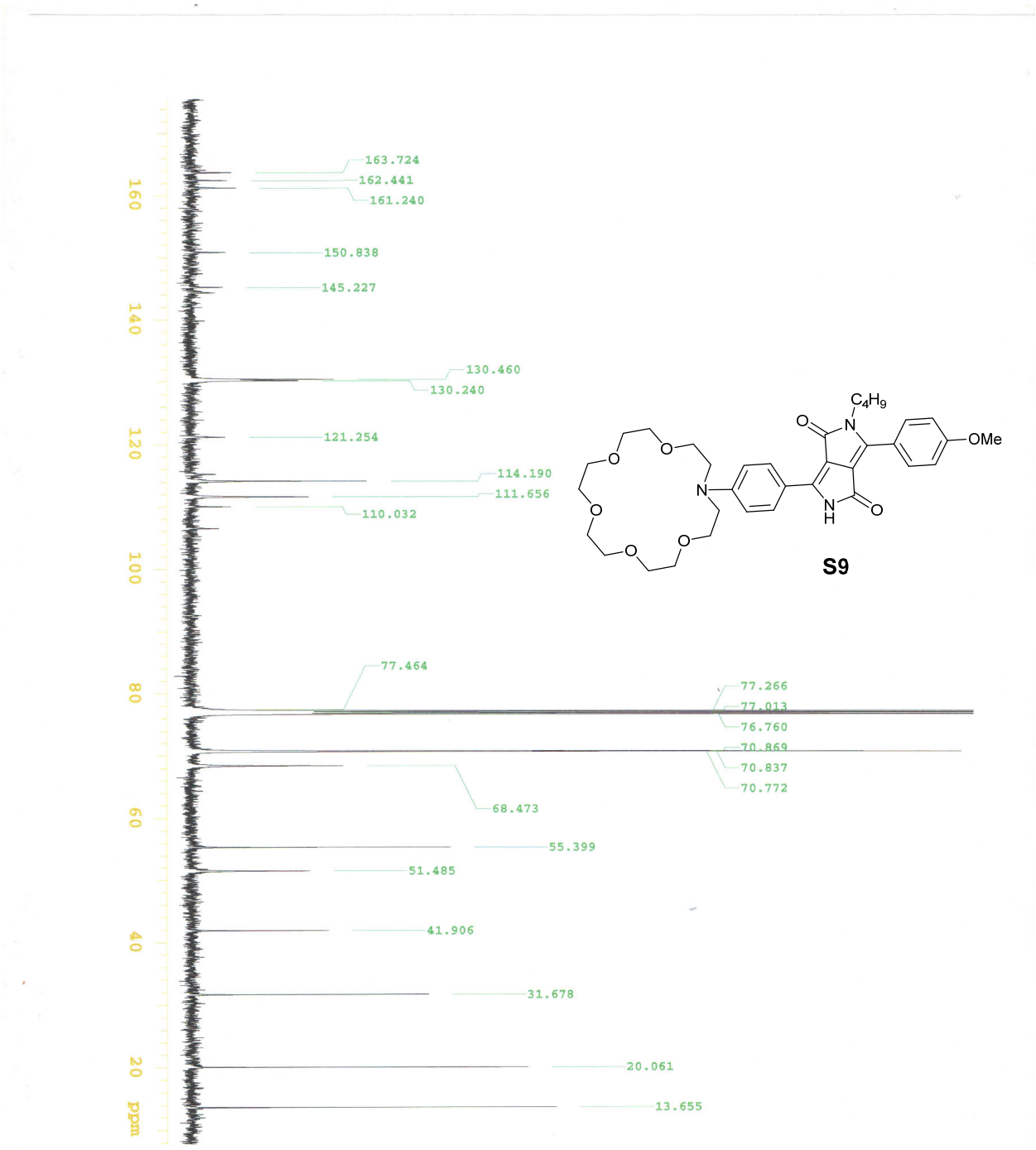
163.724
162.441
161.240
150.838
145.227
130.460
130.240
121.254
114.190
111.656
110.032
77.464
77.266
77.013
76.760
70.869
70.837
70.772
68.473
55.399
51.485
41.906
31.678
20.061
13.655
160
140
120
100
80
60
40
20
ppm
O
O
O
O
O
O
N
N
H
O
O
C_4H_9
OMe

S9

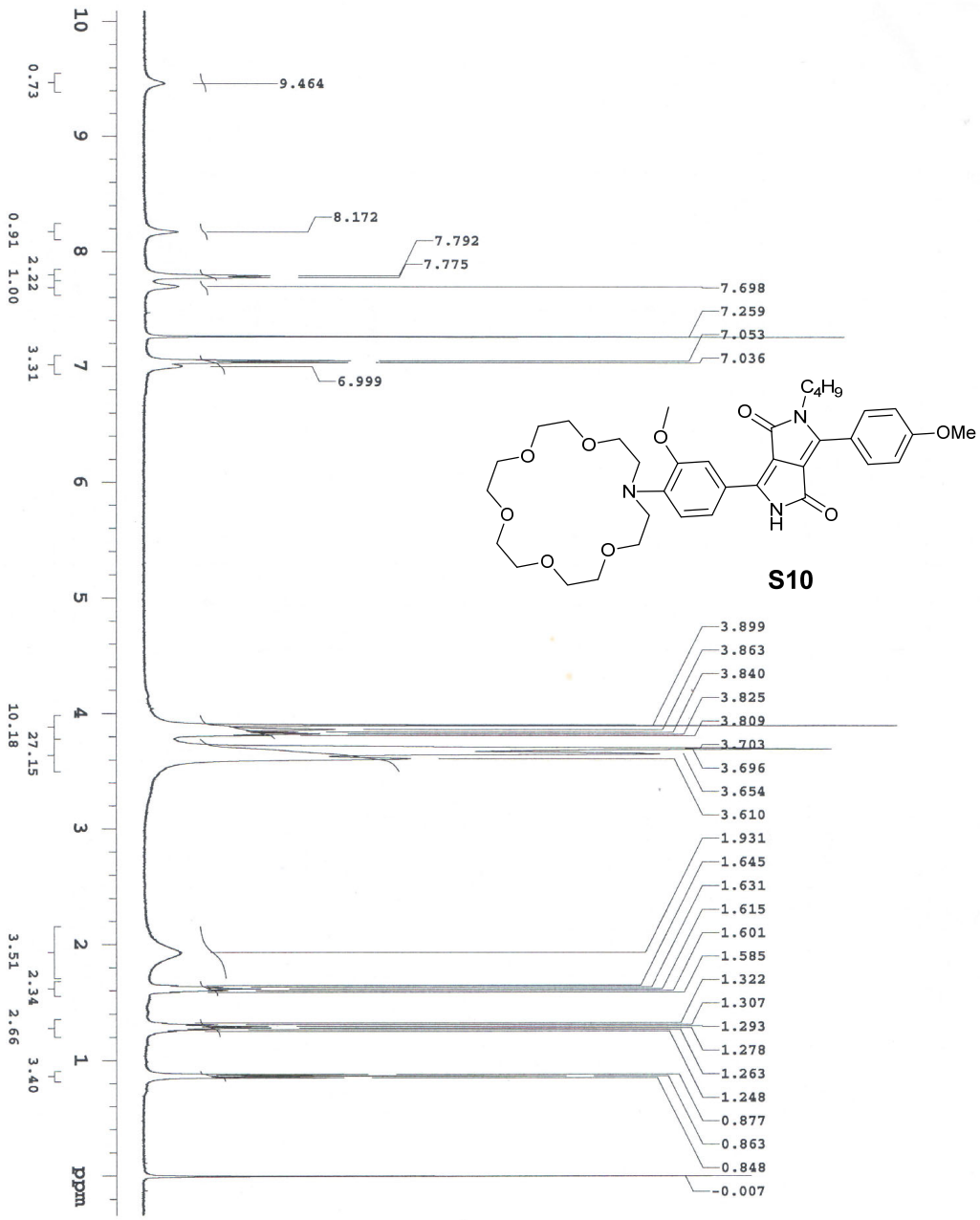
9.464
8.172
7.792
7.775
7.698
7.259
7.053
7.036
6.999
3.899
3.863
3.840
3.825
3.809
3.703
3.696
3.654
3.610
1.931
1.645
1.631
1.615
1.601
1.585
1.322
1.307
1.293
1.278
1.263
1.248
0.877
0.863
0.848
-0.007
0.73
0.91
1.00
2.22
3.31
10.18
27.15
3.51
2.34
2.66
3.40
ppm
S10

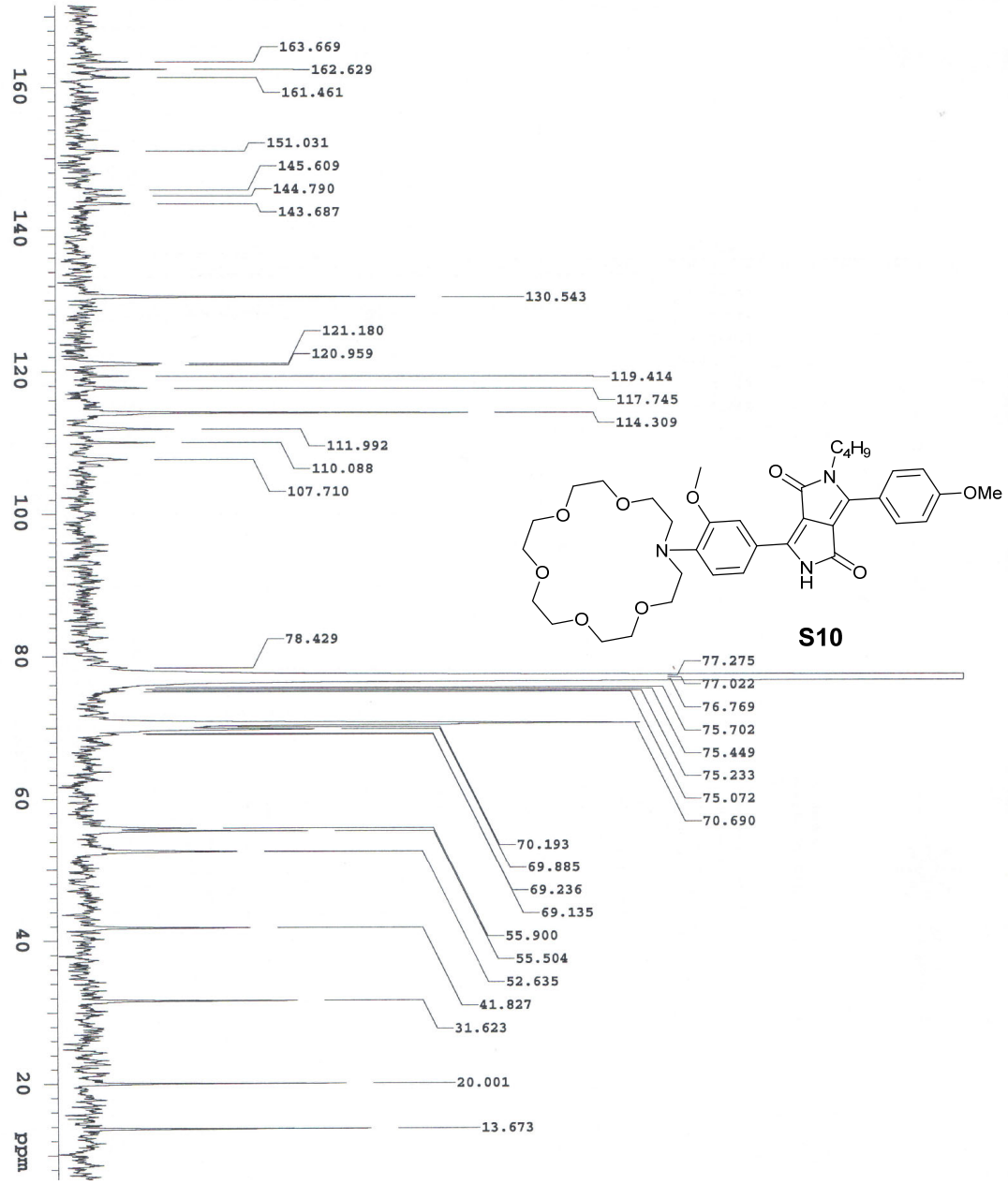
163.669
162.629
161.461
151.031
145.609
144.790
143.687
130.543
121.180
120.959
119.414
117.745
114.309
111.992
110.088
107.710
78.429
77.275
77.022
76.769
75.702
75.449
75.233
75.072
70.690
70.193
69.885
69.236
69.135
55.900
55.504
52.635
41.827
31.623
20.001
13.673
160
140
120
100
80
60
40
20
ppm
C4H9
OMe
S10

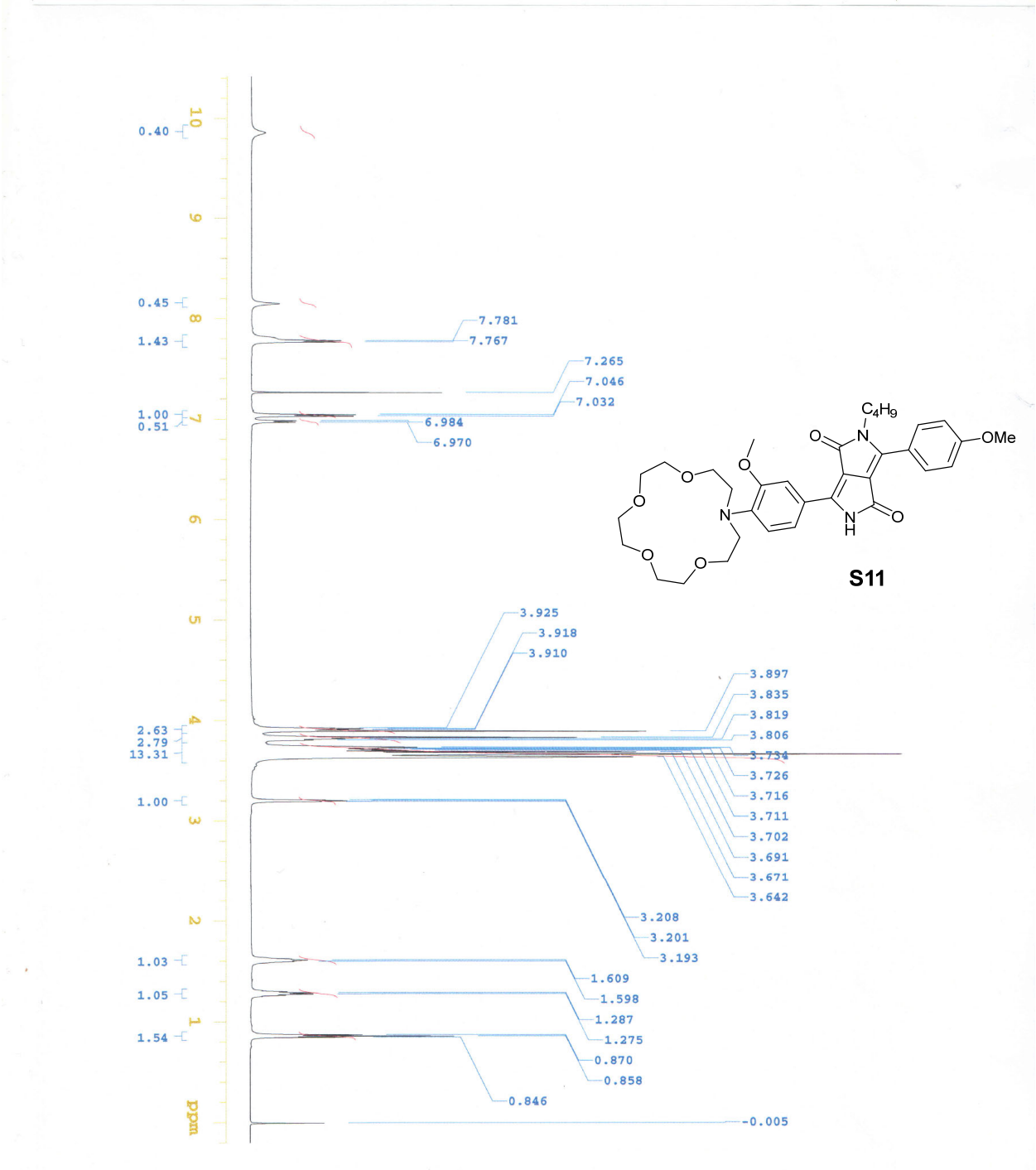
0.40
0.45
1.43
1.00
0.51
2.63
2.79
13.31
1.00
1.03
1.05
1.54
7.781
7.767
7.265
7.046
7.032
6.984
6.970
3.925
3.918
3.910
3.897
3.835
3.819
3.806
3.734
3.726
3.716
3.711
3.702
3.691
3.671
3.642
3.208
3.201
3.193
1.609
1.598
1.287
1.275
0.870
0.858
0.846
-0.005
ppm
C4H9
OMe
S11

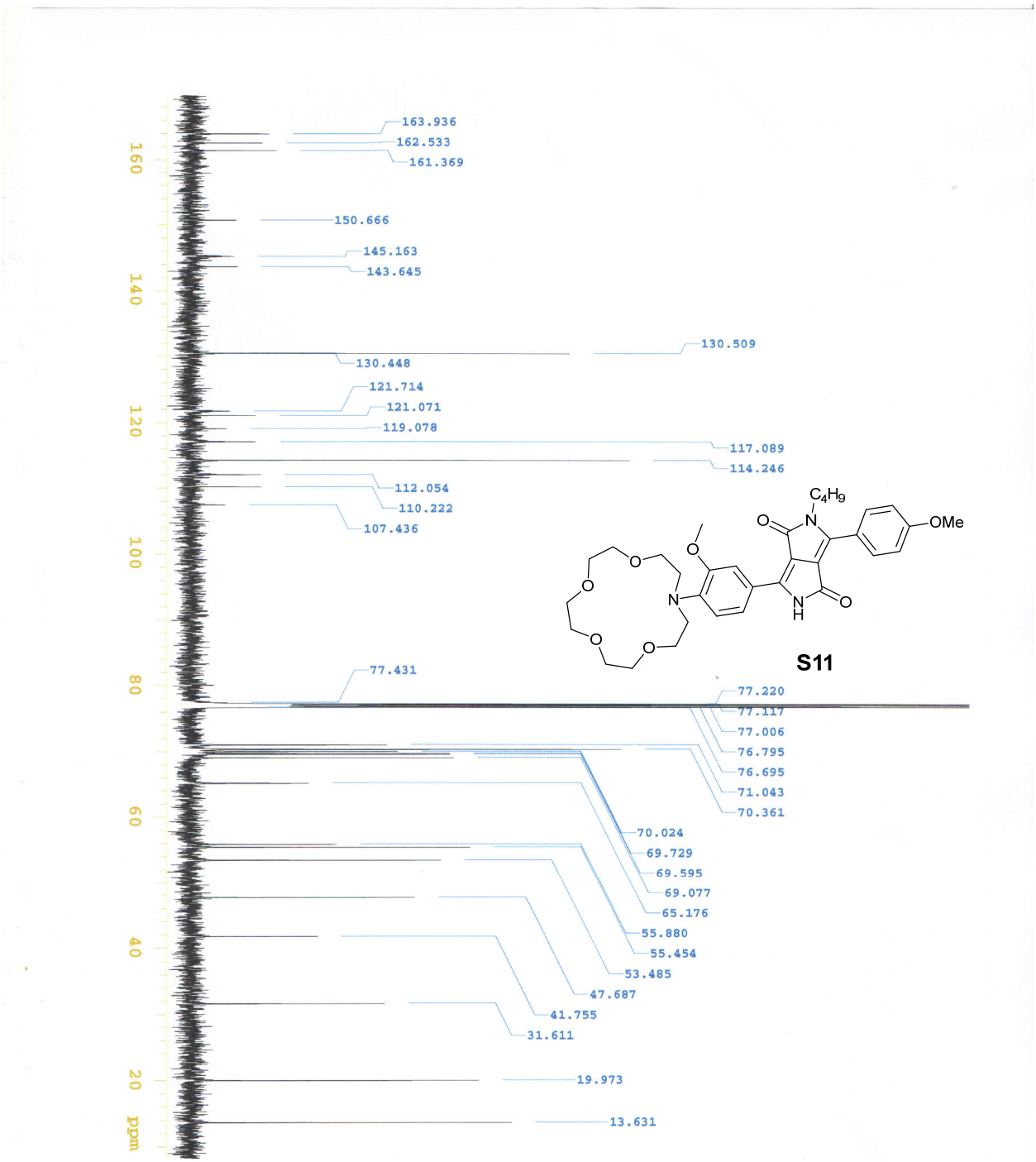
163.936
162.533
161.369
150.666
145.163
143.645
130.509
130.448
121.714
121.071
119.078
117.089
114.246
112.054
110.222
107.436
77.431
77.220
77.117
77.006
76.795
76.695
71.043
70.361
70.024
69.729
69.595
69.077
65.176
55.880
55.454
53.485
47.687
41.755
31.611
19.973
13.631
160
140
120
100
80
60
40
20
ppm
C4H9
OMe
S11

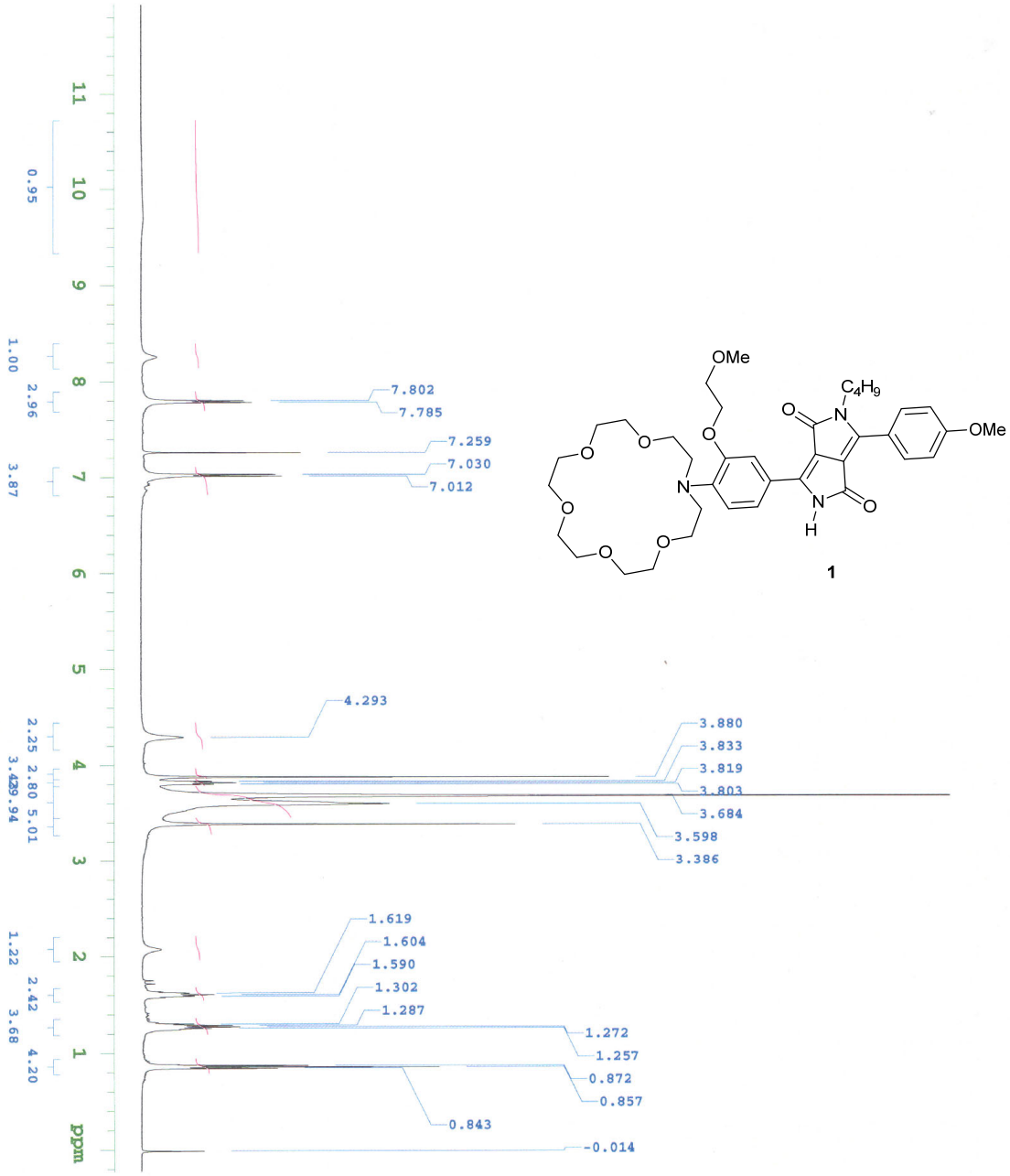
7.802
7.785
7.259
7.030
7.012
4.293
3.880
3.833
3.819
3.803
3.684
3.598
3.386
1.619
1.604
1.590
1.302
1.287
1.272
1.257
0.872
0.857
0.843
-0.014
ppm
OMe
C4H9
OMe
1

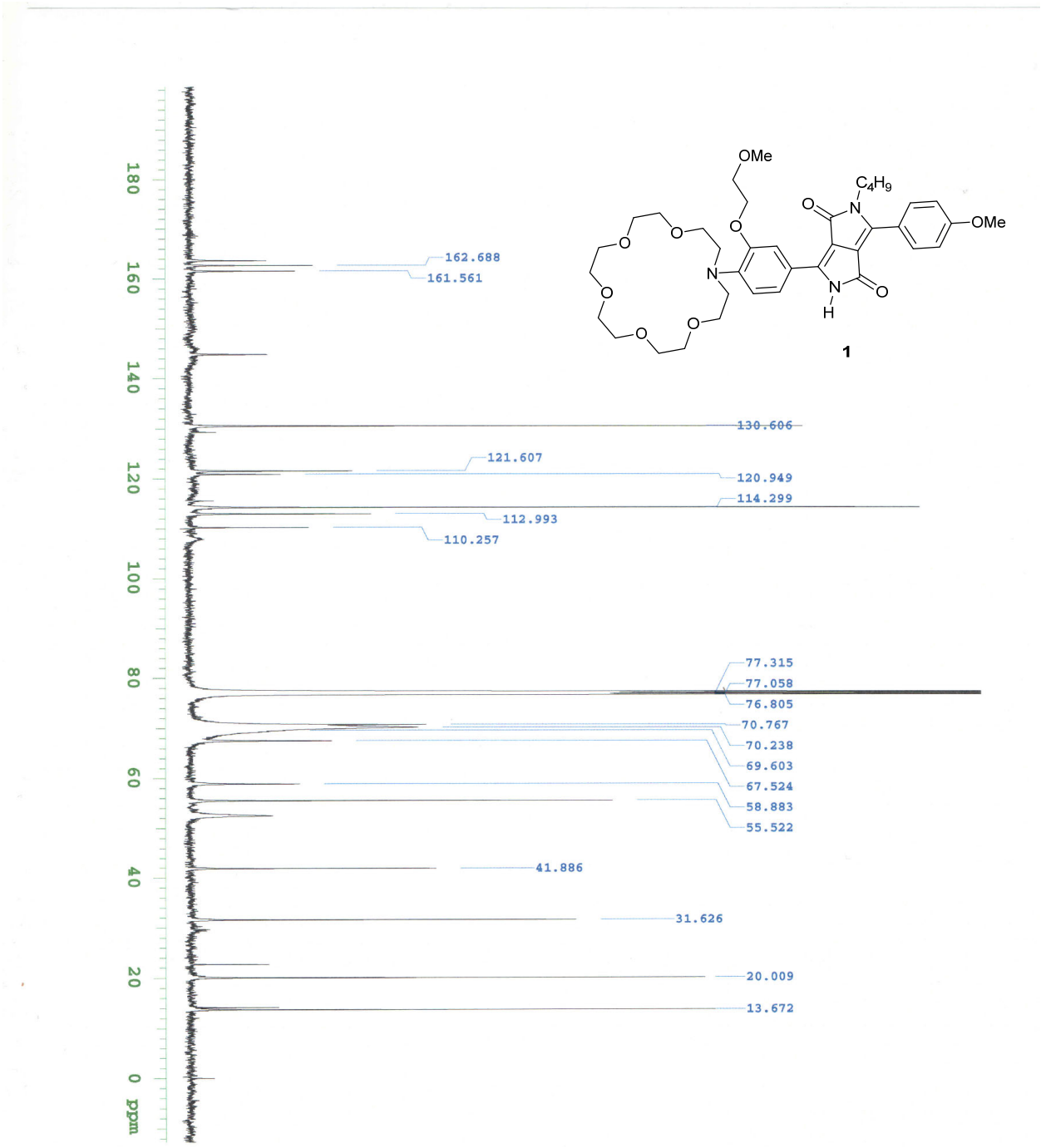
OMe
C4H9
O
N
OMe
O
O
O
N
O
O
O
N
H
O
O
1
162.688
161.561
130.606
121.607
120.949
114.299
112.993
110.257
77.315
77.058
76.805
70.767
70.238
69.603
67.524
58.883
55.522
41.886
31.626
20.009
13.672
180
160
140
120
100
80
60
40
20
0
ppm

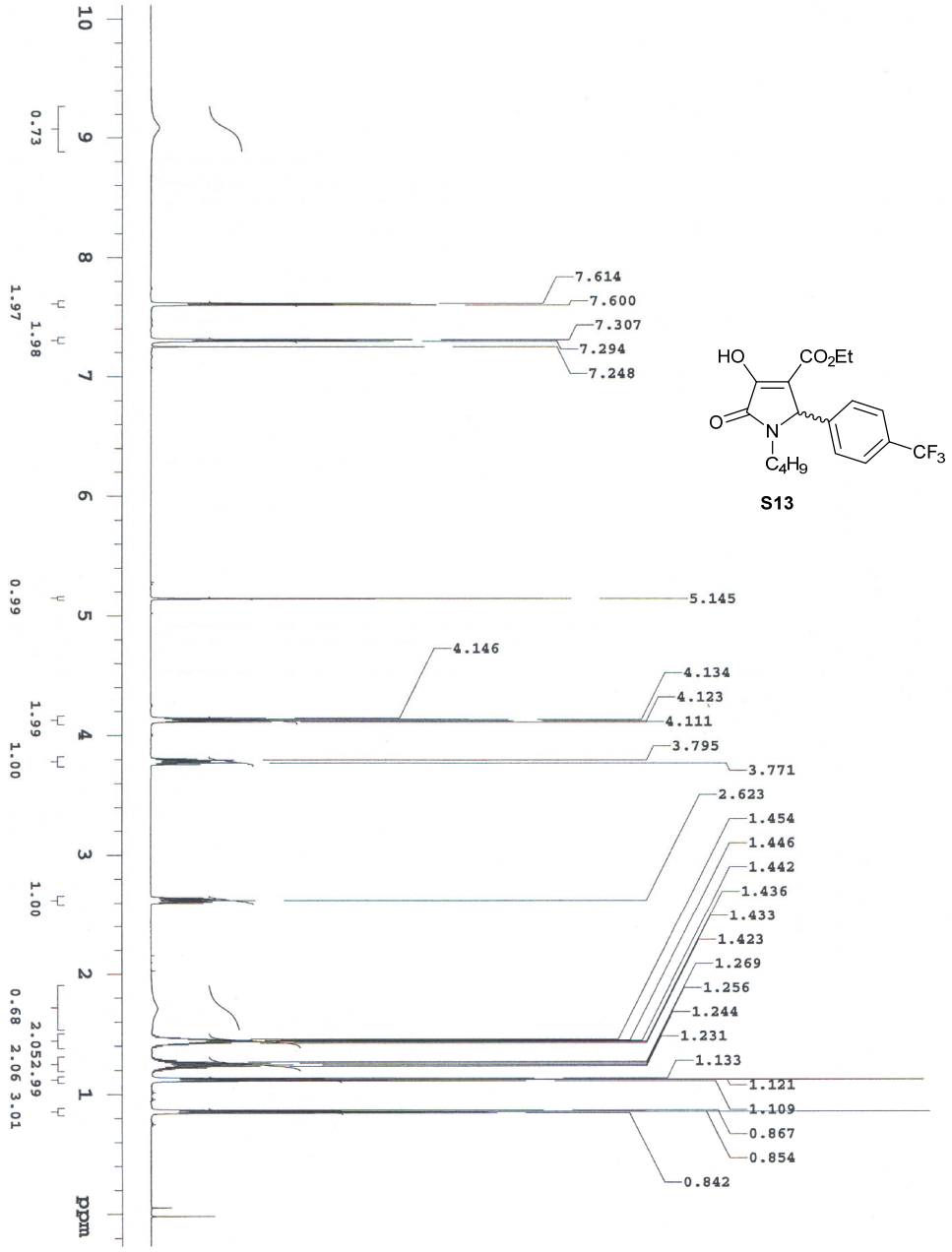
7.614
7.600
7.307
7.294
7.248
5.145
4.146
4.134
4.123
4.111
3.795
3.771
2.623
1.454
1.446
1.442
1.436
1.433
1.423
1.269
1.256
1.244
1.231
1.133
1.121
1.109
0.867
0.854
0.842
0.73
1.97
1.98
0.99
1.99
1.00
1.00
0.68
2.05
2.99
2.06
3.01
ppm
HO
CO2Et
O
N
C4H9
CF3

S13

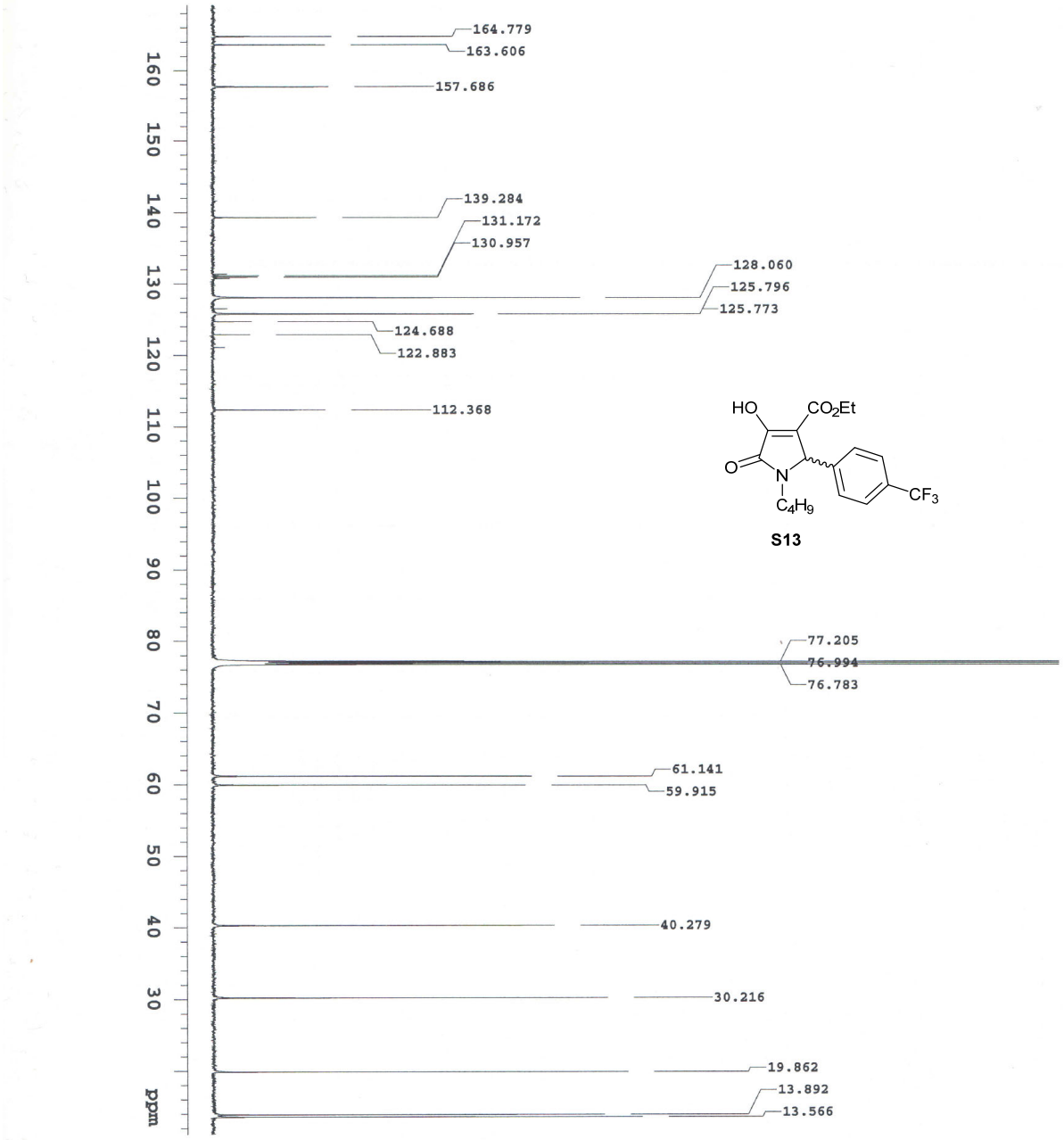
164.779
163.606
157.686
139.284
131.172
130.957
128.060
125.796
125.773
124.688
122.883
112.368
77.205
76.994
76.783
61.141
59.915
40.279
30.216
19.862
13.892
13.566
ppm
HO
CO2Et
O
N
C4H9
CF3

S13

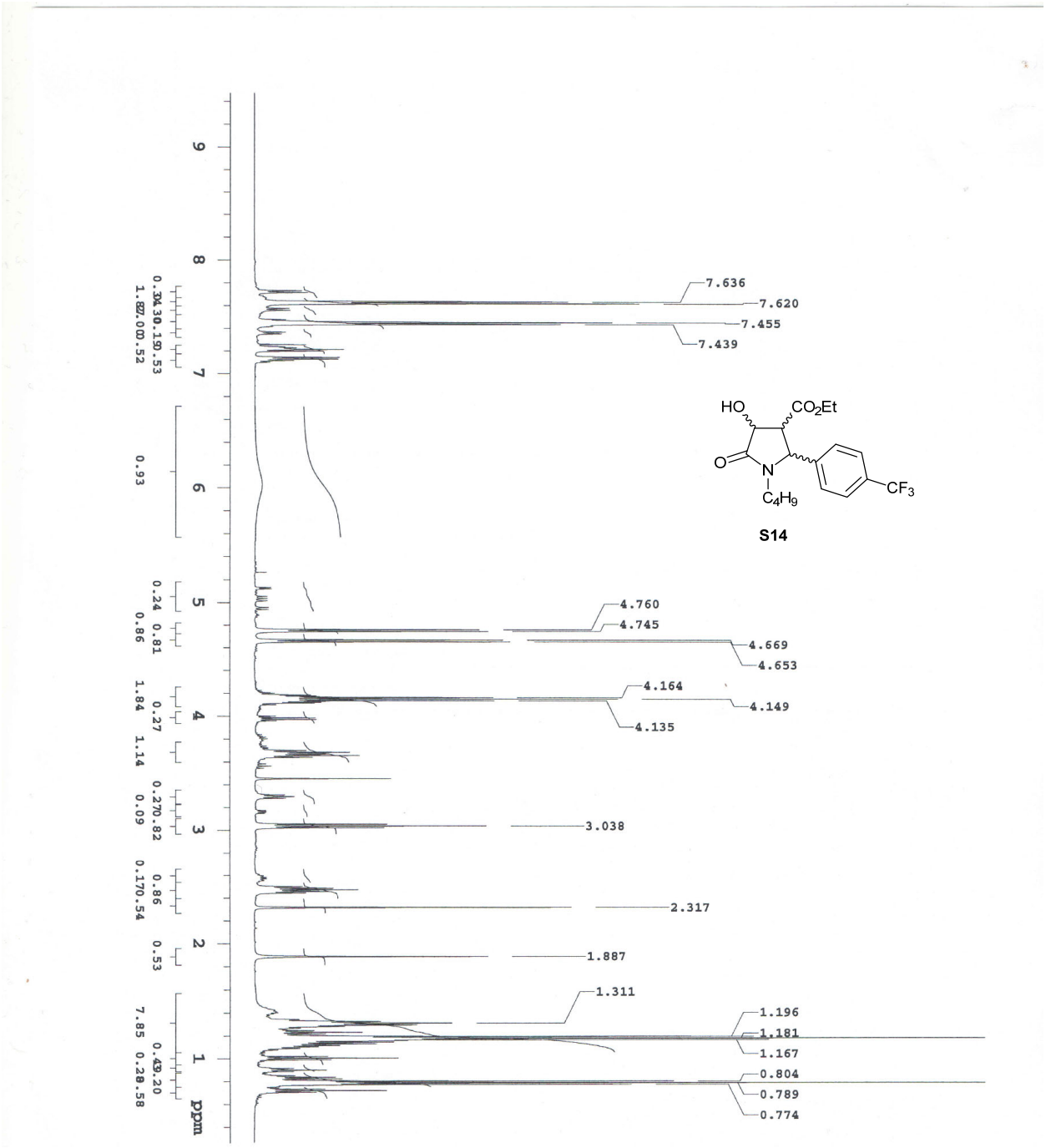
7.636
7.620
7.455
7.439
HO
CO2Et
O
N
C4H9
CF3
S14
4.760
4.745
4.669
4.653
4.164
4.149
4.135
3.038
2.317
1.887
1.311
1.196
1.181
1.167
0.804
0.789
0.774
ppm

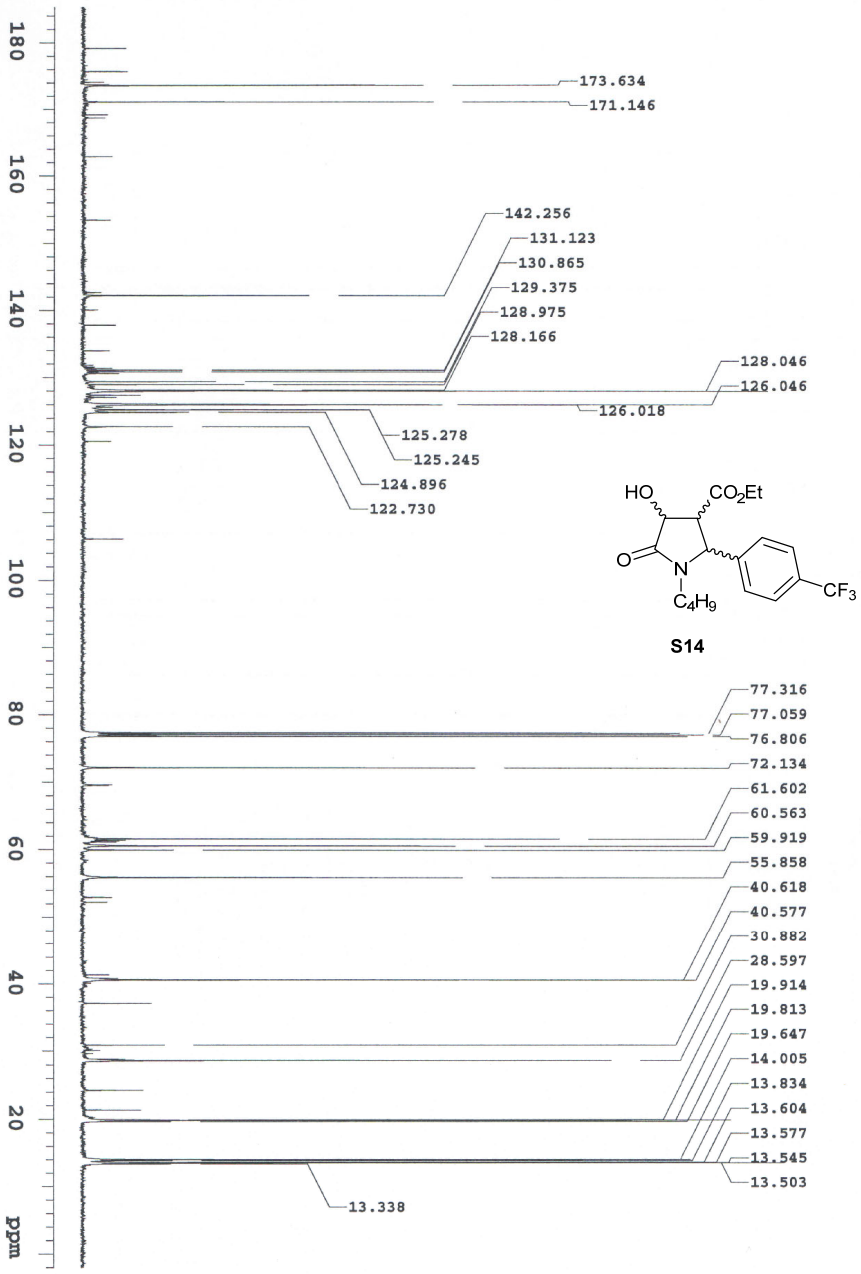
180
160
140
120
100
80
60
40
20
ppm
173.634
171.146
142.256
131.123
130.865
129.375
128.975
128.166
128.046
126.046
126.018
125.278
125.245
124.896
122.730
77.316
77.059
76.806
72.134
61.602
60.563
59.919
55.858
40.618
40.577
30.882
28.597
19.914
19.813
19.647
14.005
13.834
13.604
13.577
13.545
13.503
13.338
HO
CO2Et
O
N
C4H9
CF3

S14

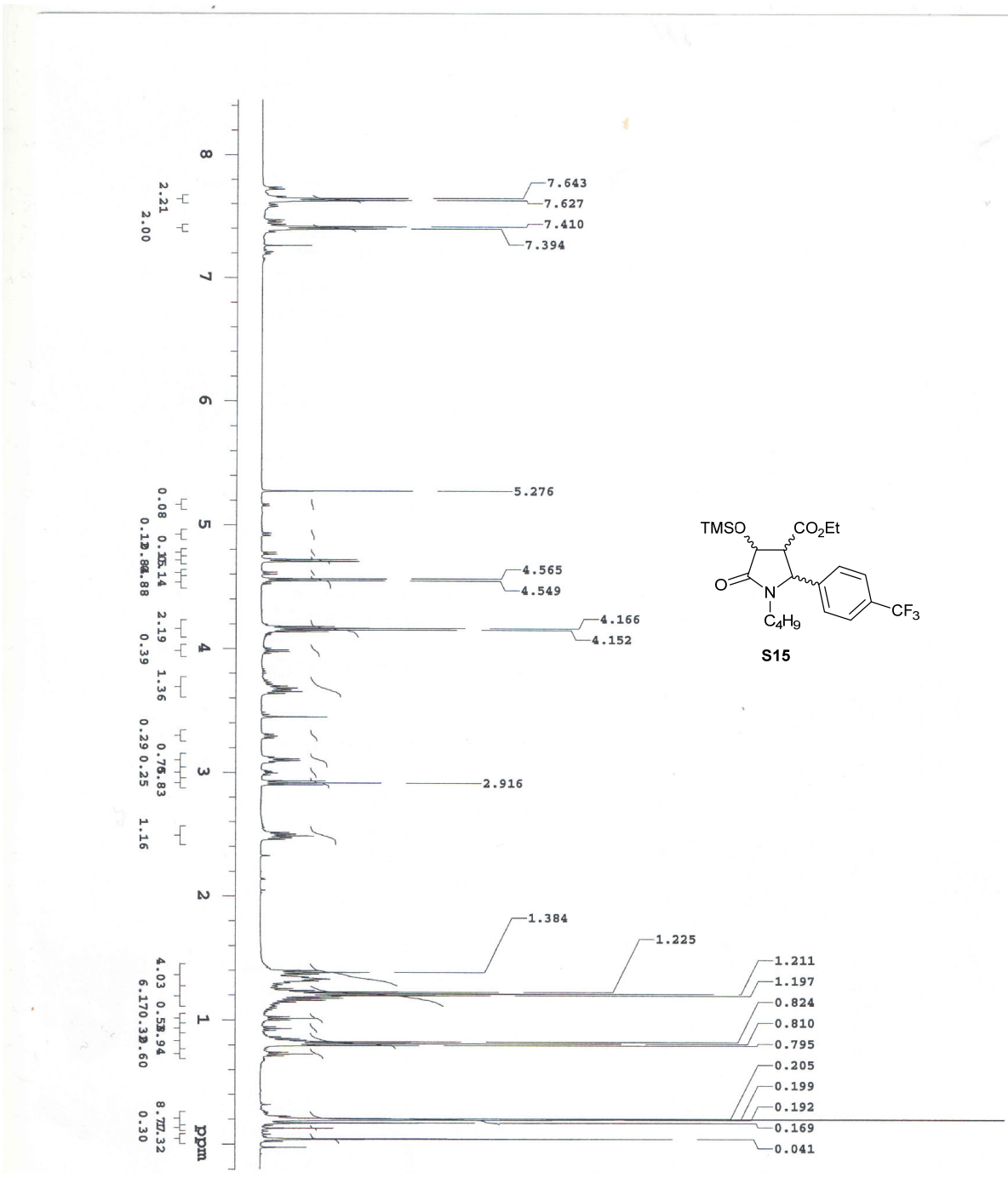
7.643
7.627
7.410
7.394
5.276
4.565
4.549
4.166
4.152
2.916
1.384
1.225
1.211
1.197
0.824
0.810
0.795
0.205
0.199
0.192
0.169
0.041
ppm
TMSO
CO2Et
O
N
C4H9
CF3

S15

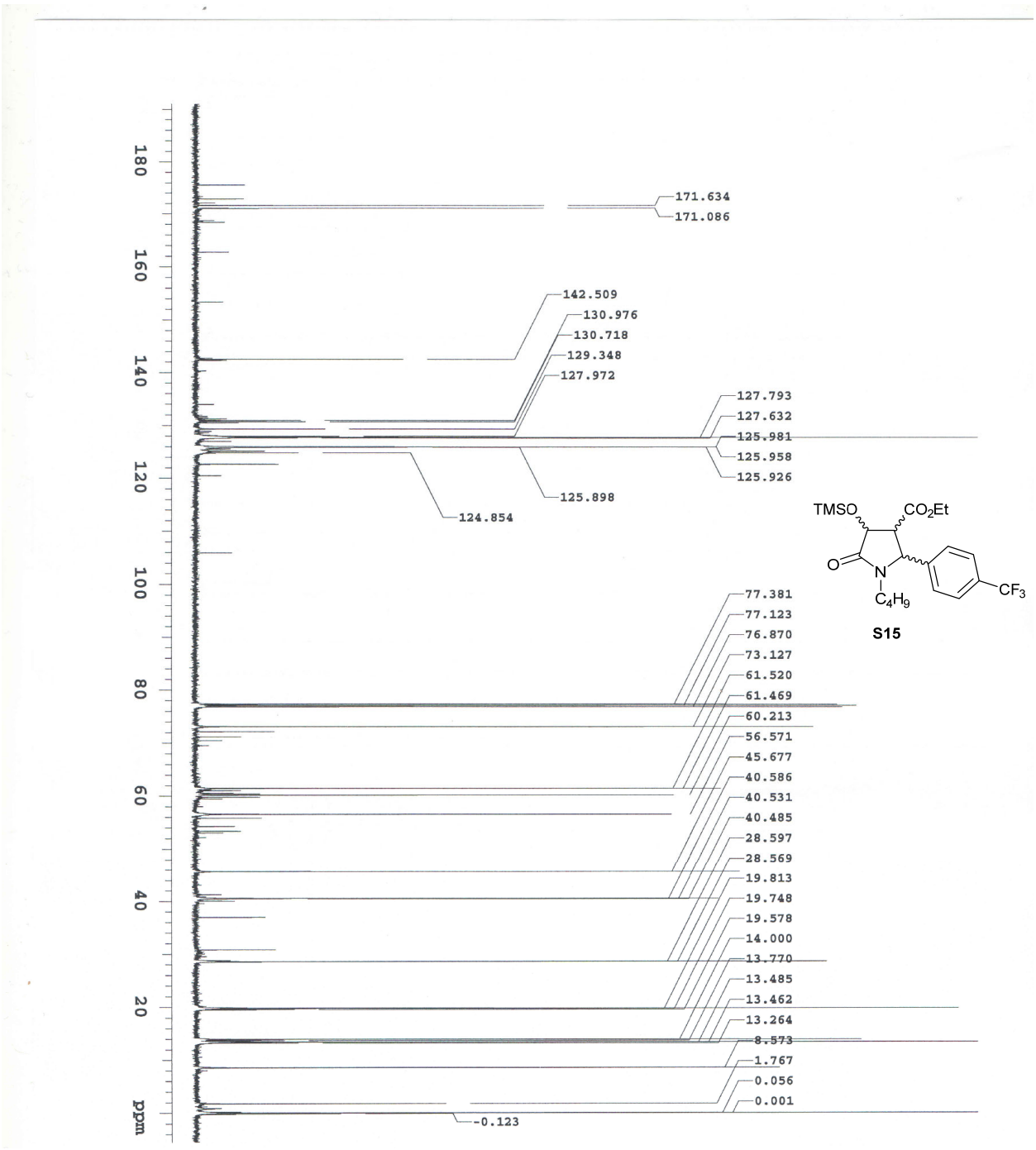
180
160
140
120
100
80
60
40
20
ppm
171.634
171.086
142.509
130.976
130.718
129.348
127.972
127.793
127.632
125.981
125.958
125.926
125.898
124.854
77.381
77.123
76.870
73.127
61.520
61.469
60.213
56.571
45.677
40.586
40.531
40.485
28.597
28.569
19.813
19.748
19.578
14.000
13.770
13.485
13.462
13.264
8.573
1.767
0.056
0.001
-0.123
TMSO
CO2Et
O
N
C4H9
CF3

S15

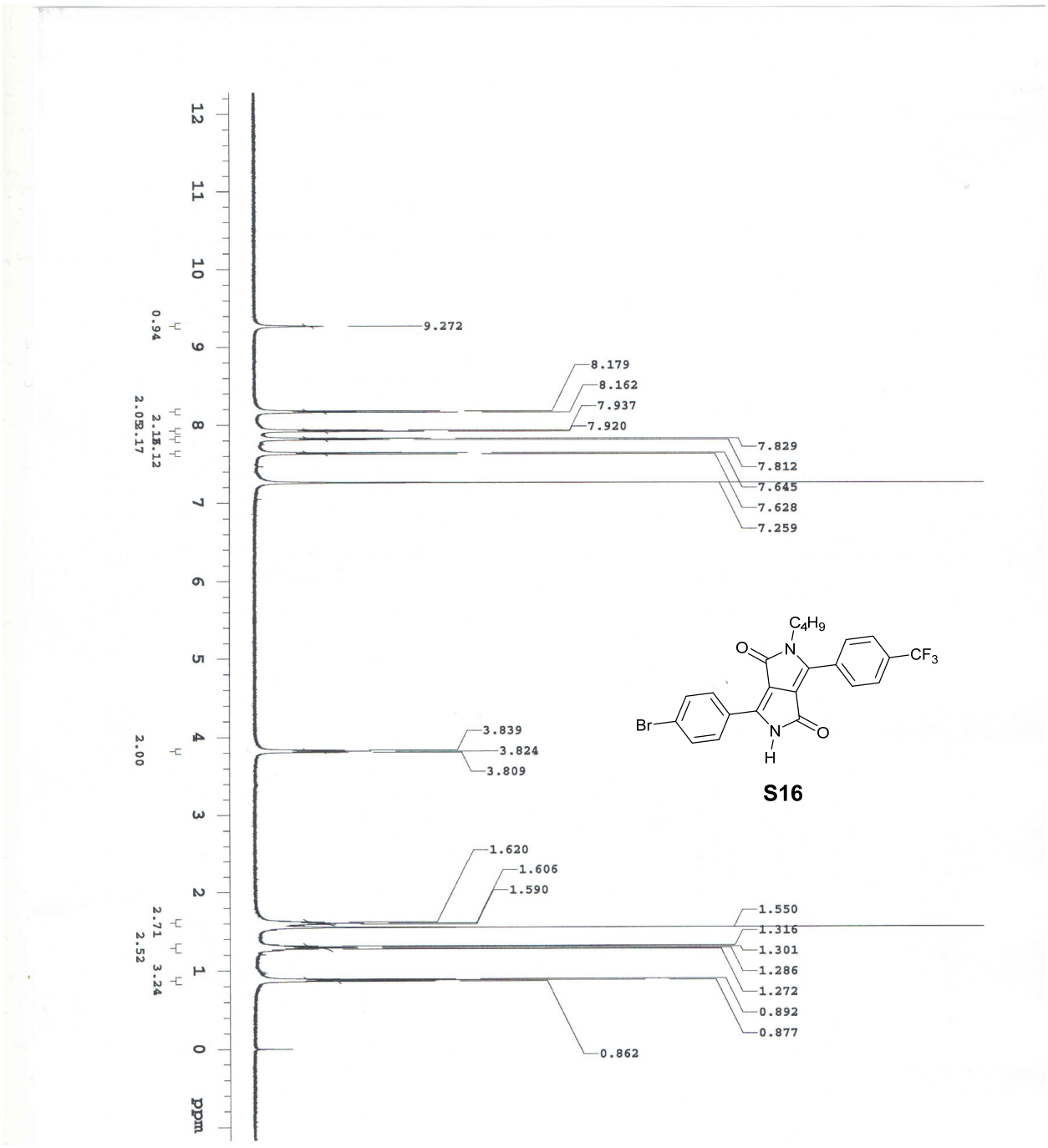
9.272
8.179
8.162
7.937
7.920
7.829
7.812
7.645
7.628
7.259
3.839
3.824
3.809
1.620
1.606
1.590
1.550
1.316
1.301
1.286
1.272
0.892
0.877
0.862
0.94
2.05
2.15
5.12
5.17
2.00
2.71
2.52
3.24
ppm
C4H9
O
N
CF3
Br
N
O
H

S16

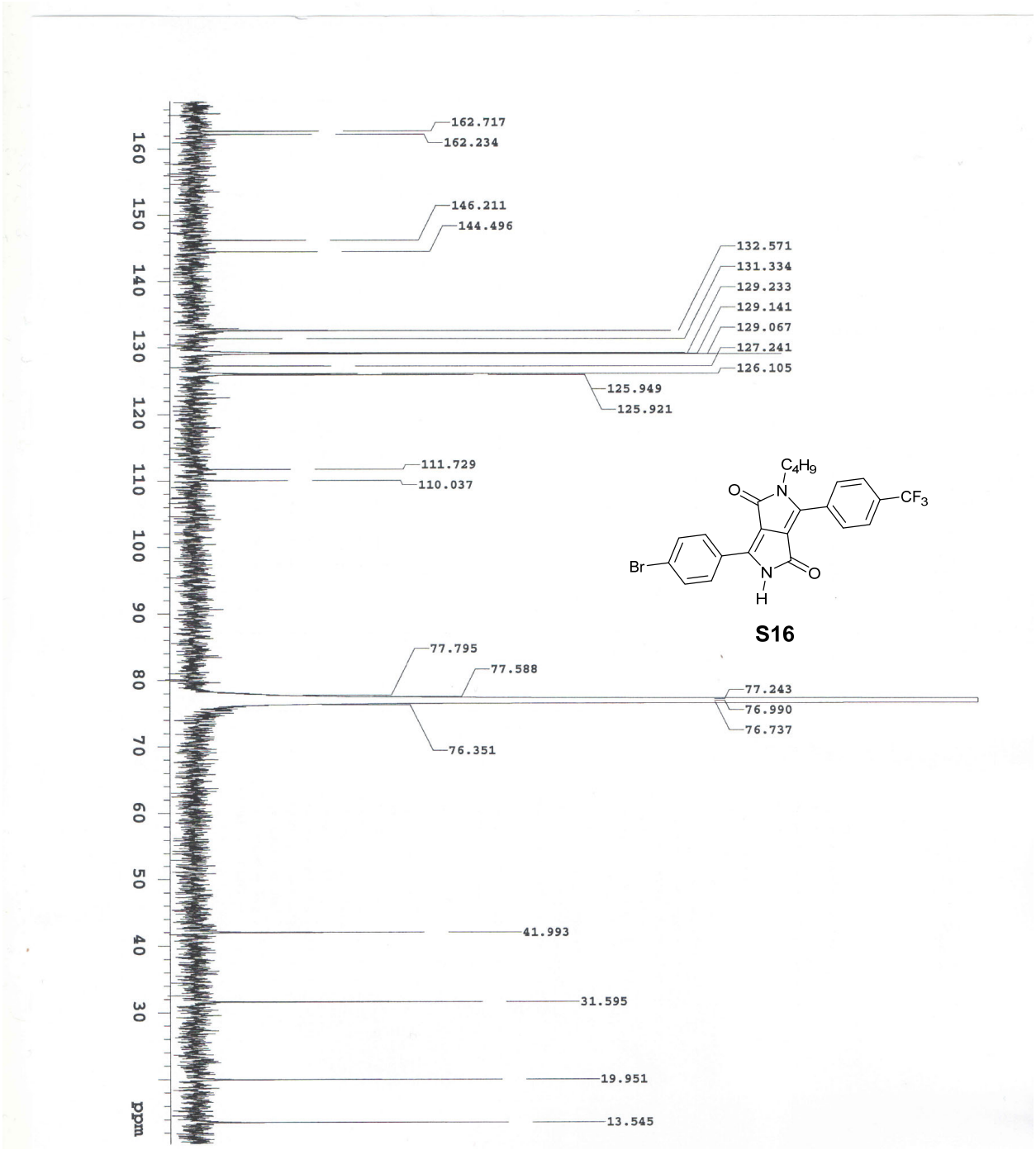
162.717
162.234
146.211
144.496
132.571
131.334
129.233
129.141
129.067
127.241
126.105
125.949
125.921
111.729
110.037
77.795
77.588
77.243
76.990
76.737
76.351
41.993
31.595
19.951
13.545
ppm
160
150
140
130
120
110
100
90
80
70
60
50
40
30
C4H9
N
O
CF3
Br
N
H
O

S16

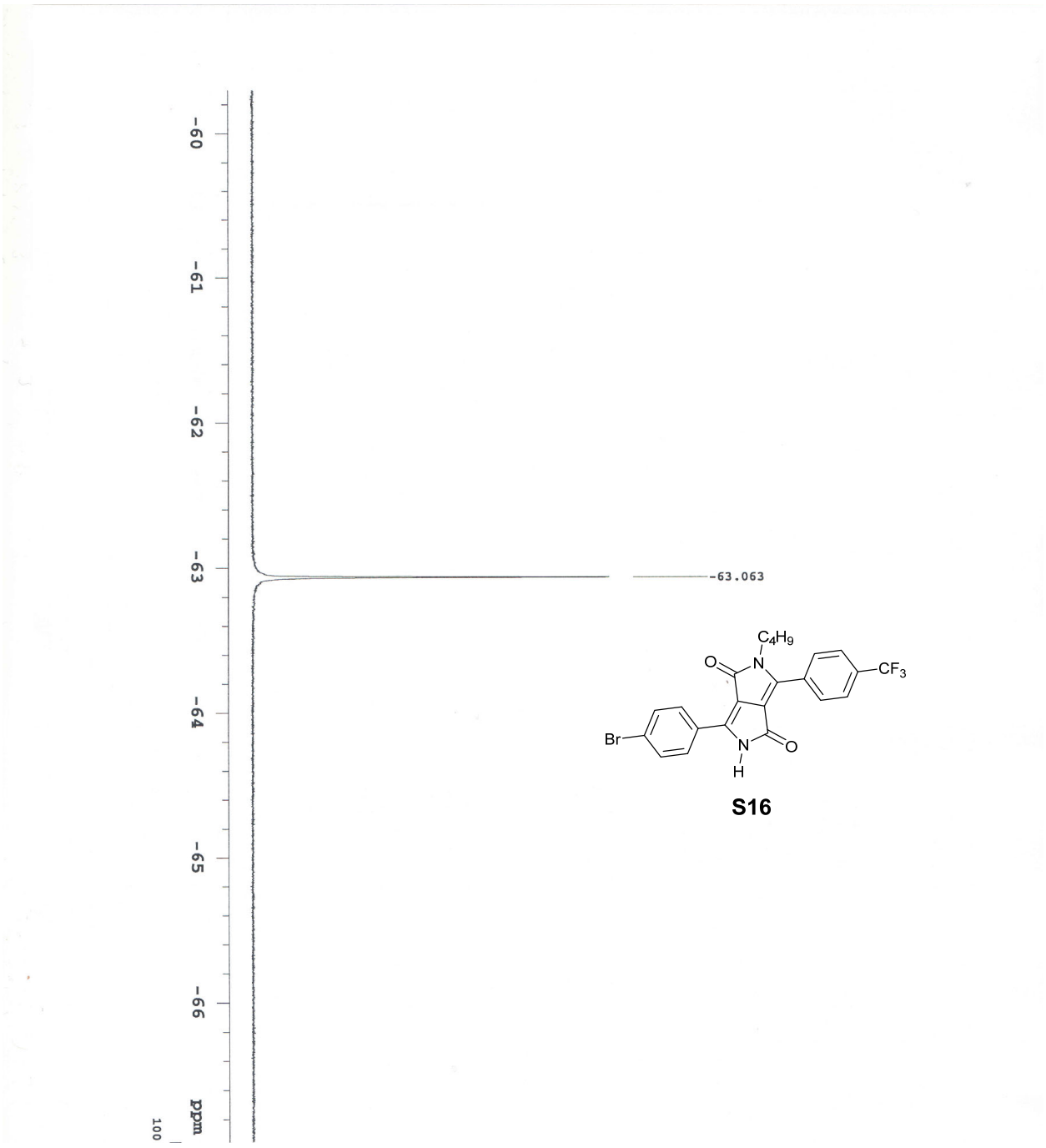

S16

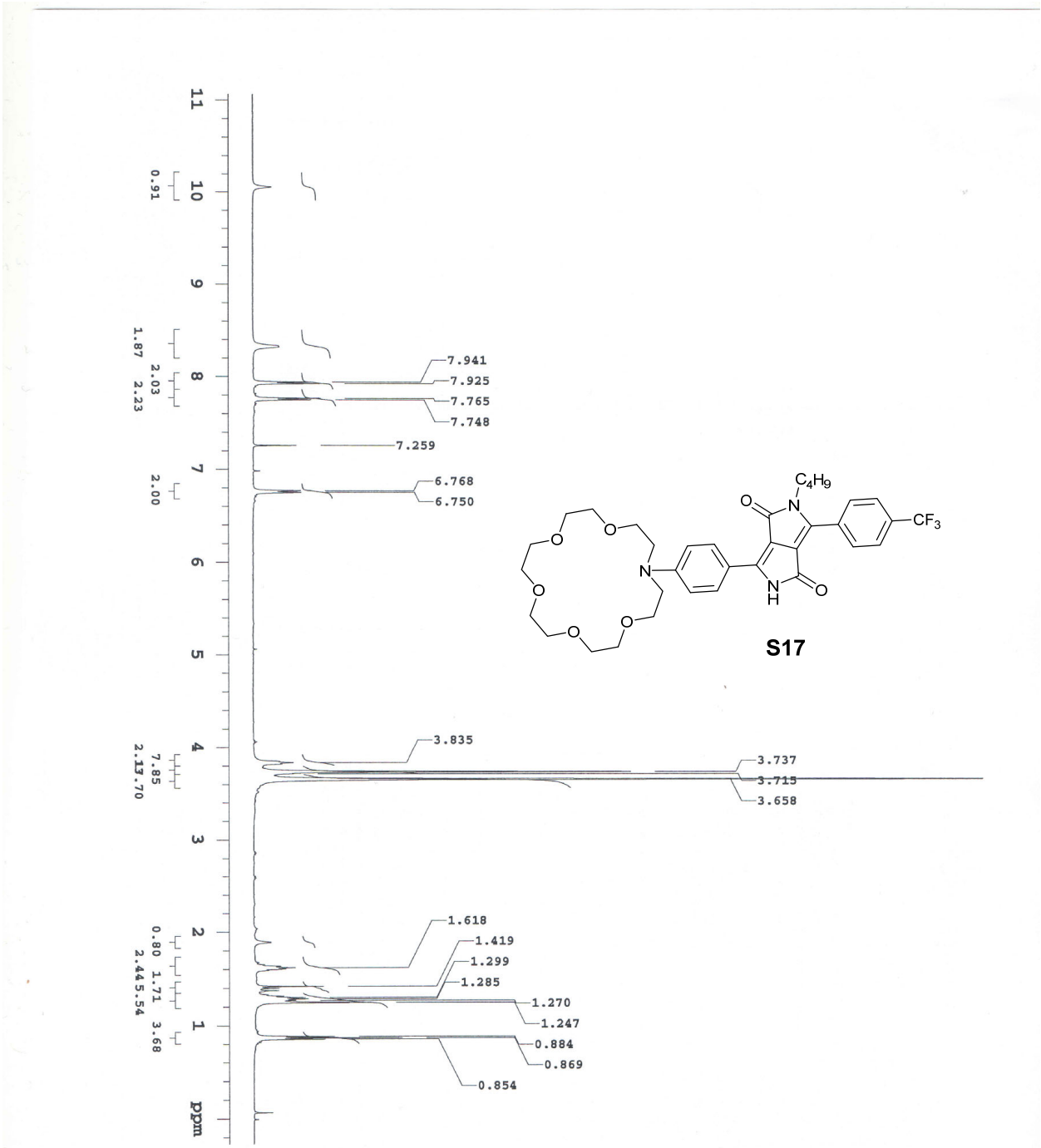
11
10
9
8
7
6
5
4
3
2
1
ppm
0.91
1.87
2.03
2.23
2.00
2.13
7.85
1.70
0.80
1.71
2.44
5.54
3.68
7.941
7.925
7.765
7.748
7.259
6.768
6.750
3.835
3.737
3.715
3.658
1.618
1.419
1.299
1.285
1.270
1.247
0.884
0.869
0.854
C4H9
CF3
S17

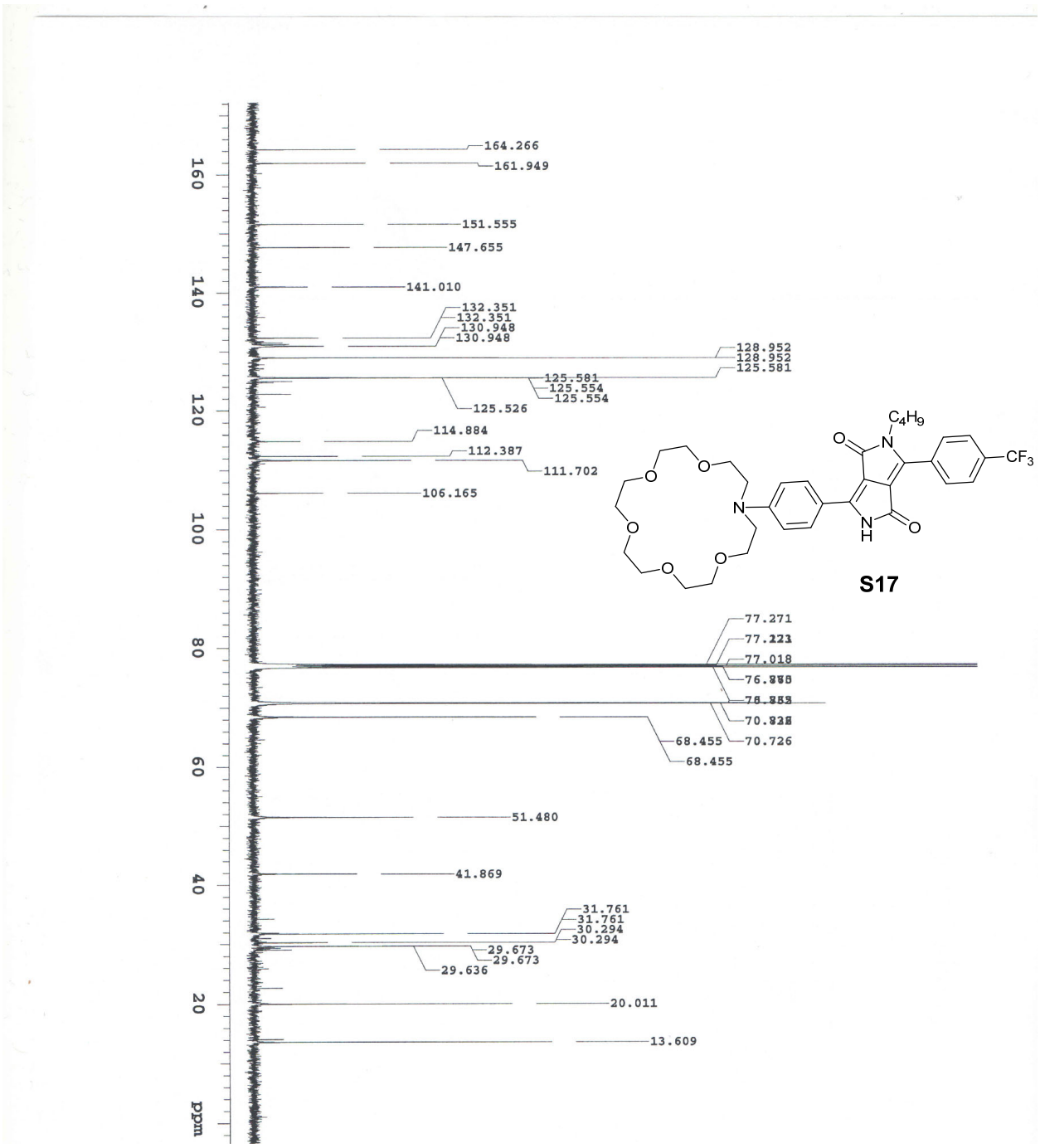
164.266
161.949
151.555
147.655
141.010
132.351
132.351
130.948
130.948
128.952
128.952
125.581
125.581
125.554
125.554
125.526
114.884
112.387
111.702
106.165
77.271
77.223
77.018
76.888
78.853
70.828
68.455
70.726
68.455
51.480
41.869
31.761
31.761
30.294
30.294
29.673
29.673
29.636
20.011
13.609
160
140
120
100
80
60
40
20
ppm
C4H9
CF3
S17

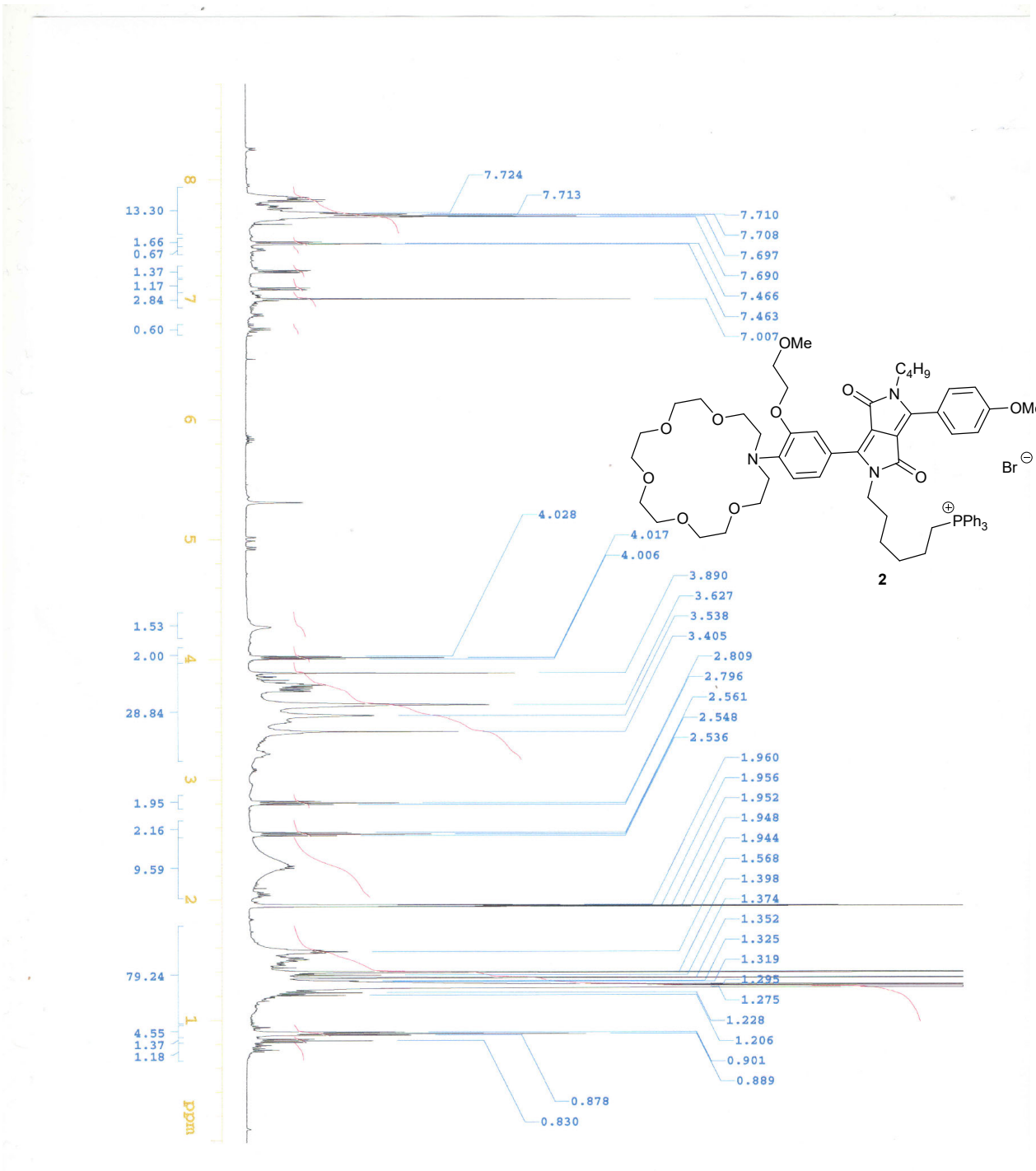
7.724
7.713
7.710
7.708
7.697
7.690
7.466
7.463
7.007
4.028
4.017
4.006
3.890
3.627
3.538
3.405
2.809
2.796
2.561
2.548
2.536
1.960
1.956
1.952
1.948
1.944
1.568
1.398
1.374
1.352
1.325
1.319
1.295
1.275
1.228
1.206
0.901
0.889
0.878
0.830
13.30
1.66
0.67
1.37
1.17
2.84
0.60
1.53
2.00
28.84
1.95
2.16
9.59
79.24
4.55
1.37
1.18
ppm
OMe
C_4H_9
OMe
Br
PPh_3
2

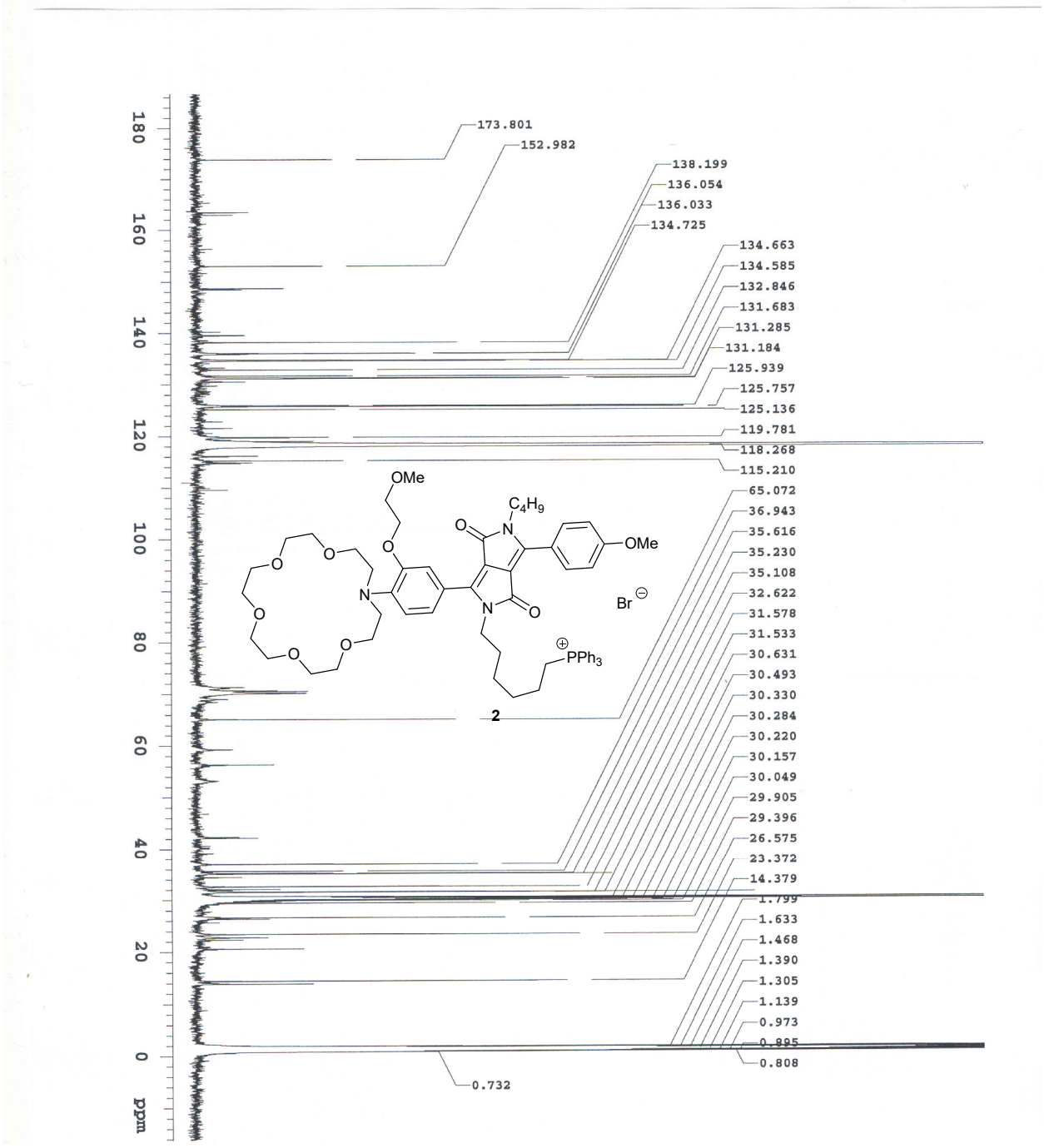
173.801
152.982
138.199
136.054
136.033
134.725
134.663
134.585
132.846
131.683
131.285
131.184
125.939
125.757
125.136
119.781
118.268
115.210
65.072
36.943
35.616
35.230
35.108
32.622
31.578
31.533
30.631
30.493
30.330
30.284
30.220
30.157
30.049
29.905
29.396
26.575
23.372
14.379
1.799
1.633
1.468
1.390
1.305
1.139
0.973
0.895
0.808
0.732
180
160
140
120
100
80
60
40
20
0
ppm
OMe
C4H9
O
N
OMe
Br
PPh3
2

MS spectra

Elemental Composition Report Page 1

Single Mass Analysis
Tolerance = 20.0 PPM / DBE: min = -1.5, max = 50.0
Selected filters: None

Monoisotopic Mass, Odd and Even Electron Ions
31 formula(e) evaluated with 1 results within limits (up to 50 best isotopic matches for each mass)
Elements Used:
C: 0-70 H: 0-100 N: 0-2 O: 0-3 Br: 1-1

D. Kumar
GDK-300
z10_dk2286 97 (3.700) Cm (82:99)

AUTOSPEC

04-Dec-2020 11:48:06
Operator: Malgorzata Grela
Voltage EI+
5.99e4

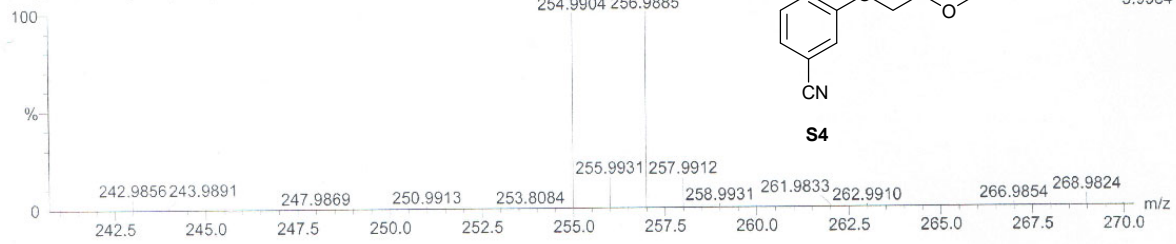

S4

Minimum:				-1.5		
Maximum:		5.0	20.0	50.0		
Mass	Calc. Mass	mDa	PPM	DBE	i-FIT	Formula
254.9904	254.9895	0.9	3.5	6.0	248.2	C10 H10 N O2 Br

C: 0-200 H: 0-200 N: 0-2 O: 0-4 Na: 0-1 Br: 0-2

Mass	Calc. Mass	mDa	PPM	DBE	Formula	i-FIT	i-FIT Norm	Fit Conf %	C	H	N	O	Na	Br
505.0726	505.0742	-1.6	-3.2	33.5	C37 H10 N2 Na	416.0	13.734	0.00	37	10	2		1	
	505.0742	-1.6	-3.2	9.5	C25 H31 O Br2	402.5	0.218	80.43	25	31		1		2
	505.0739	-1.3	-2.6	13.5	C24 H23 N2 O4 Na Br	403.9	1.634	19.52	24	23	2	4	1	1
	505.0718	0.8	1.6	6.5	C23 H32 O Na Br2	409.9	7.635	0.05	23	32		1	1	2

OV-959

z10_dk716 11 (0.243) Cm (8:20-(2:4+40:47))

1: TOF MS ES+
2.03e5

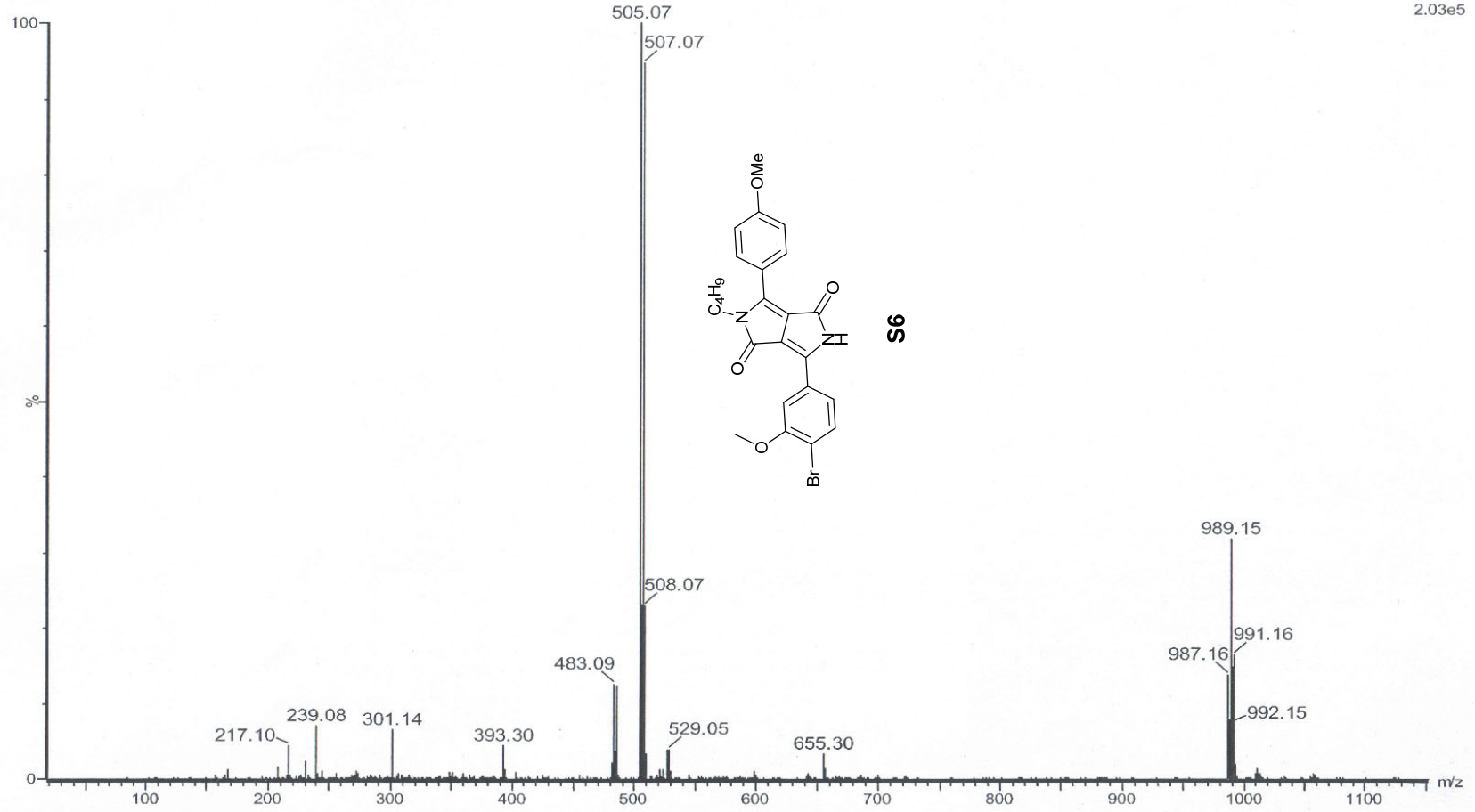

S6

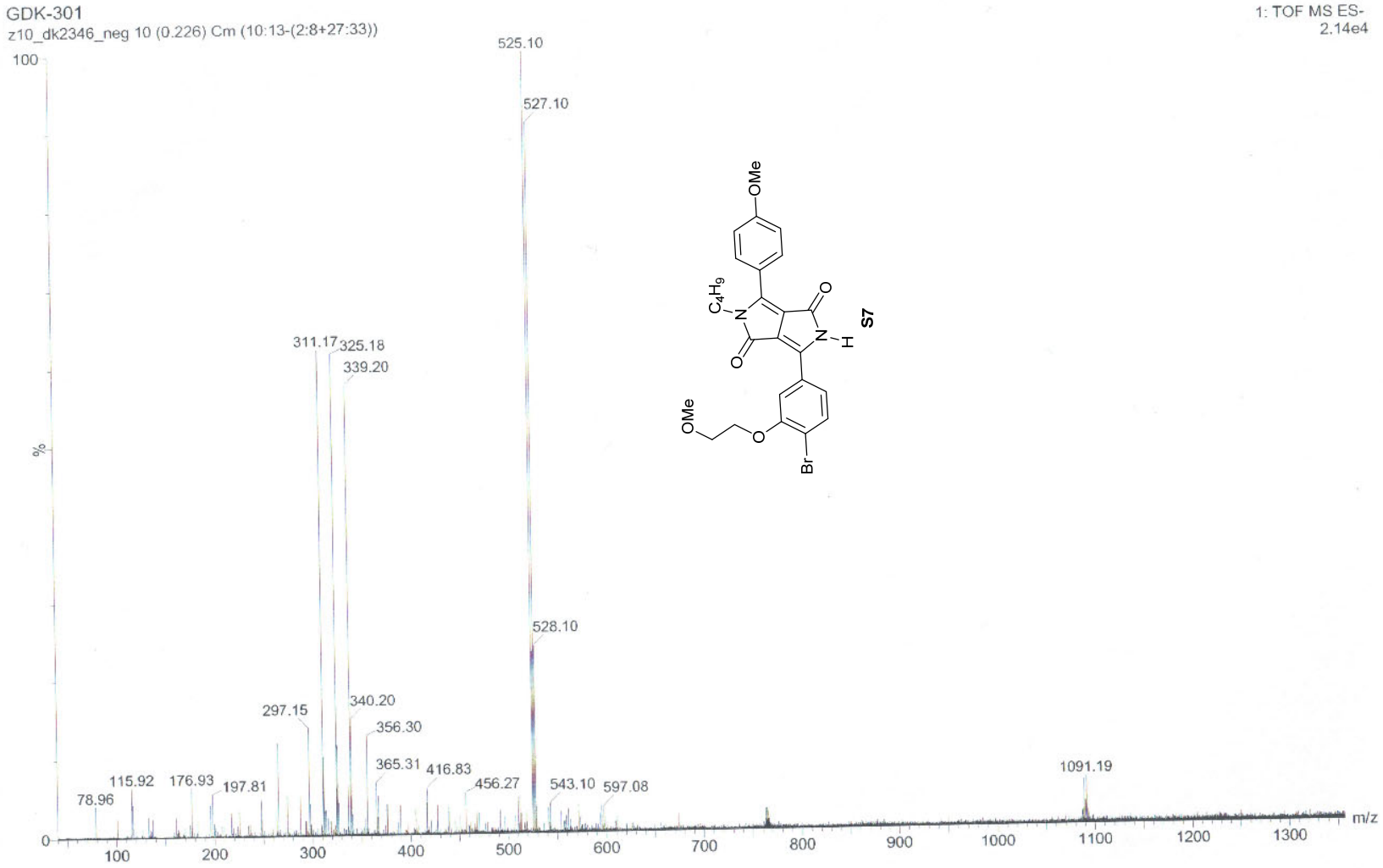
GDK-301
z10_dk2346_neg 10 (0.226) Cm (10:13-(2:8+27:33))
1: TOF MS ES-
2.14e4
100
%
0
525.10
527.10
311.17
325.18
339.20
528.10
340.20
297.15
356.30
365.31
416.83
456.27
543.10
597.08
115.92
176.93
197.81
78.96
1091.19
100
200
300
400
500
600
700
800
900
1000
1100
1200
1300
m/z
OMe
C4H9
N
O
N
H
S7
OMe
O
Br

GDK-296

z10_dk2386 12 (0.260) Cm (10:16-(4:8+41:47))

1: TOF MS ES+
2.52e6

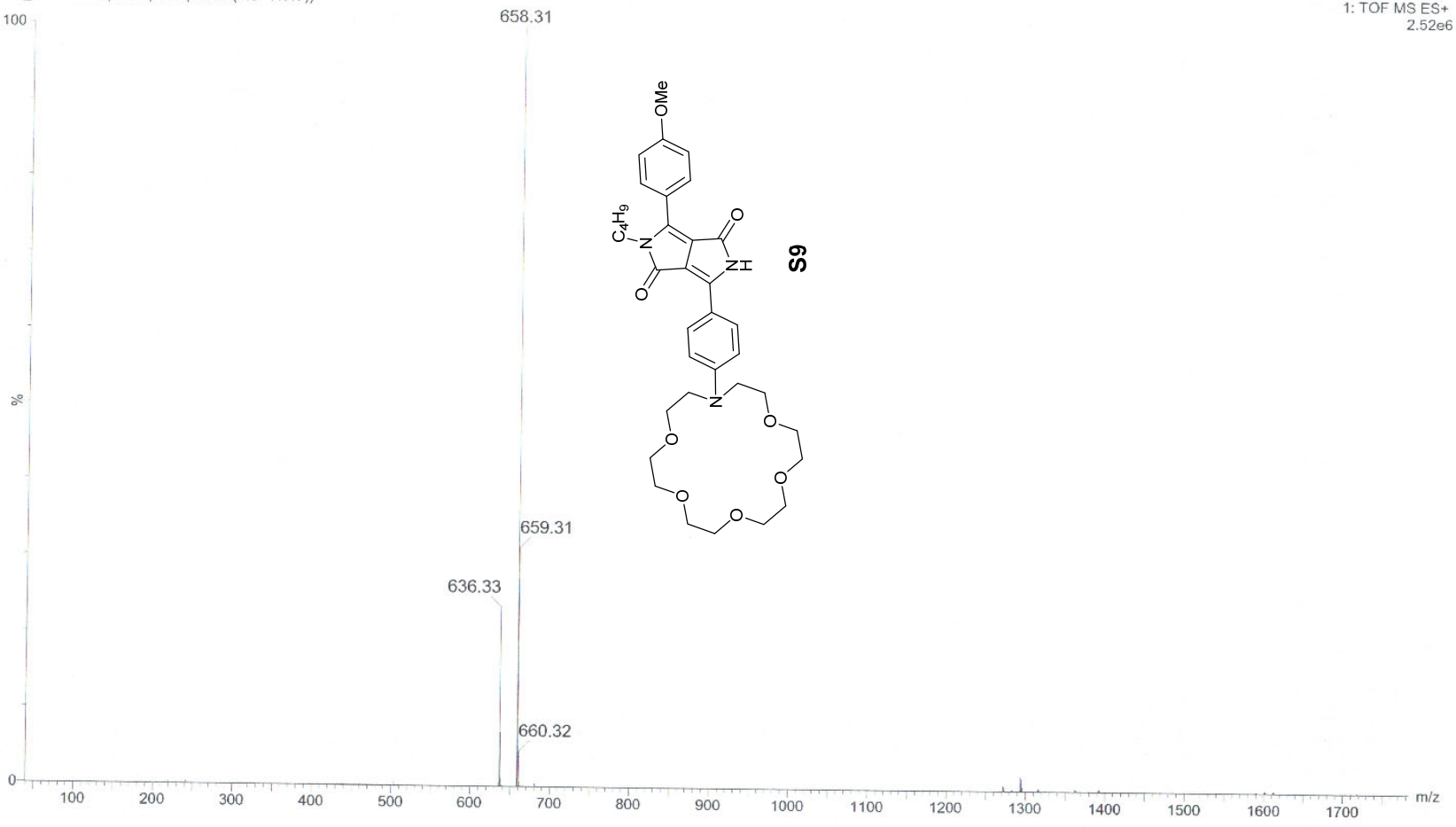

S9

Elemental Composition Report **Page 1**

Single Mass Analysis
Tolerance = 15.0 PPM / DBE: min = -1.5, max = 50.0
Selected filters: None

Monoisotopic Mass, Odd and Even Electron Ions
28 formula(e) evaluated with 1 results within limits (up to 50 best isotopic matches for each mass)
Elements Used:
C: 0-70 H: 0-100 N: 0-3 O: 9-9

D. Kumar
GDK-273
z10_dk1498h 93 (3.547) Cm (93:113)

AUTOSPEC

17-Sep-2020 11:42:39
Operator: Malgorzata Grela
Voltage EI+
3.68e3

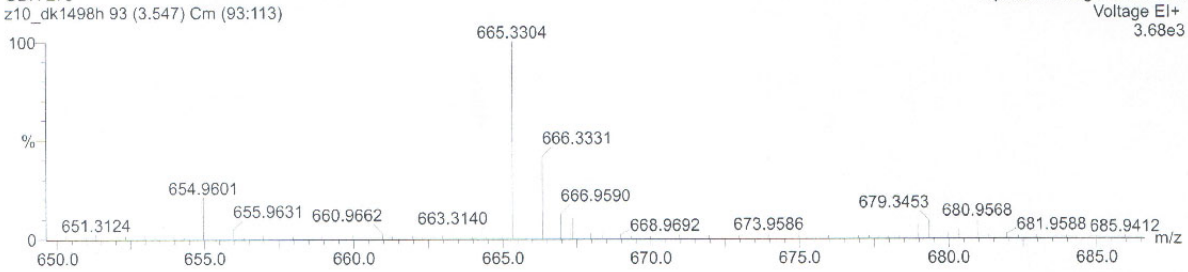

Minimum:				-1.5		
Maximum:		5.0	15.0	50.0		
Mass	Calc. Mass	mDa	PPM	DBE	i-FIT	Formula
665.3304	665.3312	-0.8	-1.2	15.0	1.2	C36 H47 N3 O9

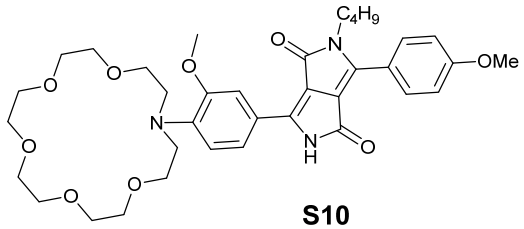

S10

GDK-293

z10_dk2345 12 (0.260) Cm (9:20-(2:8+32:40))

1: TOF MS ES+
2.38e5

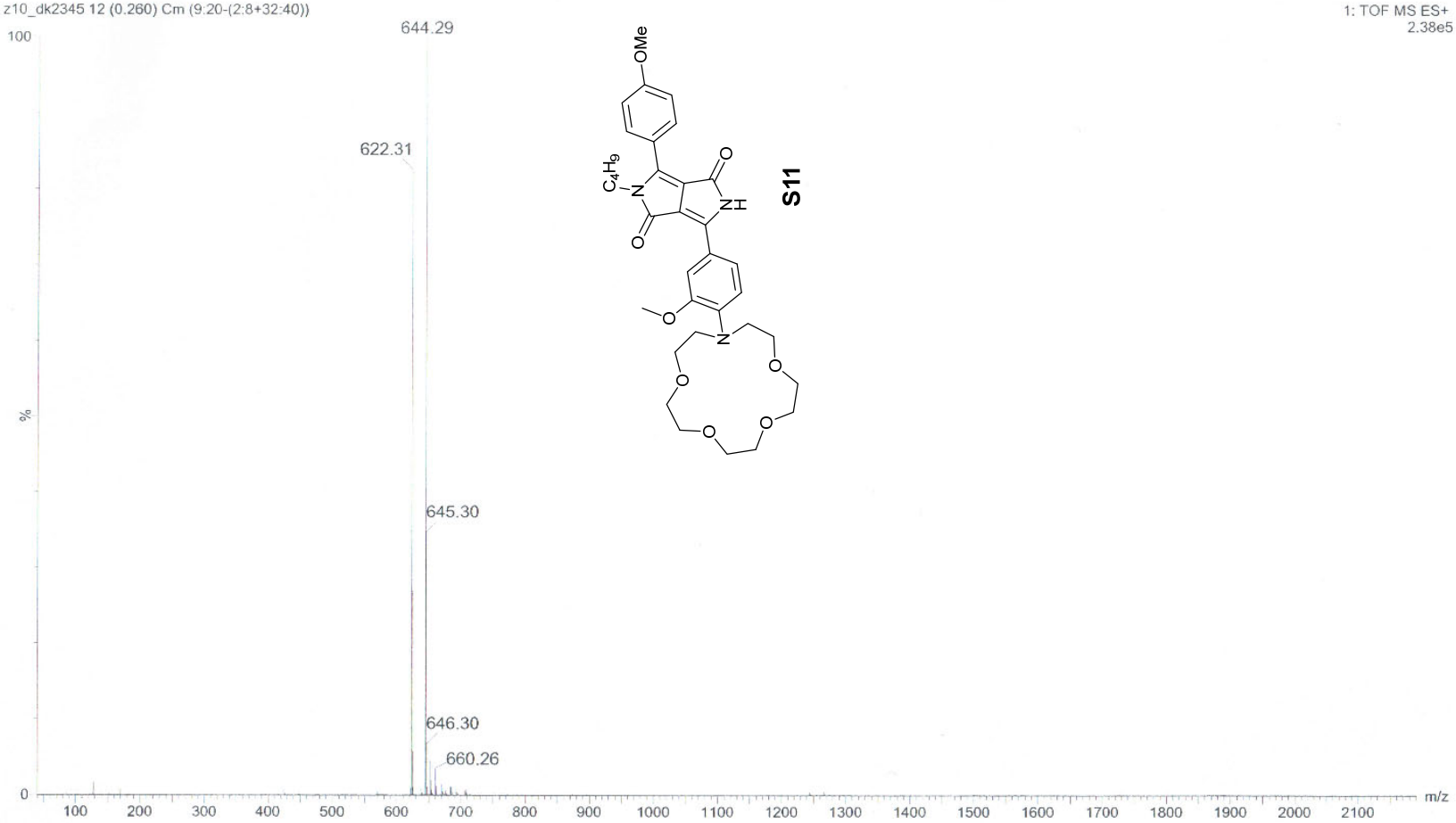

S11

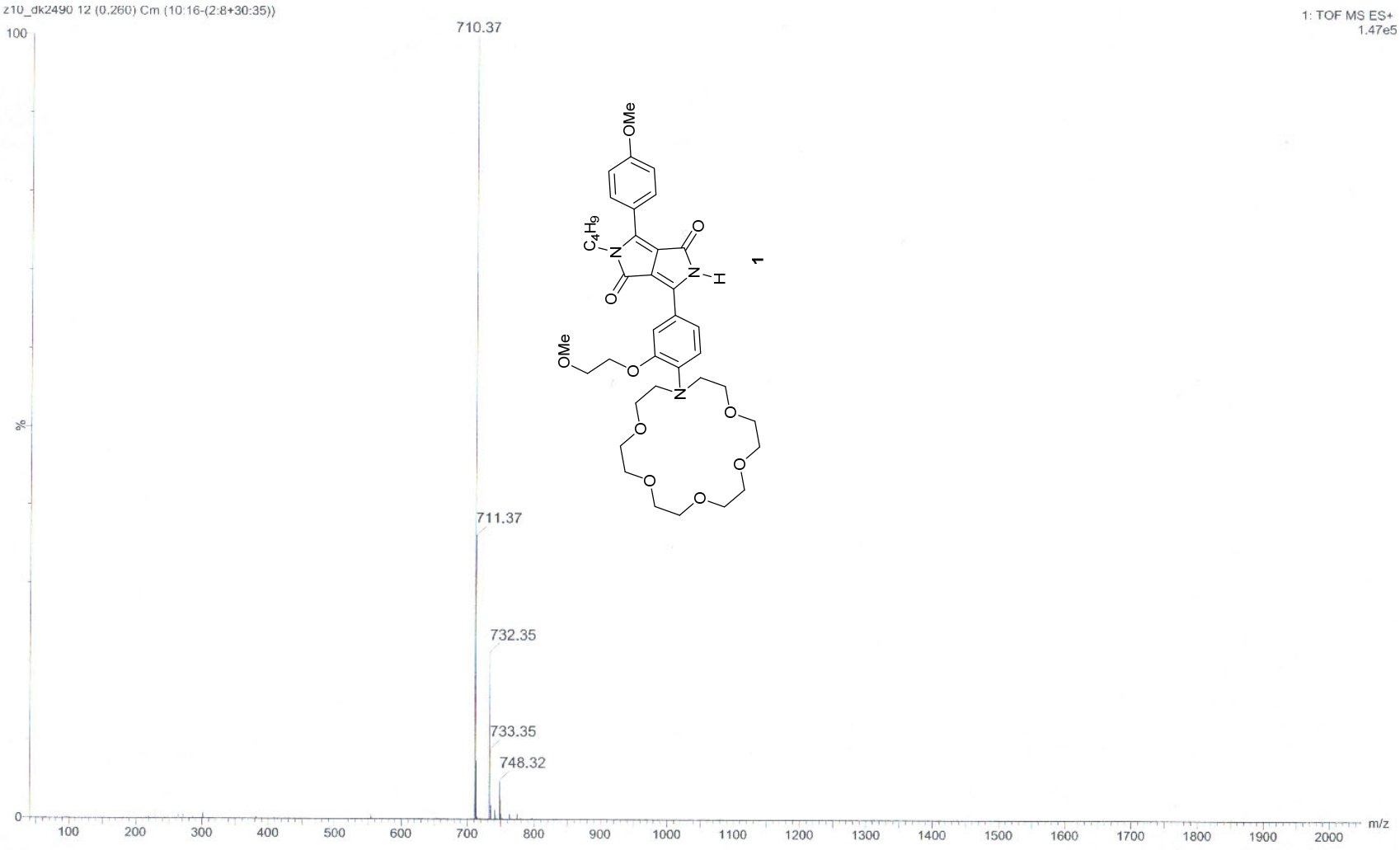
z10_dk2490 12 (0.260) Cm (10:16-(2:8+30:35))
1: TOF MS ES+
1.47e5
100
%
0
710.37
711.37
732.35
733.35
748.32
m/z
100
200
300
400
500
600
700
800
900
1000
1100
1200
1300
1400
1500
1600
1700
1800
1900
2000
OMe
C4H9
N
O
N
H
O
1
OMe
O
N
O
O
O
O
O
O

Single Mass Analysis

Tolerance = 15.0 PPM / DBE: min = -1.5, max = 50.0
Selected filters: None

Monoisotopic Mass, Odd and Even Electron Ions
42 formula(e) evaluated with 1 results within limits (up to 50 best isotopic matches for each mass)
Elements Used:
C: 0-70 H: 0-100 N: 0-1 O: 0-4 F: 3-3

K. Dinesh
GDK0344-10
z10_kd0708h 142 (5.415) Cm (136:142)

AUTOSPEC

31-Mar-2021 15:06:39
Operator: Marian Olejnik
Voltage EI+
625

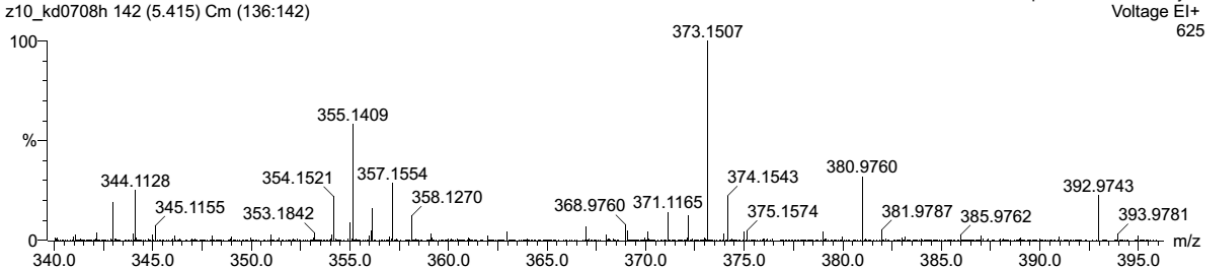

Minimum:				-1.5		
Maximum:		5.0	15.0	50.0		
Mass	Calc. Mass	mDa	PPM	DBE	i-FIT	Formula
373.1507	373.1501	0.6	1.6	7.0	2.9	C18 H22 N O4 F3

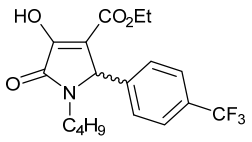

S13

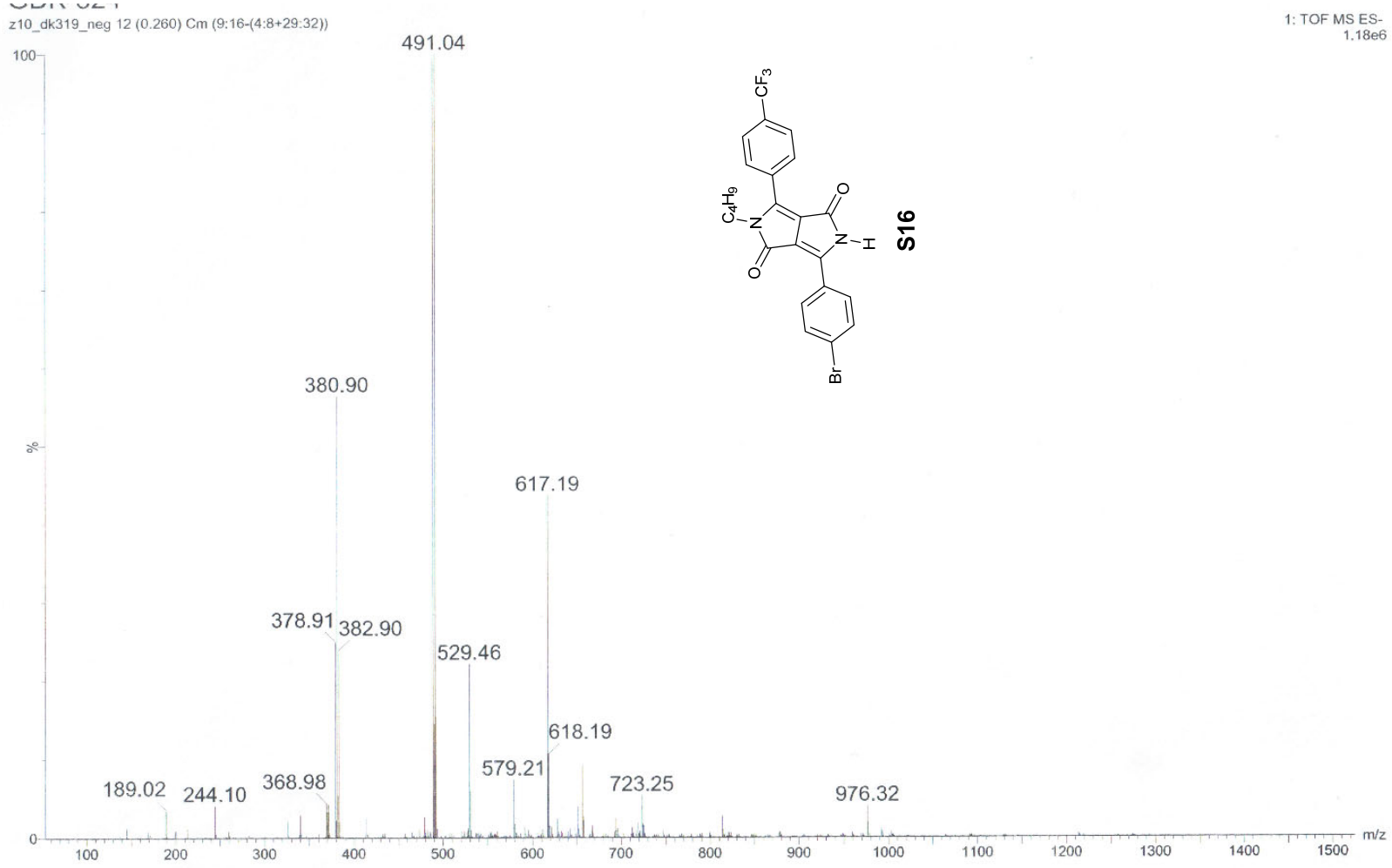
z10_dk319_neg 12 (0.260) Cm (9:16-(4:8+29:32))
1: TOF MS ES-
1.18e6
491.04
380.90
617.19
378.91
382.90
529.46
618.19
579.21
189.02
244.10
368.98
723.25
976.32
%
m/z
100
0
100
200
300
400
500
600
700
800
900
1000
1100
1200
1300
1400
1500
CF3
C4H9
N
O
O
N
H
Br
S16

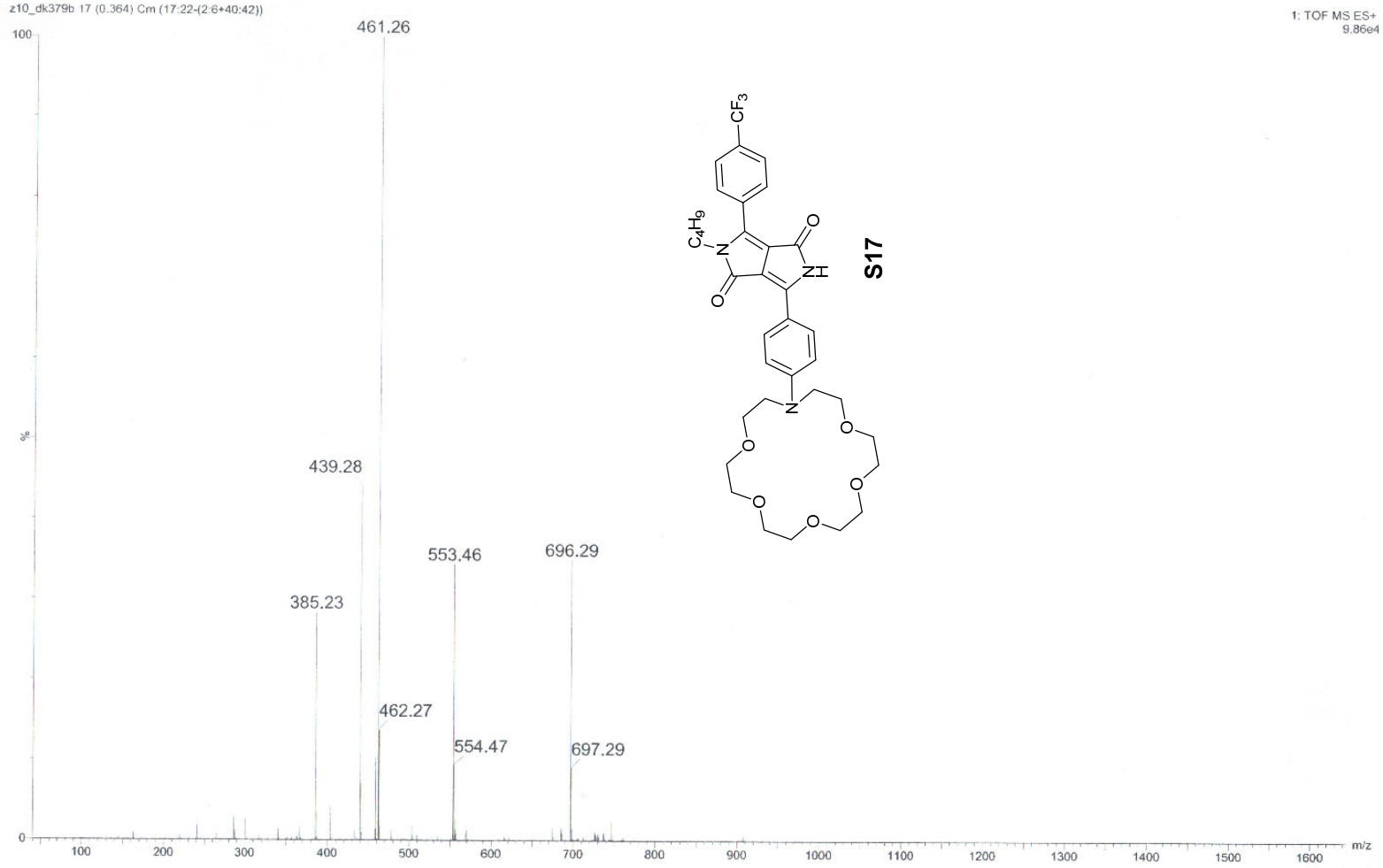
z10_dk379b 17 (0.364) Cm (17:22-(2:6+40:42))
1: TOF MS ES+
9.86e4
100
%
0
461.26
439.28
553.46
696.29
385.23
462.27
554.47
697.29
100
200
300
400
500
600
700
800
900
1000
1100
1200
1300
1400
1500
1600
m/z
CF3
C4H9
N
O
O
NH
N
O
O
O
O
O
O
S17

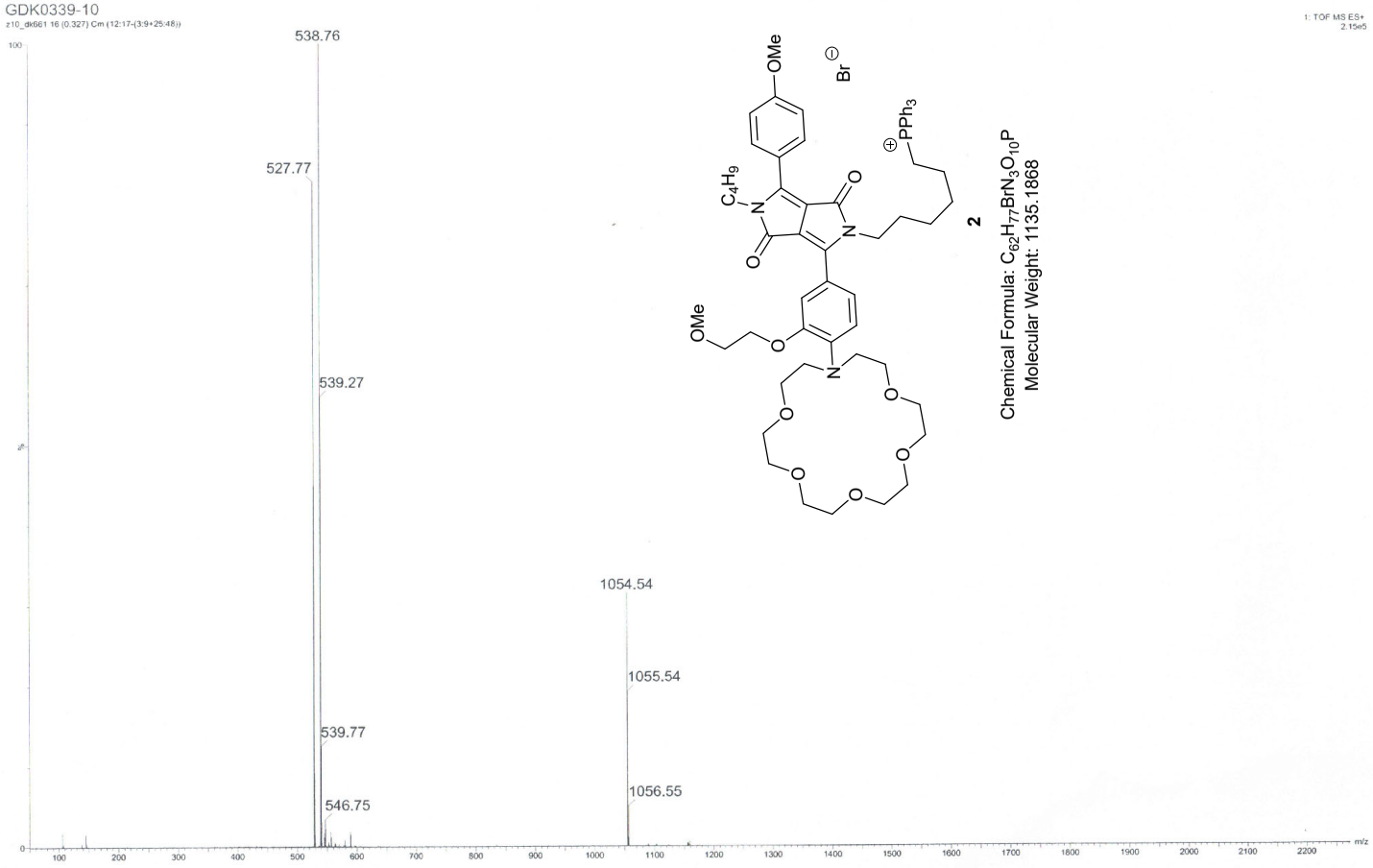
GDK0339-10
z10_dk661 16 (0.327) Cm (12:17-(3:9+25:48))
1: TOF MS ES+
2.15e5
538.76
527.77
539.27
539.77
546.75
1054.54
1055.54
1056.55
100
%
0
m/z
100
200
300
400
500
600
700
800
900
1000
1100
1200
1300
1400
1500
1600
1700
1800
1900
2000
2100
2200
OMe
Br
PPh3
C4H9
N
O
OMe
O
N
2
Chemical Formula: C62H77BrN3O10P
Molecular Weight: 1135.1868

Section S7: References

1. M. Pieczykolan, B. Sadowski and D. T. Gryko, *Angew. Chem. Int. Ed*., 2020, **59**, 7528-7535.
2. Q. Hu, J. Kunde, N. Hanke and R. W. Hartmann, *Eur. J. Med. Chem.,* 2015, **96**, 139-150.
3. D. Jacquemin, I. Duchemin, X. Blasé, *J. Chem. Theory Comput.* **2015**, *11*, 5340-5359.
4. J. Tomasi, B. Mennucci, R. Cammi, *Chem. Rev.* **2005**, *105*, 2999-3094.
5. Y. Zhao, D. G. Truhlar, *Theor. Chem. Acc.* **2008**, *120*, 215-241.
6. P. M. Vérité, C. A. Guido, D. Jacquemin, *Phys. Chem. Chem. Phys*. **2019**, *21*, 2307-2317.
7. M. J. Frisch, G. W. Trucks, H. B. Schlegel, G. E. Scuseria, M. A. Robb, J. R. Cheeseman, G. Scalmani, V. Barone, G. A. Petersson, H. Nakatsuji, X. Li, M. Caricato, A. V. Marenich, J. Bloino, B. G. Janesko, R. Gomperts, B. Mennucci, H. P. Hratchian, J. V. Ortiz, A. F. Izmaylov, J. L. Sonnenberg, Williams, F. Ding, F. Lipparini, F. Egidi, J. Goings, B. Peng, A. Petrone, T. Henderson, D. Ranasinghe, V. G. Zakrzewski, J. Gao, N. Rega, G. Zheng, W. Liang, M. Hada, M. Ehara, K. Toyota, R. Fukuda, J. Hasegawa, M. Ishida, T. Nakajima, Y. Honda, O. Kitao, H. Nakai, T. Vreven, K. Throssell, J. A. Montgomery Jr., J. E. Peralta, F. Ogliaro, M. J. Bearpark, J. J. Heyd, E. N. Brothers, K. N. Kudin, V. N. Staroverov, T. A. Keith, R. Kobayashi, J. Normand, K. Raghavachari, A. P. Rendell, J. C. Burant, S. S. Iyengar, J. Tomasi, M. Cossi, J. M. Millam, M. Klene, C. Adamo, R. Cammi, J. W. Ochterski, R. L. Martin, K. Morokuma, O. Farkas, J. B. Foresman, D. J. Fox, *Gaussian 16 Rev. B.01*, Wallingford, CT, **2016**.
8. TURBOMOLE V6.2 2010, a development of University of Karlsruhe and Forschungszentrum Karlsruhe GmbH, 1989-2007, TURBOMOLE GmbH, since 2007; available from http://www.turbomole.com.
9. a) J. Cerezo, F. Santoro, FCClasses 3.0, http://www.pi.iccom.cnr.it/fcclasses; b) F. Santoro, R. Improta, A. Lami, J. Bloino, V. Barone, *J. Chem. Phys.* **2007**, *126*, 084509; c) F. Santoro, D. Jacquemin, *Wires Comput. Mol. Sci*. **2016**, *6*, 460–486.
1.